# DISPERSION OF HEAVY PARTICLES IN AN ISOLATED PANCAKE-LIKE VORTEX

by

AURELIE GOATER

Graduée en ingénierie, Ecole Nationale Supérieure des Techniques Avancées, Paris, 2001

A THESIS SUBMITTED IN PARTIAL FULFILMENT OF
THE REQUIREMENTS FOR THE DEGREE OF
MASTER OF APPLIED SCIENCE

in

THE FACULTY OF GRADUATE STUDIES
Department of Civil Engineering
Institute of Applied Mathematics

We accept this thesis as conforming
to the required standard

THE UNIVERSITY OF BRITISH COLUMBIA
August 2003

In presenting this thesis in partial fulfilment of the requirements for an advanced degree at the University of British Columbia, I agree that the Library shall make it freely available for reference and study. I further agree that permission for extensive copying of this thesis for scholarly purposes may be granted by the head of my department or by his or her representatives. It is understood that copying or publication of this thesis for financial gain shall not be allowed without my written permission.

Department of Civil Engineering

The University of British Columbia
Vancouver, Canada

Date August 13th /2003

DE-6 (2/88)

# ABSTRACT

The objective of the present study is to characterize the dispersion of small, spherical particles (mainly heavy particles) in a quasi two-dimensional axisymmetric pancake-like vortex. The velocity field for a pancake vortex is substituted into the Maxey-Riley (1983) equation, and the resulting equations of motion are solved numerically, in non-dimensional form, for a given set of parameters.

The particles' characteristics that are of primary importance are their density and their diameter. In general, the particles considered are denser than the surrounding fluid. Therefore they move away from the vortex centre with time. The Stokes number, a function of the particle diameter and density, measures the sensitiveness of the particle to the surrounding velocity field. The lateral dispersion of the particles is examined for different values of the Stokes number, ranging from $10^{-1}$ to $10$.

The analysis is first conducted in the 2D horizontal plane of the vortex. By looking at the dynamics of individual particles, it is shown that particles of the same size and density cannot accumulate in the core of the vortex, but they can do so in the outer region of the vortex, increasing the possibility of flocculation. In addition, if the Stokes number is large enough, particles initially located in the central region of the vortex are able to overtake particles initially located further from the vortex centre.

The analysis of the concentration profiles in the horizontal plane of the vortex, when the flow is initially seeded with a homogeneous distribution of particles of the same size and density, shows that accumulation of particles takes the form of a concentration wave that grows and travels away

from the vortex centre. The larger the Stokes number is, the faster the particles are ejected, but optimal accumulation occurs for intermediate values of the Stokes number ($St \sim 1$). Also, for large Stokes numbers ($St \sim 10$), overtaking is observed. It occurs at very early times and substantially modifies the dispersion process, causing a second peak of concentration to appear. Just before the second peak of concentration detaches itself from the first one, a very high local concentration is observed, because the catch-up phenomenon adds up to the local accumulation of particles. Further calculations show that overtaking is associated with a very high probability of collision between the particles, so that, in reality, flocculation is expected to play an important role for large Stokes numbers.

The analysis is extended to the settling of heavy particles through the vortex. A 3D study shows that the second peak of concentration observed in the case of large Stokes numbers ($St \sim 10$) will not occur unless the vortex thickness is large enough.

# TABLE OF CONTENTS

Abstract ..... ii

Table of contents ..... iv

List of tables ..... ix

List of figures ..... x

List of symbols ..... xv

Acknowledgements ..... xviii

1 Review of the influence of vortex structures on the dispersion of particles ..... 1

1.1 General introduction ..... 1

1.2 Basic definitions ..... 2

1.2.1 Particle ..... 2

1.2.2 Vortex ..... 3

1.2.3 Dispersion and its traditional approach ..... 6

1.3 Model based on the Stokes number ..... 8

1.4 Review of experimental and numerical work – focus on heavy particles ..... 10

1.4.1 In wakes: demixing, focusing ..... 11

1.4.2 In mixing layers: formation of large scale particle streaks between successive vortices ..... 13

1.4.3 Summary ..... 17

1.5 Analysis of the motion of individual particles in idealized representations of the flow field ..... 18

1.6 The case of light particles ..... 21

2 Research objectives and the corresponding equations of particle motion ..... 22

2.1 Research objectives ..... 22

2.1.1 About pancake-like vortices ..... 22

2.1.2 General objectives - methodology ..... 23

2.2 Analytical model of the vortex flow field ..... 25

2.2.1 Analytical model of the velocity profile ..... 25

2.2.2 Note on the non-dimensionalization ..... 27

2.2.3 Details of the derivation of the idealized velocity field ..... 28

2.3 Assumptions that simplify the dynamics ..... 30

2.4 The Maxey-Riley equation ..... 30

2.4.1 Presentation of the equation ..... 30

2.4.2 Significance of the different terms ..... 33

2.4.3 Assumptions of the Maxey-Riley equation – corresponding restriction imposed on the parameters $(St.\delta)$ ..... 36

2.4.4 Extension to finite values of the particle Reynolds number ..... 37

2.5 The equations of motion of a particle in a pancake vortex ..... 39

2.5.1 Presentation of the equations of motion of a particle in a pancake vortex ..... 39

2.5.2 The governing parameters ..... 40

2.5.3 Importance of the initial conditions ..... 45

2.6 The bubble case ..... 46

2.6.1 General form of the equation of motion of a bubble ..... 46

2.6.1.1 The history term ..... 47

2.6.1.2 Modification of the steady drag force term ..... 47

2.6.2 The modified Stokes number as the relevant parameter ..... 48

2.6.3 Sensitivity to the acceleration of the fluid ..... 49

3 Simple analysis of light and heavy particle motion in the 2D horizontal plane of a pancake vortex ..... 50

3.1 Validity of the 2D approach ..... 50

3.1.1 Significance of the 2D approach ..... 50

3.1.2 Possibility of a quasi 2D motion ..... 51

3.1.2.1 Residence time of a particle ..... 51

3.1.2.2 Conditions for a quasi 2D motion ..... 52

3.2 Equations of motion in 2D ..... 56

3.2.1 General case ..... 56

3.2.2 Simplifications in the case of very heavy particles ..... 57

3.3 Implementation in Matlab ..... 57

3.3.1 Choosing the solver: stiff or nonstiff problem? ..... 58

3.3.2 Error tolerance ..... 59

3.3.3 Parameters of the simulation ..... 59

3.4 Equilibrium point and its stability ..... 61

3.4.1 Case of very heavy particles ..... 62

3.4.2 General case ..... 63

3.5 Influence of the density ratio ..... 66

3.5.1 Light particles versus heavy particles ..... 66

3.5.2 Case of light particles with a large Stokes number ..... 66

3.5.3 Ability of neutrally buoyant particles to track fluid particles ..... 68

3.6 Influence of the initial velocity ..... 69

4 Dynamics of heavy particles in the 2D horizontal plane of a pancake vortex ..... 73

4.1 The ejection rate ($\frac{\dot{r}}{r}$ or $\dot{r}$) : general trend ..... 74

4.2 Forces involved in the radial direction ..... 76

4.3 Analytical results for a small Stokes number ($St < 1$) ..... 80

4.4 Particle dynamics in the core region ..... 81

4.5 Particle dynamics in the outer region ..... 94

4.5.1 Ejection rate ..... 94

4.5.2 Possibility of accumulation (St=0.1/1) or overtaking (St=10) ..... 94

4.5.3 Qualitative difference between St=0.1/1 and St=10 ..... 98

5 Concentration profiles in the horizontal plane of a pancake vortex ..... 100

5.1 Snapshots of concentration profiles ..... 101

5.2 Comments ..... 109

5.3 Analytical results for small Stokes numbers ($St < 1$) ..... 117

5.4 Concentration profiles: conclusions ..... 121

5.5 Extrapolation for the 3D case ..... 122

6 The 3D study ..... 124

6.1 Role of the gravity on the dispersion ..... 124

6.2 Sinking of a planar distribution of particles through a pancake vortex ..... 125

6.2.1 Description of the 'experiment' ..... 125

6.2.2 Parameters at stake ..... 126

6.2.3 Results ..... 127

6.2.4 Extrapolation for particles being steadily seeded ..... 132

6.2.5 Influence of the vortex thickness: $\Lambda$ ..... 137

7 Discussion ..... 140

8 Conclusions ..... 149

References ..... 151

Appendix A Equations of motion with a modified added mass term ..... 155

Appendix B Justification of the neglect of the Basset history term ..... 156

Appendix C Origin of the Maxey-Riley equation's assumptions ..... 159

# LIST OF TABLES


| Table | | Page |
|---|---|---|
| 4.1 | Ejection rate in the core region for different Stokes numbers..... | 83 |
| 5.1 | Maximum value of the concentration observed $c_{max}$ and the corresponding radial position $\eta$, for St=0.1, 1, 10, at different times T ..... | 112 |
| B.1 | Comparison of the value of the Basset history term obtained, at t=100, with a time step $\Delta\tau = 0.01$, with that obtained with a time step $\Delta\tau' = 0.001$ ..... | 157 |

# LIST OF FIGURES

**Figure** **Page**


1.1 Drawings representing vortices developing in a mixing layer and in the wake of a bluff-body (Crowe et al. 1995) ..... 5

1.2 Cloud vortices observed in the wake of Selkirk Island, Chile, Landsat 7, September 1999 (photograph courtesy NASA). ..... 6

1.3 Drawing representing the concepts of mixing, spreading and transport, associated with the concept of dispersion (Crowe et al. 1993)..... ..... 6

1.4 Model based on the Stokes number (Crowe, Gore and Troutt 1985) ..... 10

1.5 Photographic results for a bluff body wake flow containing particles with a) very small Stokes numbers and b) intermediate Stokes numbers. (Tang et al. 1992) ..... 12

1.6 Numerical simulations of the particle dispersion in a wake flow: a) St=0.01, b) St=1.0, c) St=10, d) St=100 (Yang et al. 1991) ..... 13

1.7 Particle dispersion in a simulated plane mixing layer (Chein and Chung 1988) ..... 14

1.8 Stretching and folding of the large-scale particle streaks forming in between successive vortices of a mixing layer (Wen et al. 1992)..... 16

2.1 Idealized velocity and vorticity profiles of an isolated pancake-like vortex, in its 2D horizontal plane (the velocity and vorticity, usually expressed in the S.I. units, are presented in their non-dimensional form here) ..... 26

2.2 Velocity field found by following tracer particles in time (Beckers et al. 2001) ..... 27

3.1 Fluid velocity and vorticity profiles in the horizontal. The four recognizable points are: A ($r = 0$): centre of the vortex; B ($r = 1/\sqrt{2}$) distance at which $u_\theta$ is maximum; C ($r = 1$): distance at which $\omega_z$ changes sign; D ($r = \sqrt{2}$): distance at which $\omega_z$ is minimum ..... 61

3.2 Coordinates (x, y and r) and trajectory of a heavy particle and of a light particle After they are released at the cross position, close to the vortex centre. The corresponding parameters are:

$$[St - \delta - \vec{x}_p(t=0) - \vec{v}_p(t=0)] = [1 - 0.1 - (0.1;0) - \vec{u}], T = 1000.$$

and $[St - \delta - \vec{x}_p(t=0) - \vec{v}_p(t=0)] = [1 - 10 - (0.1;0) - \vec{u}],\ T = 30$ ..... 65

3.3 Coordinates (x, y and r) and trajectory of a light particle with a small Stokes number $[St-\delta-\vec{x}_p(t=0)-\vec{v}_p(t=0)]=[10-100-B-\vec{0}]$, $T=50$ ..... 67

3.4 Coordinates (x, y and r) and trajectory of a light particle with a large Stokes number $[St-\delta-\vec{x}_p(t=0)-\vec{v}_p(t=0)]=[100-100-B-\vec{0}]$, $T=50$ ..... 67

3.5 Coordinates (x, y and r) and trajectory of a neutrally buoyant particle after it is released with zero initial velocity with the following parameters: $[St-\delta-\vec{x}_p(t=0)-\vec{v}_p(t=0)]=[10-1-(1;0)-\vec{0}], T=100$ ..... 69

3.6 Trajectories of particles released from $\vec{x}_p(t=0)=(1;0)$, with zero initial velocity (left) or with the local velocity (right), for different combinations of parameters ..... 71

3.7 Trajectories (top) and coordinates (bottom) of a light particle with a large Stokes number released with zero initial velocity (left) and with the local initial velocity (right) ..... 72

4.1 Fluid vorticity and velocity profiles in the horizontal, with the distinction between the vortex core region and the outer ..... 75

4.2 Radial velocity of the particle with respect to its radial displacement ($r$). The particle is released at $(x0;y0) = (0.01;0)$ i.e. very close to the vortex centre, with a different Stokes number each time ..... 75

4.3 Logarithmic plot of the absolute values of the 'acceleration', the 'drag force' and the 'centrifugal force', with respect to time ..... 78

4.4 Absolute values of the 'acceleration', the 'drag force' and the 'centrifugal force', with respect to time, for a particle with St=10 released close to the vortex centre ..... 79

4.5 Left: distance from the vortex centre r, Cartesian x and y coordinates, with respect to time. Centre: trajectory of the particle (x position versus y position). Right: ejection rate (dr/dt)/r with respect to time. For each Stokes number: (a) St=0.01, (b) St=0.1, (c) St=1, (d) St=10, (e) St=100. Particles released at $(x0;y0) = (0.01;0)$, with the local fluid velocity ..... 82

4.6 Logarithmic plot of the ejection rate in the vortex core region, with respect to the Stokes number, as observed on simulations. (From data points corresponding to St = 0.01, 0.05, 0.1, 0.5, 1, 1.5, 2, 2.5, 3 5, 10, 50, 100.) ..... 84

4.7 Contour plot of the real and imaginary parts of the eigenvalues $\lambda_1$ and $\lambda_2$ ..... 86

4.8 a) Radial position, b) radial velocity and c) ejection rate, with respect to time, for 2 particles of Stokes number St=1 and St=10 ..... 87

4.9 Radial position with time (left) and radial velocity with respect to radial position, for three particles of Stokes number $St_1 = 0.1$, $St_2 = 1$ and $St_3 = 10$. The first and third particles are released at the radial position $r0_1 = r0_3 = 0.125$ and the second particle at $r0_2 = 0.05$ ..... 90

4.10 Radial position versus radial velocity for 3 particles of Stokes number St=0,1, St=1 and St=10, released at the same position, close to the vortex centre at $(x0; y0) = (0.01;0)$ ..... 91

4.11 Rotation rate with respect to the radial position for the same 3 particles as in the Figure 4.9 ..... 92

4.12 On the left: distance from the vortex centre with time r(t); on the right: distance from the vortex centre (r) versus the radial velocity (dr/dt). From top to bottom: St=0,1; St=1; St=8 ..... 97

4.13 Semi-logarithmic plot of the radial displacement with respect to time (left) and logarithmic plot of the absolute values of the forces involved in the radial direction (right): the 'acceleration', the 'drag force' and the 'centrifugal force'. a) St=0.1; b) St=1; c) St=10 ..... 99

5.1 Graph presenting how the concentration profiles are calculated. On the left: particle distribution pattern. On the right: concentration profile in the radial direction. The concentration is calculated for each annular region as the number of particles per unit area ..... 100

5.2 Particle distribution (left) and concentration profile (right) for St=0.1 and T=100 ..... 110

5.3 Radial position (r) of the peak of concentration, with respect to time, for each three cases: St=0.1, St=1, St=10. Corresponds to the case of $5.10^7$ particles seeded on the disc of radius [0 4] ..... 110

5.4 Value of the concentration at the peak, with respect to time, for each three cases: St=0.1, St=1, St=10. Corresponds to the case of $5.10^7$ particles seeded on the disc of radius [0 4] ..... 111

5.5 Particle distribution (left) and concentration profile (right) for St=0.1 and T=1000 (top), and for St=1 and T=100 (bottom) ..... 113

5.6 Particle distribution (left) and concentration profile (right) for St=0.1 and T=100 (top), and for St=1 and T=10 (bottom) ..... 114

5.7 Particle distribution for St=10, at T=0, 4, 6, 8, 10, 20, 30 and 50, for 32761 particles seeded uniformly on the disc $\mathbf{r} \leq \mathbf{3}$ at T=0.. ..... 116

5.8 and 5.9 Approximate predictions of the radial position of the concentration peak and of the maximum concentration involved, when a homogeneous pattern of particles is let to settle down freely through the vortex ..... 123

6.1 Settling of particles through a pancake vortex. From top to bottom: St=0.1 (T=2500), St=1 (T=250) and St=10 (T=25). Left: snapshots of the particle distribution during the settling; right: final planar distribution at the exit of the vortex ($z = -10$) ..... 128

6.2 Concentration profiles in the radial direction, at about $z \approx -3$, for each three cases: St=0.1 (T=2500), St=1 (T=250) and St=10 (T=25) ..... 130

6.3 Concentration profiles in the radial direction, at about $z \approx -10$, for each three cases: St=0.1 (T=8000), St=1 (T=800) and St=10 (T=80) ..... 130

6.4 Radial displacement of the concentration peak that forms during settling through the pancake vortex, with respect to the elevation z, for each three cases: St=0.1, St=1 and St=10 ..... 131

6.5 Value of the concentration peak (cmax/c0) during settling, for each three cases: St=0.1, St=1 and St=10, with respect to the elevation z..... 131

6.6 Vertical profiles of the particle distribution during settling through a pancake vortex. From top to bottom: St=0.1, St=1, St=10. Left: result for a slice $|dy| \leq 0.01$. Right: profile obtained by juxtaposing the radial position of all particles located in the slide $|dy| \leq 0.1$ ..... 134

6.7 On the left: final distribution of the particles in the horizontal plane for St=10. On the right: zoom that qualitatively shows to what extent two vertical slices a) and b) taken at different angles through the distribution can lead to different results. Slices a) and b) are not equivalent (see Figure 6.9) since the initial particles distribution is not perfectly axisymmetric ..... 135

6.8 Two vertical slices taken from the same experiment (St=10, see Figure 6.8). The difference in angle is pi/8. The fact that the two slices are not equivalent reminds that the solution is not perfectly axisymmetric ..... 135

6.9 Vertical profiles for St=1, St=2, St=5 and St=10 ..... 136

6.10 Final concentration profiles (in the radial direction) after particles have settled through a pancake of thickness $\Lambda = 0.2$, for each three cases: St=0.1, St=1 and St=10 ..... 138

6.11 Same as Figure 6.11 but with a vortex thickness $\Lambda = 0.3$ ..... 138

6.12 Same as Figure 6.11 but with a vortex thickness $\Lambda = 0.4$ ..... 139

6.13 Same as Figure 6.11 but with a vortex thickness $\Lambda = 0.5$ ..... 139

7.1 Definition sketch for the othokinetic flocculation in 2D ..... 142

7.2 Profile of the absolute value of the velocity gradient in the radial direction, in the horizontal plane of symmetry of a pancake vortex ..... 144

7.3 Profiles of the particle concentration and of the collision rate in the radial direction for St=1 and T=0, 10, 50, 100, 500 and 1000 ..... 145

7.4 Evolution of the maximum of the collision rate $\frac{dN}{dt}$, in the radial direction, with respect to time, for St=0.1, St=1 and St=10 ..... 147

B.1 Absolute value of the drag term and of the Basset History term, with respect to time, in the case of a particle of Stokes number St=1, released at (x0;y0)=(0.01;0) with the local fluid velocity..... 158

# LIST OF SYMBOLS

*The following symbols are used in this thesis:*

$c(z)$ Accounts for the variation of the velocity profile in the vertical – function of the elevation $z$

$c(r,t)$ Particle concentration

$c_D$ Drag coefficient

$\delta$ Density ratio ($= \rho_f / \rho_p$)

$d$ Particle diameter

$\frac{dN}{dt}$ Rate of collision

$f_1$ Ratio between the actual steady drag force and the Stokes drag

$Fr$ Froude number

$Fr_i$ Internal Froude number

$F_{drag}$ Drag force

$g$ Gravity

$\kappa$ Viscosity ratio ($= \mu_p / \mu_f$)

$\lambda$ Thickness of the vortex (dimensional)

$\lambda_1$, $\lambda_2$ Eigenvalues of the equations of motion linearized around the vortex centre

$\Lambda$ Non-dimensional thickness of the vortex

$L$ Characteristic length scale of the vortex

$\mu$ Dynamic viscosity of the fluid (also written as $\mu_f$)

$\mu_p$ Dynamic viscosity of the material of the particle

| | |
|---|---|
| $\nu$ | Kinematic viscosity of the fluid |
| $\nu_p$ | Kinematic viscosity of the material of the particle |
| $N$ | Local buoyancy frequency of the fluid |
| $\omega_z$ | Vertical vorticity |
| $\omega_M$ | Maximum value of the vertical vorticity (dimensional) |
| $\Omega$ | Characteristic rotation rate in the horizontal plane considered |
| $P$ | Total number of particles |
| $Q$ | Flow rate used to derive the expression for the collision rate (in the study of flocculation) |
| $\rho_f$ | Fluid density |
| $\rho_p$ | Particle density |
| $r, \theta, z$ | Cylindrical coordinates of the particle (' $z = 0$ ' corresponds to the symmetry plane of the vortex) |
| $r_i, r_j$ | Radius of the i-particle, radius of the j-particle |
| $R$ | Sum of the radius of two colliding particles (in the study of flocculation) |
| $\mathrm{Re}_p$ | Particle Reynolds number |
| $\mathrm{Re}_f$ | Reynolds number of the flow |
| $St$ | Stokes number |
| $\tau_A$ | Relaxation time (or aerodynamic response time) of the particle |
| $\tau_F$ | Time associated with the fluid motion in the vortex scales |
| $\tau_S$ | Settling time of the particle |
| $T$ | Indicates a time (simulation time in general) |
| $u$ | Fluid velocity (also written as $\vec{u}$ ) |

$u_r, u_\theta, u_z$ Radial, circumferential and axial velocity components of the fluid velocity

$U$ Representative velocity of the vortex

$U_{term}$ Terminal velocity of the particle

$\vec{v}_p$ Particle velocity

$V$ Particle volume

$\vec{w}$ Relative velocity of the fluid with respect to the particle a $(= \vec{u}(\vec{x},t) - \vec{v}_p(t))$

$w$ Total height of the vortex $(= 2\lambda)$

$\vec{x}_p$ Particle position

$\Delta z$ Indicates a vertical displacement

$Z$ Complex coordinate of the particle $(= x + iy)$

## *Miscellaneous*

$A$ Non-dimensional strain parameter (in the model of a Burgers vortex)

$r_{\max}, z_{\max}$ Experimental constants of the model of the vortex velocity used by Bonnier et al. (2000)

$u = \overline{U} + u'$ Decomposition of the fluid velocity into a mean component and a fluctuating component (turbulence model)

$u = \overline{U} + U_{large-scale\ structure} + u'$ Decomposition of the fluid velocity into a mean component, a component associated with the large-scale structures, and a fluctuating component

# ACKNOWLEDGEMENTS

Doing research at the University of British Columbia has been a wonderful experience. The story started back in Paris, when Dr. Sabine Ortiz-Clerc, Professor at the École Nationale Supérieure des Techniques Avancées (ENSTA), told me about UBC and its program in Environmental Fluid Mechanics. I am very grateful to her for her encouragement, and to the Government of Canada for providing me with essential financial support during the first year of my program.

Naturally, I am much indebted to my supervisor, Dr. Gregory Lawrence, for guiding and encouraging me during my research work, especially since I chose a topic of my own interest. In addition, I would like to thank the other members of my supervisory committee, Dr. Pierre Bérubé and Dr. Susan Allen, for their helpful suggestions in the preparation of this document.

I also address special thanks to my officemates, Dr. Violeta Martin, Albert Leung and Trent Hoover, for making my student life even more enjoyable.

Finally, I gratefully acknowledge the support of a University Graduate Fellowship from the University of British Columbia.

# 1. REVIEW OF THE INFLUENCE OF VORTEX STRUCTURES ON THE DISPERSION OF PARTICLES

## 1.1 General introduction

Many turbulent flows of practical interest involve the dispersion of particles, drops and bubbles. Applications range from power production to pollution control. As it has been shown in recent years, the particle dispersion is highly influenced by the large-scale coherent structures of the flow, and namely by vortical flow structures. As Hunt (1991) reports in his review of industrial and environmental flows, vortices are sometimes generated in flows where they do not usually exist, in order to enhance mass and heat transfer [as in the Oxford dialysis machine, where channels have undulating walls to generate recirculating flows]. In a patented process (ALCAN International Ltd. 1988), vortices are generated by baffle plates in the turbulent flow along a channel of liquid aluminium containing small particles; these vortices capture the particles as they travel over the baffles and then deposit them farther down the channel, holding them in suspension for longer than they would be otherwise.

The vortical structures that are present in free shear flows such as mixing layers, jets and wakes have received wide attention. These vortices (especially the primary quasi two-dimensional vortices) are real actors in the dispersion process. In recent years, progress has been made in enlarging the two-dimensional study to a more complete and realistic three-dimensional view, partly thanks to advances in computational capabilities. Also, some recent studies have included the effect of the particles themselves on the flow (on the stability of the flow in particular). This 'two-way coupling' becomes relevant when the particle concentration is high enough for interaction to occur. Even when the two-way coupling is taken into account, studies usually stick to a sufficiently dilute particulate phase, for which collisions between particles do not need to be

integrated. The studies to be mentioned in this review are essentially two-dimensional, though, they do not include the feedback of the particles on the flow, and they mainly consider the dispersion of heavy particles.

The usual way to approach such problems is first to choose and model a vortical flow, or to numerically generate such a flow. Then, the particle dynamics is integrated. The Maxey-Riley (1983) equation has been used extensively to describe the particle dynamics, but one has to be aware of the assumptions used to derive the Maxey-Riley equation. In fact, most of the studies have used simplified versions of this equation by only considering bubbles or heavy particles. The ratio of the fluid density to the particle density is indeed an important parameter, as well as the Stokes number, which is the ratio of the aerodynamic response time of the particle to the characteristic flow time scale, and the Froude number, when gravity is included. Experimental, numerical and analytical work has enabled some insight into the dispersion process occurring in different types of flows -in free shear flows in particular- and into the role played by the non-dimensional parameters just mentioned.

## 1.2 Basic definitions

### 1.2.1 Particle

The term 'particle' will refer to a self-contained body, with maximum dimension ranging from $0.1\mu m$ to $10cm$, separated from the surrounding medium by a recognizable interface. It has to be distinguished from the term 'particle' as used by the nuclear physicist.

The particle can either be in the solid, liquid or gaseous phase. We might refer to the particle as a rigid sphere, a drop or a bubble, correspondingly. The term 'fluid particles' refers to both drops

and bubbles. A particle is said to be heavy if its density is larger than the density of the surrounding fluid. The particles considered will be **heavy particles, unless stated otherwise.** Moreover, it will be assumed that the particles considered are rigid, have a spherical shape, and that they are passive (i.e. passively transported by the flow).

### 1.2.2 Vortex

- Vorticity

The vorticity field $\vec{\omega}$ of a flow with velocity distribution $\vec{u}$ is the curl of the velocity distribution: $\vec{\omega} = \vec{\nabla} \times \vec{u}$ . Vorticity is a local measure of how fast the fluid elements rotate about themselves.

$\vec{\omega}$ is a vector, each component having the dimension of a frequency. In the case of two-dimensional flows which are confined to a horizontal plane ($u_z = 0$), the vorticity vector only has one non-zero component $\omega_z$ in the direction perpendicular to that plane.

A very specific example is now examined in order to apply the concept of vorticity: that of a body of fluid in solid body rotation $u_\theta(r,\theta,z) = \Omega r$ (e.g. a cup of coffee centred on a turntable and gradually spun up to speed). In this case, the vorticity everywhere is a constant (equal to twice the angular velocity of each infinitesimal fluid element about the centre of the turntable). Indeed, each particle rotates about its own axis at the same angular velocity as it rotates around the centre of the turntable.

Note that the fact that a fluid is rotating at a large scale does not necessary imply that the vorticity is locally non-zero, and that even if the streamlines of a flow are not curved, the flow itself may be rotational.

- Vortex

There is not a definition on which everybody agrees, but it is generally admitted that a fluid vortex should be a region of concentrated vorticity. It should be pointed out that this definition does not cover all cases.

Organized vortex structures are systematically produced in free shear flows (Figure 1.1). In a mixing layer, where two fluids having a different mean velocity are in contact, instabilities develop and lead to the formation of vortices. A vortex pairing phenomena is observed. A different phenomenon is observed in the wake of a bluff body. Vortices of opposite sign form on each side of the body and move downstream in a regular organized pattern (they do not pair).

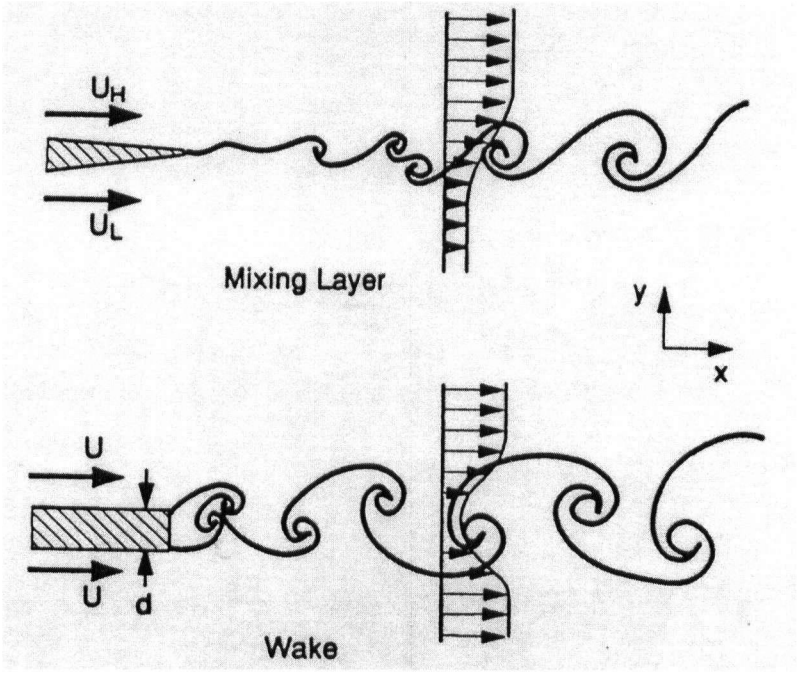


**Figure 1.1** Drawings representing vortices developing in a mixing layer and in the wake of a bluff-body (Crowe et al. 1995)

Even at the small scale, the turbulent flow may consist of small recognizable vortices, which interact, grow and dissipate. Some conceptual models even say that turbulence is in fact a collection of vortices. On the other hand, vortices are also observed at the large scale of geophysical flows. For instance, in the ocean, vortices named meddies originate from the Mediterranean Sea and travel west, transporting unusually high amount of salt into the Atlantic (Armi et al. 1989). Moreover, many Karman vortex streets have been observed in the atmosphere in the wake of islands. Figure 1.2 shows a street of cloud vortices in the wake of Selkirk Island, Chile (a 33 square mile island that rises over a mile above sea-level).

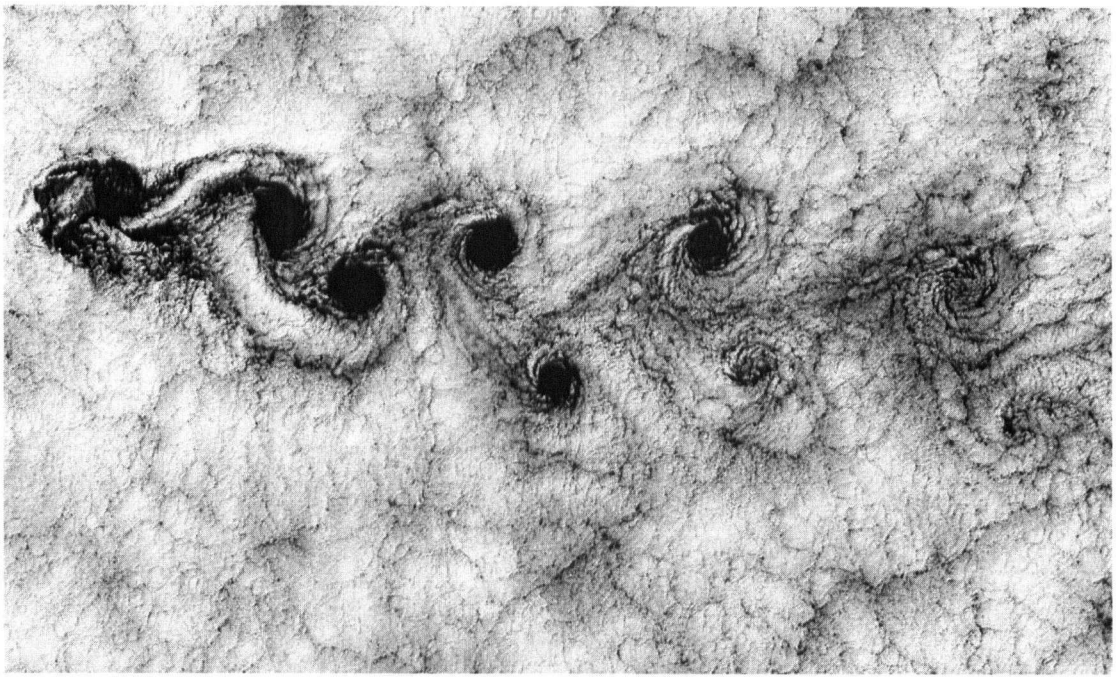

**Figure 1.2** Cloud vortices observed in the wake of Selkirk Island (left), Chile, by Landsat 7, September 1999 (photograph courtesy NASA).

### 1.2.3 Dispersion and its traditional approach

The term 'dispersion' refers to the mixing, spreading and transport of the particles (Figure 1.3).

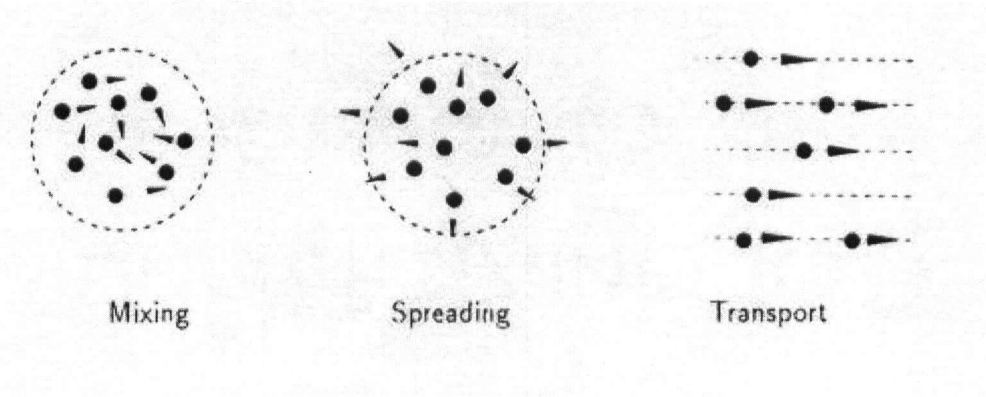


**Figure 1.3** Drawing representing the concepts of mixing, spreading and transport, associated with the concept of dispersion (Crowe et al. 1993).

The traditional approach

Turbulence is usually considered as the key mechanism responsible for the mixing and spreading of particles in a fluid flow. Turbulence is decomposed into a mean velocity and a superimposed fluctuation component:

$$u = \overline{U} + u'$$

The fluctuating component $u'$ is usually approximated by a random process, and assumed isotropic. The particle dispersion is then treated as a diffusion process. The problem then centres on finding a suitable dispersion coefficient to use in the equations of motion.

A popular method for including particle dispersion in a numerical model is the Monte Carlo approach. In this approach, a local velocity fluctuation is selected randomly for each particle. The velocity experienced by the particle is the sum of the mean velocity and the fluctuation velocity.

This approach is far from being satisfying when organized structures are involved because the effect of those structures are ignored, even though they play an important role in the particle dispersion process.

The velocity field: $u = \overline{U} + u'$

should be substituted by: $u = \overline{U} + U_{large-scale\ structures} + u'$

where the effect of the large scale structures on the particle dispersion is important.

## 1.3 Model based on the Stokes number

The importance of large scale organized vortex structures as the controlling mechanism in the dispersion process has been demonstrated by numerous numerical and experimental investigations, making it clear that the traditional approach of treating particle dispersion as a diffusion process has little relevance for flows exhibiting these structures.

Crowe et al. (1985) investigated turbulent free shear flows and analyzed the influence of the large-scale structures on the dispersion of the particulate phase. Their two-dimensional vortex dynamics simulations of a turbulent mixing layer demonstrated the tendency of very small particles to closely follow the fluid elements, as the dominant Stokes drag force dictates their dynamics. Very heavy particles, on the other hand, were barely affected by the forces exerted upon them by the fluid, due to their large inertia. However, they observed that intermediate size particles were ejected into the free stream and were strongly dispersed, sometimes more than the fluid particles themselves. This mechanism was observed to be most effective when the aerodynamic response time of the particles was of the same magnitude as the characteristic flow time associated with the vortical structures. Chung and Troutt (1988) demonstrated the same effects in axisymetric jets, while Chein and Chung (1987) observed that vortex pairing events result in even higher lateral dispersion rates.

Crowe et al. (1985) developed a conceptual model of particle dispersion that accounts for entrainment by the vortices and the centrifugal effect in the rotating vortices based on the Stokes number (St). They defined the Stokes number as the ratio of the relaxation time $\tau_A$ to the time associated with the fluid motion in the vortex $\tau_F$:

$$St = \frac{\tau_A}{\tau_F} \tag{1.1}$$

The relaxation time, also known as the aerodynamic response time, is defined as:

$$\tau_A = \frac{\rho_p d^2}{18\mu} \tag{1.2}$$

where $\rho_p$ is the material density of the particles, $d$ is the particle diameter and $\mu$ is the dynamic viscosity of the fluid. It expresses the time it takes the particle to respond to unsteady forcing by fluctuating fluid velocities. More specifically, this is the time it would take for a particle released from rest in a flow to achieve 63% of the free stream velocity, assuming Stokes' drag law is applicable.

The time associated with the fluid motion is:

$$\tau_F = \frac{L}{U} \tag{1.3}$$

where $L$ is the characteristic length scale of the vortex and $U$ a representative velocity. The Stokes number is therefore expressed as:

$$St = \frac{\tau_A}{\tau_F} = \frac{\rho_p d^2 U}{18\mu L}. \tag{1.4}$$

The Stokes number measures the responsiveness of the particles to the flow. This simple conceptual model predicts that small particles (St<<1) essentially track the fluid flow and therefore spread and mix as the fluid elements. Larger particles (St~1) are entrapped by the vortices and centrifuged beyond the vortex, effecting a spreading rate exceeding that of the fluid particles. Even larger particles will pass through the vortex structures with little change in their

trajectory, due to their large inertial resistance to changes in the flow. In other words, the degree of dispersion depends on the Stokes number. An illustration is provided by Figure 1.4.

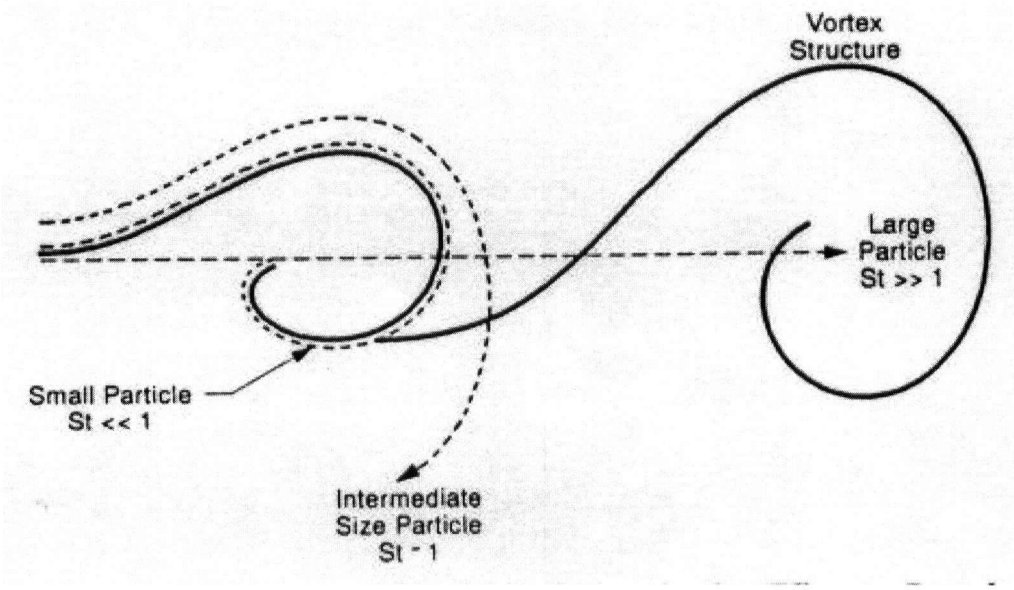


**Figure 1.4** Model based on the Stokes number (Crowe, Gore and Troutt 1985)

## 1.4 Review of experimental and numerical work – focus on heavy particles

Both numerical and experimental studies have verified the appropriateness of the Stokes number as the scaling factor for particle dispersion in large-scale structures.

Several shear flow configurations have been studied experimentally: mixing layers (Kamalu et al. 1989; Lazaro & Lasheras 1989, 1992; Wen 1990; Kiger & Lasheras 1995), plane wakes (Yang 1993) and axisymetric jets (Longmire & Eaton 1992; Hardalupas et al. 1989). Those experiments mainly focused on the dispersion of heavy particles whose density is large compared to the fluid density. Under these conditions, the dynamics of heavy particles is dominated by the drag force and is therefore easier to analyze. All the experimental investigations agree on the fact that:

- large scale vortices play a prominent role on the dispersion of particles
- particles characterized by an intermediate Stokes number are preferably dispersed
- highly non-homogeneous and strongly response time dependent dispersion patterns could result from the action of the vortices.

These results were confirmed by numerical experiments. The cases of a wake and of a mixing layer are now considered as an illustration.

### 1.4.1 In wakes: demixing, focusing

Photographs of a bluff body wake flow (Figure 1.5) clearly illustrate the high degree of non-homogeneity in particle distribution when the Stokes number is intermediate (Figure 1.5 b). Particles are indeed focused into thin regions, and do not disperse homogeneously, contrary to what is intuitively expected when dealing with turbulent flows. The comparison between Figure a) and Figure b) shows that particles of intermediate Stokes number tend to migrate away from the centre of the vortex structures, whereas particles of small Stokes number are dispersed throughout the vortex structures.

The focusing effect was confirmed by mathematical calculations which demonstrated that for a Stokes number close to one, there is a one-dimensional attractor in the dynamical system governing the particle motion (Burns, Davis & Moore 1999).

a)

b)

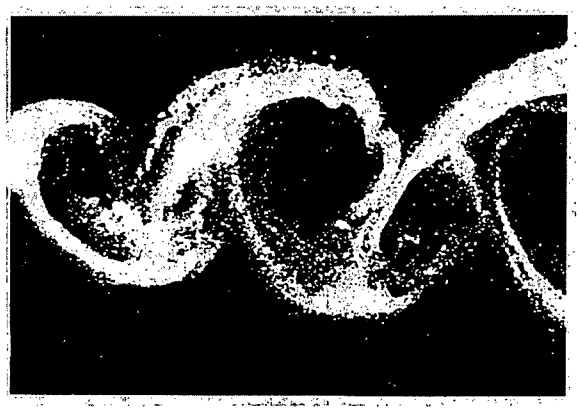

**Figure 1.5** Photographic results for a bluff body wake flow containing particles with a) very small Stokes numbers and b) intermediate Stokes numbers (Yang 1993)

Numerical simulations of the particle dispersion in a plane wake downstream of a thick plate (Figure 1.6) are in agreement with the experimental results. Again, the patterns obtained are closely correlated with the Stokes number. The focusing that occurs with particles of intermediate Stokes number is quite significant. The conventional wisdom concerning the utility of the wake flow as a mixing process is therefore, under certain conditions, incorrect.

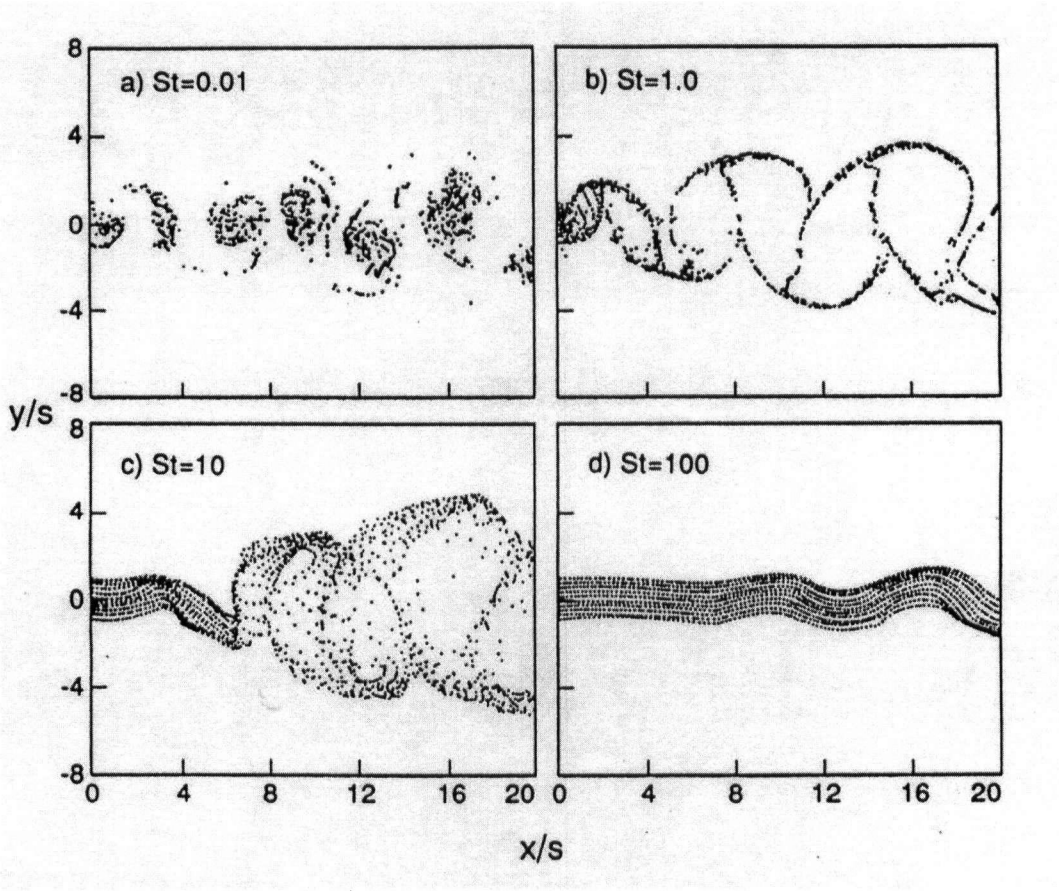


**Figure 1.6** Numerical simulations of the particle dispersion in a wake flow: a) St=0.01, b) St=1.0, c) St=10, d) St=100 (Tang et al. 1992)

### 1.4.2 In mixing layers: formation of large scale particle streaks between successive vortices

In mixing layers, both numerical simulations and flow visualization experiments demonstrate the ejection of heavy particles from the vortex centres and the formation of large-scale particle streaks in the braid regions between successive vortices (Longmire & Eaton 1992, Wen et al. 1992).

In Figure 1.7, uniform size particles (St=0.1, 1, 10, 50) are released at a constant rate into a simulated plane mixing layer. Particles with a Stokes number in the order of one are centrifuged to the boundaries of the vortex structures, yielding the larger spread.

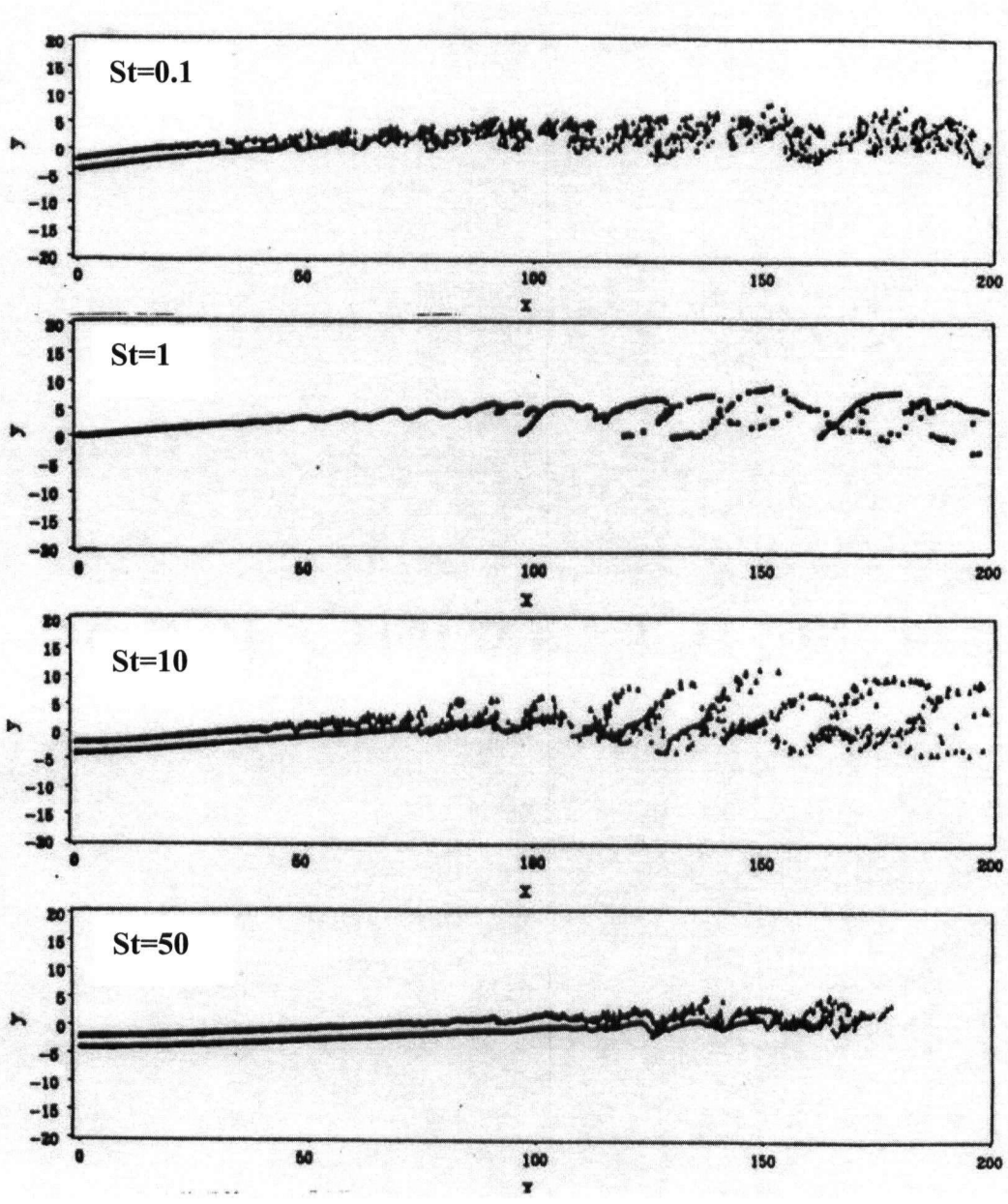


**Figure 1.7** Particle dispersion in a simulated plane mixing layer (Chein and Chung 1988)

The particle streaks between the vortices are closely aligned with the extensional direction of the stagnation point flow field (Martin & Meiburg 1994) and dominate the dispersion process. Using an idealization of the spatially periodic mixing layer as a row of point vortices, it was demonstrated that the formation of these concentrated particle streaks proceeded with maximum efficiency for a Stokes number close to one, in agreement with experimental and numerical observations of preferential particle dispersion at Stokes number of order unity.

Since the braid region was shown to be so important for the particle dispersion process, Marcu & Meiburg (1996) analyzed the effects of the concentrated and strained counter-rotating streamwise vortices that are known to form in that region (Corcos & Lin 1984), to gain some insight on the role played by those three-dimensional secondary vortex structures. The flow field was modeled by two superimposed rows of Stuart vortices of opposite sign, with an additional two-dimensional strain field corresponding to the extensional strain field created by the evolving spanwise Kelvin-Helmholtz vortices. Equilibrium points for the particles, as well as their stability criteria, were determined analytically, both in the absence and in the presence of gravity.

In addition, two specific mechanisms were identified: the stretching and folding of the particle streaks (Wen et al. 1992). The stretching is associated with the regions of high velocity gradients (i.e. high shear) on the boundaries of adjacent vortex structures, where particles concentrate. The folding is associated with the pairing of adjacent large-scale vortices (Figure 1.8).

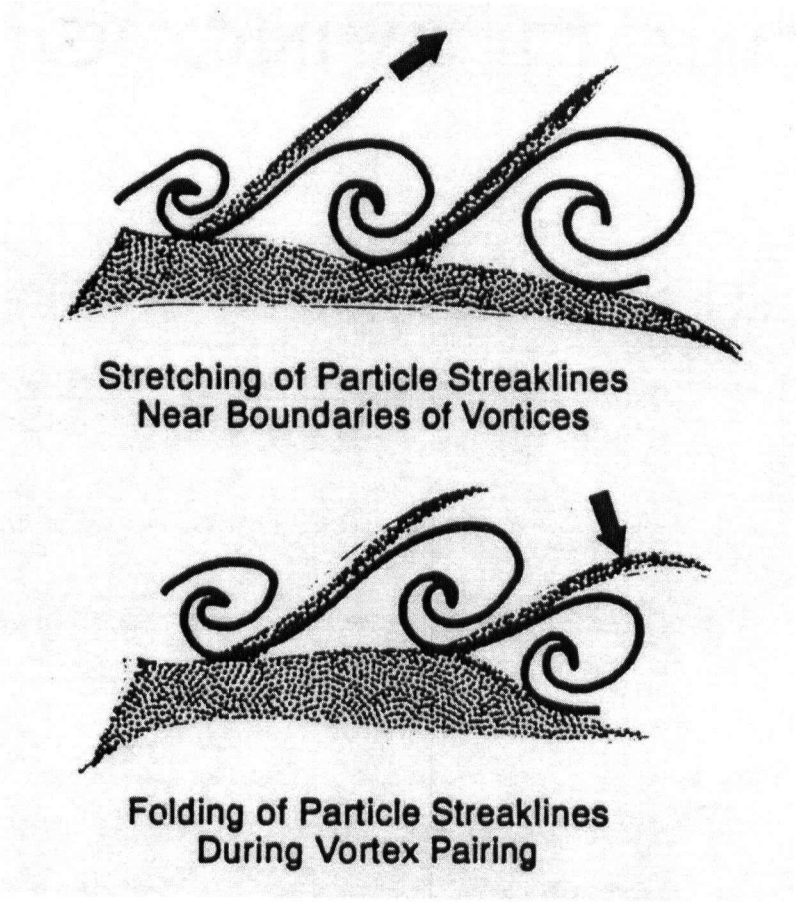


**Figure 1.8** Stretching and folding of the large scale particle streaks forming in between successive vortices of a mixing layer (Wen et al. 1992)

### 1.4.3 Summary

Experimental and numerical investigations with heavy particles agree on the facts that:

1- Large scale organized vortex structures are a controlling mechanism in the dispersion process

2- The particle dispersion patterns produced by the vortices may be highly non-homogeneous and strongly dependent on the Stokes number

3- The particles that are the most likely to be concentrated near the outer edges of the vortex structures are those of intermediate or relatively large size (i.e. lateral particle dispersion is maximum for an intermediate particle Stokes number).

Note:

It is often said that particle dispersion is maximized for an intermediate Stokes number, conveying the idea that the particle phase is optimally dispersed throughout a region. However, as discussed above, in the wake of a bluff body, particles of intermediate Stokes number tend to focus on lines at the edge of the vortices. Therefore, it is more appropriate to think in terms of 'lateral dispersion' rather than in terms of 'optimal dispersion'.

Indeed, particles with a small Stokes number mix and spread as the fluid particles, whereas those with an intermediate Stokes number are ejected and those with an even larger Stokes number are barely affected and therefore not laterally dispersed.

## 1.5 Analysis of the motion of individual particles in idealized representations of the flow field

Several studies analysed the motion of individual particles in idealized representations of the flow field. A few examples are provided here.

- Noting that the global features of bubble and particle dispersion were dominated by their dynamics in three distinctly different regions of the flow field: the viscously dominated vortex core, the outer region of the vortices and the stagnation zones, Raju & Meiburg (1997) considered idealized representations of these flow regions (in order: a solid body vortex: $(u_\theta = \frac{r}{2};\ u_r = 0)$, a point vortex: $(u_\theta = \frac{1}{2r};\ u_r = 0)$, and a stagnation point zone ($u_x = y$, $u_y = x$)). This study provided the basis for the present research project. The particle dynamics was integrated via the Maxey-Riley equation, across the entire spectrum of density ratios, from light to heavy particles, and history effects were neglected. The governing fourth order system obtained was reduced to two second-order equations for all three model flows. The two governing parameters were the Stokes number and the density ratio. These simplifications enabled the authors to make analytical progress in terms of the quantification of ejection/entrapment trends and accumulation behaviour. For a solid body vortex, an optimal ejection or entrapment was found to occur for intermediate values of the Stokes number, as the difference between the inward and outward forces reaches a maximum. This optimal Stokes number is a function of the density ratio (but hasn't been expressed analytically). For a point vortex flow, up to three different regimes, corresponding to three different force balances, were found. Optimal accumulation was observed for intermediate Stokes number. In the stagnation point flow, a criterion for optimal accumulation was found in the case of heavy particles, but light particles did not exhibit optimal behaviour.

- Rows of Stuart vortices have been used as a representation of mixing layer vortices (Gañán-Calvo and Lasheras 1991, Tio et al. 1993a and 1993b) and a non-linear dynamical systems approach was applied in studying the behaviour of the particle. The authors observed that if gravity was moderate, the particles could stay suspended above or below the mixing layer, in which case trajectories were periodic, quasi-periodic or chaotic. On the other hand, when gravity was dominant, sedimentation occurred.

- As mentioned earlier, two superimposed rows of Stuart vortices of opposite sign were used to model the counter-rotating streamwise vortices present in the braid regions between vortices (Marcu & Meiburg 1996).

Note: Stuart vortices are a particular flow model based on the solution to the steady two-dimensional Euler equations. They describe a periodic flow of liked-signed vortices. The dimensionless streamfunction of the Stuart vortices is:

$$\Psi = \frac{1}{4\pi}\ln[\cosh(2\pi(y-y_0)) - k\cos(2\pi(z-z_0))] \qquad \textbf{(1.5)}$$

where $(z_0, y_0)$ denotes the location of a vortex centre. The parameter $k$ determines the degree to which the vorticity is concentrated in the vortex cores. For $k = 1$, the flow is that induced by a row of corotating point vortices, while for $k = 0$ we have a uniform shear layer with a tanh velocity profile.

- The dynamics of heavy particles in Burgers vortices was also addressed (Marcu, Meiburg & Newton 1995). It provided some useful information regarding two-phase turbulence. Indeed, Burgers vortex-like structures are prominent in the small scales of turbulence. The flow field of a Burgers vortex was modeled as:

$$\begin{cases} u_z = 2Az \\ u_r = -Ar \\ u_\theta = \dfrac{1}{2\pi r}[1-\exp(-\dfrac{r^2}{2})] \end{cases} \quad \textbf{(1.6)}$$

where $u_z$, $u_r$ and $u_\theta$ are the axial, radial and circumferential velocity components, respectively, r the distance from the vortex centre, and A the non-dimensional strain parameter (1/A is also known as the vortex Reynolds number).

In the absence of gravity, the vortex centre is a stable equilibrium point for particles up to a critical value of the Stokes number:

$$St^* = 16\pi^2 A$$

as the inward drag force created by the radially inward fluid motion overcomes the destabilizing centrifugal force. For Stokes number exceeding the critical value, particles asymptotically approach closed circular orbits. When gravity is considered, the centre is not an equilibrium point anymore, but the location of one or three other equilibrium points is calculated and their stability is determined.

Although the most complete quantitative data will always be provided by direct numerical simulations and experimental measurements, the analysis of simplified flow models enables investigation into the interaction of several important mechanisms in isolation. As such, it potentially contributes to the understanding and ultimately the modeling of such data. In the present study, a simplified flow model of a pancake vortex is considered. The dispersion of particles in pancake vortices has not been studied yet, as far as the author knows.

## 1.6 The case of light particles

Fewer studies have focused on the dispersion of light particles, such as bubbles, in vortical flows. In particular, numerical simulation of bubble motion is difficult because of the sensitivity of the bubble acceleration to the flow acceleration, and because of the need to include the effect of pressure and Reynolds number on the bubble size and shape. Anyhow, it is well known that, contrary to heavy particles, light particles tend to migrate towards the vortex centres. The Maxey-Riley equation (Equation 2.13) taken in the limit of vanishing small density ratio shows indeed that the acceleration of the bubbles is centripetal. Stuart's calculations (1967) also demonstrated that bubbles migrate towards the vortex centre, when a Stuart's vortex is considered.

# 2 RESEARCH OBJECTIVES AND THE CORRESPONDING EQUATIONS OF PARTICLE MOTION

## 2.1 Research objectives

### 2.1.1 About pancake-like vortices

The horizontal extent of pancake vortices is large compared to their vertical extent. They are observed in stratified fluids like oceanic and atmospheric flows, where vertical motions tend to be inhibited. Mesoscale atmospheric vortices can be generated by horizontal shear of the horizontal wind – for instance when flow passes terrain obstacles such as mountains and islands while the vertical ascent over the obstacle is inhibited by a stable atmospheric stratification. Pancake vortices are also observed in many laboratory experiments that investigate the decaying turbulence generated by moving rakes, grids or bluff bodies in a stratified fluid.

A quantity called the internal Froude number, defined as $Fr_i = \frac{U}{LN}$, is generally introduced to estimate whether the milieu is stratified enough to enable such vortices to form. $L$ is the characteristic length scale of the vortex, $U$ a representative velocity, and $N$ the local buoyancy frequency of the fluid. $N$ is related to the density gradient $\frac{d\rho_f}{dz}$ as:

$$N^2(z) = -(\frac{g}{\rho_f})\frac{d\rho_f}{dz}.$$

Where $g$ stands for the gravity intensity, $\rho_f$ for the fluid density, z for the vertical coordinate. The lower the internal Froude number is, the stronger the stratification is.

When they interact with each other, pancake vortices generally increase in size and decrease in number. Their emergence in stratified flows has some analogies with the self-organizing process observed in purely two-dimensional flows (McWilliams 1984). Still, coherent vortices in stratified flows do have a three dimensional structure and a certain thickness. Shearing forces generated by the viscosity diffuses the vorticity. The thickness of pancake-like vortices increases in time, corresponding to a decrease of strength due to vertical diffusion of momentum.

### 2.1.2 General objectives – methodology

The objective of the present study is to characterize the dispersion of particles (mainly heavy particles) in a quasi-two-dimensional axisymetric pancake-like vortex. Contrary to most studies, there is no mean flow in addition to the flow generated by the vortex: the action of the vortex alone is considered. Under this circumstance, scenarios where particles with a large Stokes number are entrained by the mean flow while being barely affected by the vortex are not possible.

For the purpose of the study, an idealized representation of the velocity field of an isolated pancake-like vortex will be considered. Then, the particle dynamics will be integrated into it via the Maxey-Riley equation, the generic equation of motion. The equations of motion for the problem will thus be derived, the assumptions will be presented, and the neglect of some effects justified (Chapter 2). Turbulence and its effects will not be included.

In the first place, some well known scenarios will be reproduced, showing in particular the influence of the density ratio and of the Stokes number on individual particles (Chapter 3). Then the particle dynamics will be explored further, by first studying the dynamics in the horizontal plane (Chapters 4 and 5). This approach assumes that the particle motion in the vertical is decoupled from its horizontal motion. The relevance of this approach will be discussed, and

numerical results will be presented. Chapter 4 focuses on the motion of individual particles, whereas Chapter 5 addresses the case where the flow is initially loaded homogeneously with a large number of particles (of uniform size). The time evolution of the concentration profiles in the horizontal is examined, revealing some interesting features. Then, the vertical motion will be fully integrated in the study (Chapter 6). As the particles settle, their distribution in the horizontal is modified by the presence of the vortex. The concentration profiles obtained as a result of the settling through the vortex are examined.

A semi-analytical approach

Insight into the dynamics of particles has been gained in the past by analyzing the motion of individual particles in idealized representations of the flow field (see section 1.5). The same approach is applied here.

The advantage of considering an idealized representation of the flow field instead of simulating a realistic (and therefore non-analytical) flow field is that not only can the forces acting on the particle be approximated in the equation of motion, but that these forces can be expressed analytically. Because the flow field is not an unknown anymore, the equations of motion depend only on the particle position and velocity and on some key governing parameters. These simplifications enable analytical progress in the quantification of ejection/entrapment trends for instance, and facilitate the evaluation of the different forces involved.

## 2.2 Analytical model of the vortex flow field

### 2.2.1 Analytical model of the velocity profile

For the purpose of this study, a steady quasi-two-dimensional axisymetric pancake-like vortex is considered. A cylindrical coordinate system is introduced for a convenient analysis of the flow: $r$ is the radial coordinate, $\theta$ is the azimuthal and $z$ the vertical upward coordinate. '$z = 0$' corresponds to the symmetry plane of the vortex. The velocity distribution inside the vortex is modeled as follows (Beckers et al. 2001).:

$$\begin{cases} u_\theta(r,z) = \frac{r}{2}\exp(-r^2)\exp(-\frac{z^2}{2\Lambda^2}) & \textbf{(2.1)} \\ u_r = u_z = 0 & \textbf{(2.2)} \end{cases}$$

$\Lambda$ is a non-dimensional constant called the thickness of the vortex. Its value is determined experimentally by taking some measures of the vertical profile of the velocity field.

In the 2D study of particle motion in the horizontal plane of a pancake vortex, Equation 2.1 can be simplified to:

$$u_\theta(r,z) = c\frac{r}{2}\exp(-r^2) \qquad \textbf{(2.3)}$$

with $$c(z) = \exp(-\frac{z^2}{2\Lambda^2}). \qquad \textbf{(2.4)}$$

Note that we'll write $c(z) = c$ for convenience. In the two-dimensional study, c will be taken as the constant 1. Figure 2.1 shows the velocity and vorticity profiles associated with the vortex.

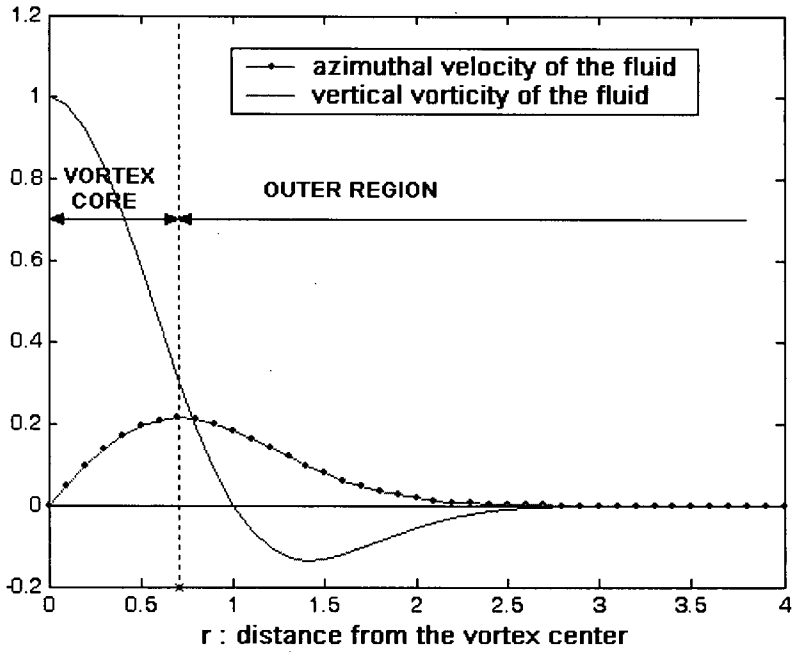


**Figure 2.1** Idealized velocity and vorticity profiles of an isolated pancake-like vortex, in its 2D horizontal plane of symmetry (the velocity and vorticity, usually expressed in the S.I. units, are presented in their non-dimensional form here).

The velocity profile was derived from experimental observations (Beckers et al. 2001). For illustration, Figure 2.2 shows the result of a particle tracking experiment carried out in an isolated pancake like-vortex. The trend of the velocity profile observed (an initial increase in the azimuthal velocity with distance from the vortex centre, followed by a decrease) is in agreement with the model.

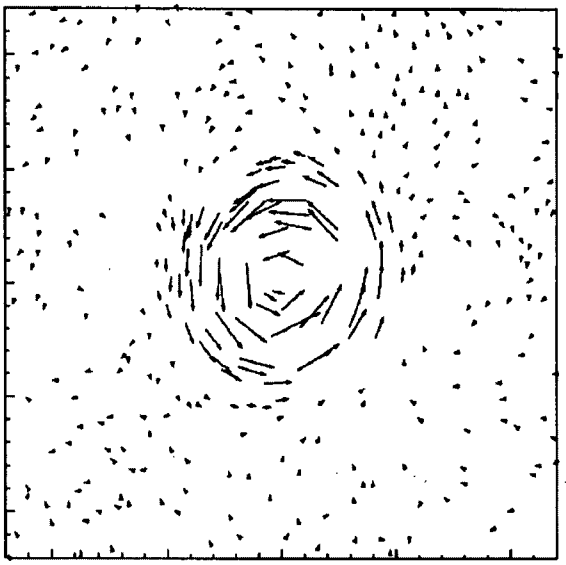

**Figure 2.2** Velocity field found by following tracer particles in time (Beckers et al. 2001)

### 2.2.2 Note on the non-dimensionalization

All the variables have been non-dimensionalized in the model for the velocity field (Equations 2.1 and 2.2). The distances $r$ and $z$ have been non-dimensionalized by the characteristic length scale $L$, defined by the radial position in the vortex plane where the vorticity changes sign. Beckers et al. (2001) estimated $L$ from experimental cross-sections. As for the velocity scale, it is estimated by:

$$U = L\omega_M \qquad \textbf{(2.5)}$$

$\lambda = L\Lambda$ is the (dimensional) experimentally observed thickness of the vortex and $\omega_M$ the (dimensional) maximum value of the vertical vorticity.

### 2.2.3 Details of the derivation of the idealized velocity field

The velocity profile of the pancake vortex was derived from experimental observations by Beckers et al. (2001). They in fact modeled the time evolution of the velocity field as well, but that aspect will not be considered in the present study. Many observers reported cases of pancake vortices that were surprisingly robust in geophysical environments (McWilliams 1985, Armi et al. 1989).

To derive this expression, Beckers et al. first assumed a zero vertical velocity. This is a relevant first order approximation since the motion in strongly stratified flows is quasi-two-dimensional. They also assumed axisymmetry ($\frac{\partial}{\partial\theta}=0$) and incompressibility of the flow ($\vec{\nabla}.\vec{u}=0$), implying the absence of a radial fluid motion ($u_r=0$). Using the method of separation of variables, they wrote:

$$u_\theta(r,z)=G(r)H(z). \tag{2.6}$$

Their experimental observations suggested that the radial distribution of the vertical vorticity fitted well with the $\alpha-$profile, introduced by Carton et al. (1989):

$$\omega_z(r)=(1-\frac{1}{2}\alpha r^\alpha)\exp(-r^\alpha) \tag{2.7}$$

with the specific value $\alpha=2$:

$$\omega_z(r)=(1-r^2)\exp(-r^2). \tag{2.8}$$

This distribution corresponds to a vortex core of positive vorticity surrounded by a ring of negative vorticity (see Figure 2.1). Experiments also showed that the distribution of the planar flow field in the vertical direction was Gaussian in shape. This type of distribution arises naturally when diffusion acts on a layer with initially zero thickness. Given those experimental observations, Beckers et al. opted for:

$$G(r) = \frac{r}{2}\exp(-r^2) \tag{2.9}$$

$$H(z) = \frac{1}{\sqrt{2\pi\Lambda^2}}\exp(-\frac{z^2}{2\Lambda^2}) \tag{2.10}$$

which leads to the expression of the azimuthal velocity proposed earlier, except that the constant $(\sqrt{2\pi\Lambda^2})^{-1}$ used to normalize the Gaussian distribution is dropped in our model (Equation 2.3). This constant accounts for the fact that, for a given vortex that one follows in time, the thicker the weaker (i.e. the larger $\Lambda$ is, the smaller the velocity involved is). This constant is dropped given that the evolution of the vortex with time won't be considered, and that it is more intuitive to have the velocity in the horizontal plane independent on $\Lambda$ (i.e. the thickness of the vortex). This way, the characteristic velocity is completely independent of the thickness $\Lambda$ of the vortex, and corresponds to the actual typical velocity (which makes more sense physically).

The expression for the velocity field is very similar to the one used by Bonnier et al. (2000) to interpret the density profiles they obtained inside the vortices present in the far wake of a sphere towed through a stratified fluid:

$$u_\theta = U\frac{r}{r_{max}}\exp(\frac{1}{2}(1-\frac{r^2}{r_{max}^2}-\frac{z^2}{z_{max}^2})), \tag{2.11}$$

where $U$ , $r_{max}$ and $z_{max}$ were determined experimentally.

## 2.3 Assumptions that simplify the dynamics

In order to evaluate the forces acting on the particles, we will assume that:

- the particles have a spherical shape
- particle-particle interactions, as well as the action of the particles on the flow itself, are negligible (dilute regime assumption); if the particle concentration was high, a multi-phase flow system approach would be necessary.

The only forces considered are:

- the forces from the fluid-particle interactions
- the gravity effect (or buoyancy force)

Therefore, this study considers the one-way coupling from the fluid to the particle as the prevailing actor of the dispersion.

## 2.4 The Maxey-Riley equation

### 2.4.1 Presentation of the equation

Under the assumptions presented in section 2.3, the dynamics of the particle is governed by the Maxey-Riley equation (1983), the general form of which is presented in this section:

| **Particle Acceleration** | = | **Stokes drag** | + | **buoyancy force** | + | **pressure gradient force** | + | **virtual mass** | + | **Basset history term** |
|---|---|---|---|---|---|---|---|---|---|---|

Assuming that the particle diameter is small compared to the flow scale, the Faxen correction terms can be neglected (indeed, a small particle diameter implies that the velocity curvature has

negligible effect on the calculation of the drag force on the sphere at low particle Reynolds number, which is what the Faxen correction terms stand for).

Neglecting the Faxen correction terms, the different terms of the equations are:

- **Particle acceleration term:** $V\rho_p \frac{d\vec{v}_p}{dt}$

- **Stokes drag:** $3\pi d\mu\left[\vec{u}(\vec{x},t) - \vec{v}_p(t)\right]_{\vec{x}=\vec{x}_p(t)}$

- **Buoyancy force:** $V(\rho_p - \rho_f)\vec{g}$

- **Pressure gradient term:** $V\rho_f\left[\frac{D\vec{u}}{Dt}\right]_{\vec{x}=\vec{x}_p(t)}$

- **Virtual mass:** $\frac{1}{2}V\rho_f \frac{d}{dt}\left[\vec{u}(\vec{x},t) - \vec{v}_p(t)\right]_{\vec{x}=\vec{x}_p(t)}$

  **(or added mass effect)**

- **Basset history term:** $-\frac{3}{2}\pi d^2\mu\int_0^t \left\{\frac{d/d\tau\left[\vec{v}_p(\tau) - \vec{u}(\vec{x},\tau)\right]_{\vec{x}=\vec{x}_p(t)}}{\left[\pi\mu(t-\tau)\nu\right]^{\frac{1}{2}}}\right\}d\tau$

$\vec{v}_p$ is the particle velocity, $V$ its volume, $d$ its diameter and $\rho_p$ its density, whereas $\vec{u}$, $\rho_f$ and $\mu$ are the velocity, density and dynamical viscosity of the fluid respectively.

The equation reads:

$$\frac{d\vec{v}_p}{dt}=\frac{3\pi d\,\mu}{V\rho_p}[\vec{w}(\vec{x},t)]+(1-\frac{\rho_f}{\rho_p})\vec{g}+\frac{\rho_f}{\rho_p}\left[\frac{D\vec{u}}{Dt}\right]+\frac{1}{2}\frac{\rho_f}{\rho_p}\frac{d}{dt}[\vec{w}(\vec{x},t)]-\frac{3\pi d^2\mu}{2V\rho_p}\int_0^t\left\{\frac{d/d\tau[-\vec{w}(\vec{x},t)]}{[\pi\mu(t-\tau)\nu]^{\frac{1}{2}}}\right\}d\tau$$

| **Particle Acc.** | **Stokes drag** | **buoyancy force** | **pressure gradient force** | **virtual mass** | **Basset history term** |
|---|---|---|---|---|---|

**(2.12)**

or, in non-dimensional form:

$$\frac{d\vec{v}_p}{dt}=\frac{1}{St}[\vec{w}(\vec{x},t)]-\frac{(1-\delta)}{Fr^2}\vec{e}_z+\delta\left[\frac{D\vec{u}}{Dt}\right]+\frac{\delta}{2}\frac{d}{dt}[\vec{w}(\vec{x},t)]-9\delta(\frac{\nu}{Ud})\int_0^t\left\{\frac{d/d\tau[-\vec{w}(\vec{x},\tau)]}{[\pi\mu(t-\tau)\nu]^{\frac{1}{2}}}\right\}d\tau$$

| **Particle Acc.** | **Stokes drag** | **buoyancy force** | **pressure gradient force** | **virtual mass** | **Basset history term** |
|---|---|---|---|---|---|

**(2.13)**

where $\vec{w}(\vec{x},t)=\vec{u}(\vec{x},t)-\vec{v}_p(t)$ and the terms in square brackets are evaluated at $\vec{x}=\vec{x}_p(t)$ or $\vec{x}=\vec{x}_p(\tau)$.

The governing parameters are:

- the Stokes number $St=\frac{\rho_p d^2 U}{18\mu L}$
- the density ratio $\delta=\frac{\rho_f}{\rho_p}$
- the Froude number $Fr=\frac{U}{\sqrt{gL}}$.

The exact expression of the governing parameters will be given later in the case of a particle evolving in a pancake like vortex (section 2.5.2).

As Maxey and Riley pointed out, it is important to note the distinction between the two different time derivatives. The derivative $\frac{d}{dt}$ is used here to denote a time derivative following the moving sphere:

$$\frac{d}{dt}u_i\left[\vec{x}_p,t\right]=\left(\frac{\partial u_i}{\partial t}+\vec{v}_p.\vec{\nabla}u_i\right)_{\vec{x}=\vec{x}_p(t)}.$$

On the other hand, $\frac{D}{Dt}$ is used to denote the time derivative following a fluid element. For instance, the fluid acceleration as observed at the instantaneous centre of the sphere is given by:

$$\left.\frac{Du_i}{Dt}\right|_{\vec{x}_p(t)}=\left(\frac{\partial u_i}{\partial t}+\vec{u}.\vec{\nabla}u_i\right)_{\vec{x}=\vec{x}_p(t)}$$

### 2.4.2 Significance of the different terms

The Stokes drag, the virtual mass and the Basset history term account for the drag acting on the particle:

- the Stokes drag is the drag corresponding to steady motion at the instantaneous velocity
- the virtual mass contribution (or added mass effect) arises because acceleration of the particle requires acceleration of the fluid surrounding the body.
- the Basset history term adjusts the particle acceleration by taking into account the past acceleration on the particle motion, including the effect of the conditions that prevailed during development of the flow. Its form results from diffusion of vorticity from the particle (Clift et al. 1978).

The pressure gradient force accounts for the acceleration of the displaced fluid (i.e. the force a fluid sphere of the same size would experience in absence of the particle).

The buoyancy force accounts for the effect of gravity on the particle.

About the added mass term

To account for the fluid mass being accelerated, the mass of the body is increased, giving rise to the added mass term. For a sphere, the added mass is half the mass of the fluid displaced by the body, hence the coefficient $1/2$. The added mass is proportional to the density ratio $\delta = \frac{\rho_f}{\rho_p}$, and therefore has a negligible effect when the carrier fluid is of low density compared to the particle.

Some authors (Manton 1974; Auton 1981) have replaced the acceleration following the particle by the acceleration following a fluid element in the added mass term, i.e. $\frac{du}{dt}$ by $\frac{Du}{Dt}$. In fact, the distinction between the two is negligible given the low particle Reynolds number approximation used to derive the Maxey-Riley equation. Regardless, the term $\frac{du}{dt}$ will be kept for the added mass term, unless stated otherwise.

Neglect of the Basset history term

The Basset history term is expected to increase the drag force when:

- the particle is accelerating or decelerating (unsteady motions)
- the Reynolds number for the relative motion is low (Clift at al. 1978).

However, some studies have shown that the history effects are less important as originally thought:

- the Basset history term initially decays as $t^{-\frac{1}{2}}$ and later as $t^{-2}$ (Mei et al. 1991a, 1991b, Mei and Adrian 1992, Mei 1994; Lovalenti and Brady 1993a, 1993b, 1993c, 1995; Chang and Maxey 1994)
- departure from Stokes flow lessens the history effect

In the two-dimensional study, where gravity is absent, we expect this term to be negligible, especially if the particle is not released from rest but with an initial velocity corresponding to the ambient fluid velocity. Moreover, the Basset history term is proportional to the density ratio $\delta$, so the heavier the particle, the smaller this term is.

Therefore, given that the thesis focuses on the case of heavy particles, the Basset history term will be neglected. The only terms that are really important in the present case are the particle inertia, the drag, and the gravity terms.

The neglect of the Basset history term will be justified afterwards (Appendix B): its magnitude will be evaluated and compared to that of the drag term, showing that it is at least seven orders of magnitude smaller than the drag term.

### 2.4.3 Assumptions of the Maxey-Riley equation-corresponding restriction imposed on the parameters $(St.\delta)$

The Maxey-Riley equation is based on some assumptions (see explanations in Appendix C).

1. Assumption 1: $\mathrm{Re}_p = \frac{Ud}{\nu}\left|\vec{v}_p - \vec{u}\right|_{\dim ensionless} << 1$ **(2.14)**

   The particle Reynolds number is small compared to one so that the flow can be approximated to a Stokes flow.

2. Assumption 2: $(\frac{d}{L})^2 \mathrm{Re}_f = \frac{d^2 U}{L\nu} << 1$ **(2.15)**

   The ratio of the particle diameter squared times the characteristic velocity scale to the product of the kinematic viscosity of the fluid and of its characteristic length scale (i.e. the gradients of the velocity U) is assumed small compared to one. $\mathrm{Re}_f$ stands for the flow Reynolds number.

3. Assumption 3: $\frac{d}{L} << 1$ **(2.16)**

   The particle diameter is assumed to be small compared to the characteristic length scale of the fluid motion

It seems reasonable to impose <u>at least</u> that the following inequalities be satisfied:

$$\frac{d}{L} \le 10^{-3} \text{ and } \frac{Ud}{\nu} \le 10^{2}. \quad \textbf{(2.17)}$$

Now: $$\frac{Ud}{\nu} = 18\,St\,\delta\,(\frac{L}{d}) \qquad \textbf{(2.18)}$$

implying: $$\underline{St\,\delta \leq 5.6*10^{-3}}. \qquad \textbf{(2.19)}$$

In other words, the product $(St\,\delta)$ should be of order $10^{-3}$ or less for the Maxey-Riley equation to be applied. As a consequence, the present study will mainly focus on the case of **heavy particles in air** for which the density ratio $\delta$ is about $10^{-4}$. That way, the assumptions will be verified for a wide range of Stokes number. Light particles will only be looked at for simple verifications.

Restrictions imposed by the physics

By looking at a variety of flows for which particle dispersion is involved, we notice that, usually, significant values of $St$ are obtained only for heavy particles (small $\delta$), so that the product $St\,\delta$ is relatively small. This restriction on the parameters $(St\,\delta)$ is similar as the one imposed by the assumptions of the Maxey-Riley equation.

### 2.4.4 Extension to finite values of the particle Reynolds number

The Maxey-Riley equation is normally restricted to flows with particle Reynolds numbers that are small compared to one. It is nevertheless possible to model the departure from the Stokes regime (when the inertial effects become comparable to the drag effects) in the Stokes drag term. Corrections are indeed available for this term (and are used in the present study). They are described below.

Unfortunately, it is not possible to model the departure from the Stokes regime for the other terms. The best thing to do seems to limit the study to situations where the inertial effects are not prevailing, implying that the Stokes number shouldn't be too large.

Please note that the influence of the particle Reynolds number on the particle dynamics is expected to be small anyway.

Model of the departure from the Stokes drag

Strictly speaking, the following corrections apply only to rigid spheres, but they will be used for fluid particles as well. An empirical multiplicative fáctor $f_1$ is introduced in the drag coefficient $c_D$. This factor $f_1$ is the ratio between the actual steady drag force and the Stokes drag defined for $\mathrm{Re}_p = 0$.

**Oseen correction to the Stokes drag for $\mathrm{Re}_p \leq 0.01$**

Usually, $f_1$ is taken to be equal to 1 for the limit of creeping flows. Oseen (1910) noted a difficulty in applying this creeping flow equation to particles in unbounded media. Indeed, the ratio of the neglected inertia terms over the retained viscous terms is of order $O(\mathrm{Re}_p(\frac{r}{d}))$ where r is the distance from the particle, so that the expression of the drag coefficient is valid only for a distance $r \leq \frac{d}{\mathrm{Re}}$ from the particle. Oseen proposed an approximation coming from linearizing the inertia terms instead of neglecting them:

$$c_D = \frac{24}{\mathrm{Re}_p}(1+\frac{3}{16}\mathrm{Re}_p), \text{ i.e. } f_1 = 1+\frac{3}{16}\mathrm{Re}_p. \qquad \textbf{(2.20)}$$

**Correction of the drag term for** $0.01 < \mathrm{Re}_p < 20$

In the range $0.01 < \mathrm{Re}_p < 20$, the correction coefficient is given by Clift et al. (1978) as:

$$f_1 = 1 + 0.1315\,\mathrm{Re}_p^{(0.82-0.05\log \mathrm{Re}_p)}. \qquad \textbf{(2.21)}$$

It takes into account the effect of the wake behind the sphere on the drag.

## 2.5 The equations of motion of a particle in a pancake vortex

### 2.5.1 Presentation of the equations of motion of a particle in a pancake vortex

The system of coordinates was chosen so that the horizontal plan (x,y) or (r, $\theta$) corresponds to the symmetry plan of the vortex. The gravity vector is assumed to be perpendicular to the horizontal plan. Integrating the analytical model of the pancake vortex velocity field into the Maxey Riley equation leads to the following non-dimensional equations of motion:

- in polar coordinates:

$$\begin{cases} (1+\frac{\delta}{2})\frac{\ddot{r}}{r} = -\frac{1}{St}\frac{\dot{r}}{r} - \frac{c}{4}\delta\dot{\theta}\exp(-r^2) - (\frac{c}{2})^2\delta\exp(-2r^2) + (1+\frac{\delta}{2})\dot{\theta}^2 \\ (1+\frac{\delta}{2})\frac{d}{dt}(r^2\dot{\theta}) = \frac{1}{St}(\frac{c}{2}r^2\exp(-r^2) - r^2\dot{\theta}) + \frac{c}{4}\delta(1-2r^2)r\dot{r}\exp(-r^2) - \frac{\delta c}{4\Lambda^2}z\dot{z}r^2\exp(-r^2) \\ (1+\frac{\delta}{2})\ddot{z} = -\frac{1}{St}\dot{z} - (1-\delta)g \end{cases} \qquad \textbf{(2.22)}$$

where $\dot{r} = \frac{\partial r}{\partial t}$ and $\ddot{r} = \frac{\partial^2 r}{\partial t^2}$.

- in Cartesian coordinates:

$$\begin{cases} (1+\frac{\delta}{2})\ddot{x} = \frac{1}{St}(-\frac{c}{2}y\exp(-r^2) - \dot{x}) - (\frac{c}{2})^2\delta x\exp(-2r^2) + (\frac{c}{4})\delta(2x\dot{x}y + 2\dot{y}y^2 - \dot{y} + \frac{z\dot{z}y}{\Lambda^2})\exp(-r^2) \\ (1+\frac{\delta}{2})\ddot{y} = \frac{1}{St}(\frac{c}{2}x\exp(-r^2) - \dot{y}) - (\frac{c}{2})^2\delta y\exp(-2r^2) - (\frac{c}{4})\delta(2xy\dot{y} + 2\dot{x}x^2 - \dot{x} + \frac{z\dot{z}x}{\Lambda^2})\exp(-r^2) \\ (1+\frac{\delta}{2})\ddot{z} = -\frac{1}{St}\dot{z} - (1-\delta)g \end{cases}$$

**(2.23)**

In the radial equation (i.e. the equation for $r$), the first three terms on the right hand side of the equation favour inward motion, whereas the last term favours outward motion.

(See Appendix A for the equations that use $\frac{Du}{Dt}$, the acceleration following a fluid element, instead of $\frac{du}{dt}$, the acceleration following the particle, in the added mass term.)

### 2.5.2 The governing parameters ( $\Lambda$ , $St$, $\delta$ and $Fr$ )

There are four governing parameters in Equations 2.22 and 2.23. However, in the 2D study, it is **only the Stokes number ($St$) and the density ratio ($\delta$) that play a role on the particle dynamics and the dispersion process**. The effect of gravity and the influence of the vortex thickness are addressed in the 3D study (Chapter 6).

The aspect ratio $\Lambda$

This is the non-dimensional thickness of the vortex: $\Lambda = \frac{\lambda}{L}$. It describes how the planar flow field changes along the vertical axis. It is indeed the standard deviation of the Gaussian distribution that the planar flow field exhibits along the vertical axis.

As previously discussed, c is not an independent parameter since it directly depends on the aspect ratio: $c = c_\Lambda(z)$.

The Stokes number

In the present study, the Stokes number is: $St = \tau_A \Omega$ where $\Omega$ denotes the characteristic rotation rate in the horizontal plane considered. Given the definition of the characteristic length and velocity scale, $\Omega$ can be written as $\Omega = \frac{U}{L} = \omega_M$ ($\omega_M$ being the maximum value of the vertical vorticity observed experimentally in the horizontal plane z=0, at the centre of the vortex).

As a result: $$St = \tau_A \Omega = \frac{d^2}{18\nu\delta}\frac{U}{L} \quad \textbf{(2.24)}$$

or $$St = \frac{\rho_p d^2}{18\mu}\omega_M \quad \textbf{(2.25)}$$

or $$St = (\frac{d}{L})^2 \frac{\mathrm{Re}_f}{18 * \delta} \quad \text{with} \quad \mathrm{Re}_f = \frac{UL}{\nu} \quad \textbf{(2.26)}$$

$St$ is the only parameter that depends on the particle diameter (it varies as the diameter square $d^2$) and is therefore independent of all the other parameters.

The density ratio

Due to the stratification of the background flow field, $\delta$ varies with z according to:

$$\delta = \delta_0(1 - \frac{N^2}{g}Lz) \tag{2.27}$$

with $\delta_0 = \frac{\rho_{f0}}{\rho_p}$ the density ratio at $z = 0$, z the dimensionless elevation, and $N$ the local buoyancy frequency of the fluid, determined by calculating the density gradient:

$$N^2(z) = -(\frac{g}{\rho})\frac{d\rho}{dz}. \tag{2.28}$$

$\delta_0$ varies as the inverse of the particle density $\rho_p$. Because it is the only parameter that depends on the particle density, it is independent of all the other parameters.

In fact, it has been observed that the core of pancake vortices coincides with an intensification of the background stratification (in both the laminar and turbulent regime). This pinching of the isopycnals accounts for a hydrostatic balance with the pressure drop in the vertical direction (Bonnier at al. 2000). This local intensification of the density gradient is also observed in geophysical applications like in the core of a cyclone, even though the earth's rotation has to be taken into account. Still, in rotating systems, the geostrophic balance replaces the centrifugal balance in the horizontal direction. Whereas cyclonic submesoscale vortices are characterized by a core of low pressure like in our model, anticyclonic submesoscale eddies have a core of high pressure. To maintain a balanced state, the background stratification has to be smoothed (i.e. the isopycnals are further apart), leading to a homogeneous core, as observed, for example, by Armi et al. (1989).

This being said, the local intensification of the density gradient is negligible for the present study.

The Froude number

The Froude number expresses, in non-dimensional form, the relative importance of inertial forces and gravitational forces for the particle motion. Large Froude numbers describe a particle motion dominated by inertia, for which gravity is not important. As the Froude number decreases, gravity becomes more important for the dynamical behaviour of the particle. The Froude number only affects the vertical motion.

In the equations of motion (Equations 2.22 and 2.23), the gravity term scales as the inverse of the Froude number squared:

$$g' = \frac{1}{Fr^2} = \frac{Lg}{U^2} = \frac{g}{L\omega_M{}^2} \qquad \textbf{(2.29)}$$

The Froude number is the only parameter that depends on the gravity. Let's point out that the Froude number that Beckers et al. (2001) referred to in their study of pancake-like vortices in stratified flows was the 'internal Froude number' (see section 2.1.1). The internal Froude number does not belong to the parameters of the present study.

Possible values of the different parameters

The purpose here is to get an idea about the values of the Stokes number, Froude number and particle Reynolds number that can be obtained in nature. Two sets of values will be considered.

- The first one is taken from the experiments carried out by Beckers et al. (2001). Beckers was not studying the particle dispersion but the evolution of pancake-like vortices in water with:

$$U = 2.3 \ cm\ s^{-1}$$

$$L = 3 \ cm$$

$$\nu = 1.02 * 10^{-6} \ m^2\ s^{-1}$$

- The second set originates from the experimental values given by Yang (1993). It corresponds to the study of the particle dispersion in the coherent vortex structures present in the wake flow of a bluff body (in air):

$$U = 3.3 \ m\ s^{-1}$$

$$L = 3 \ cm$$

$$\nu = 1.5 * 10^{-5} \ m^2\ s^{-1}$$

**The Stokes number**

The Stokes number in the horizontal plane is:

- For set #1: $St = \frac{d^2}{18\nu\delta}\frac{U}{L} \approx 4 * 10^4 * \frac{d^2}{\delta}$.
- For set #2: $St = \frac{d^2}{18\nu\delta}\frac{U}{L} \approx 4 * 10^5 * \frac{d^2}{\delta}$.

If we consider particles of diameter $d = 30\mu m$ and of density $\rho_p = 2.4 \ g\ cm^{-3}$:

- For set #1: $\delta = 10^{-1} \Rightarrow \quad St \approx 4 * 10^{-4}$
- For set #2: $\delta = 10^{-4} \Rightarrow \quad St \approx 4$

In particular, it illustrates the fact that it is reasonable to consider large values of the Stokes number only for heavy particles in gas (when $\delta << 1$).

**The Froude number**

- For set #1: $Fr = \frac{U}{\sqrt{gL}} \approx 0.04$.
- For set #2: $Fr = \frac{U}{\sqrt{gL}} \approx 6$.

As a result, we expect the effect of gravity to be much more significant in the first example.

**The particle Reynolds number**

The particle Reynolds number is given by:

$$\mathrm{Re}_p = \frac{d\left|\vec{v}_p - \vec{u}\right|}{\nu} \qquad \textbf{(2.30)}$$

It has to be reasonably low (small compared to one) for the Maxey-Riley equation to be valid. But, as mentioned earlier, values up to 20 will be allowed. Now, under reasonable initial condition for the particle velocity, $\left|\vec{v}_p - \vec{u}\right|$ is less than the local fluid velocity, and a first approximation would be: $\mathrm{Re}_p < \frac{dU}{\nu}$. If $d = 30\mu m$, this translates as:

- For set #1: $\mathrm{Re}_p < 0.67$
- For set #2: $\mathrm{Re}_p < 6.6$.

### 2.5.3 Importance of the initial conditions

The relaxation time $\tau_A$ (i.e. the time after which the particle velocity is not affected by the initial velocity), is proportional to the Stokes number, since the later is the ratio of the relaxation time to the time associated with the vortex motion. It follows that the smaller the Stokes number, the less

important the initial conditions are. Also, the lighter the particle, the more sensitive it is to the initial conditions, as the equations and the simulations will show.

## 2.6 The bubble case

The purpose here is to give some idea of the specificities of the bubble behaviour in vortical flows. It is mainly given for reference, given that the bubble case is barely addressed in this project (it mainly focuses on heavy particles).

The behaviour of bubbles in vortical flows is really different from that of heavy particles (almost opposite). The density ratio $\delta$ therefore plays a key role in the particle dynamics. In addition to the difference in dynamics due to the density ratio, the equations of motion for a bubble slightly differ from that for a heavy particle, as it is going to be shown now.

### 2.6.1 General form of the equation of motion of a bubble

The Maxey-Riley equation of motion retains the same form for bubbles, except for the history term, and under the assumption that they are small and non-deforming. In fact, bubbles tend to grow and change in shape as they are accelerated towards the vortex axis (Chahine 1995). Still, assuming that they are non-deforming is a reasonable assumption in flows where the length scale of the bubble is small compared to the flow length scale, and when a large surface tension exists which keeps the spherical shape.

#### 2.6.1.1 The history term

Morrison and Stewart (1976) have derived the term that replaces the history term in the case of bubbles. This new term depends on the time rate of change of the relative velocity ($\vec{w}(\vec{x},t) = \vec{u}(\vec{x},t) - \vec{v}_p(t)$). For flows in which the frequency of the oscillatory motion of the carrier fluid is small, the Basset term can be neglected.

#### 2.6.1.2 Modification of the steady drag force term

Another difference with the equations for solid spheres is to be mentioned: the drag force on a bubble in low Reynolds number flows is $\frac{2}{3}$ that of a particle of the same size. The origin of this coefficient can be explained as follows.

For a rigid particle, the only boundary conditions that need to be considered at its interface with the carrier fluid are the velocity boundary conditions (the normal and tangential velocity in each phase are equal at the interface). For fluid particles, additional boundary conditions are required: the normal and shearing stresses are required to be balanced at the interface separating the two fluids. The equation expressing the continuity of tangential stress across the interface makes use of the viscosity ratio: $\kappa = \frac{\mu_p}{\mu_f}$. This ratio shows up in the calculation of the drag coefficient, which is, in the case of small particle Reynolds numbers (Stokes regime):

$$c_D = \frac{8}{\mathrm{Re}_p}\left(\frac{2+3\kappa}{1+\kappa}\right) \qquad \textbf{(2.31)}$$

the drag force being:

$$F_{drag} = c_D * \frac{1}{2}\rho_f v_p \left(\pi \frac{d^2}{4}\right) \qquad \textbf{(2.32)}$$

For a bubble: $\kappa = 0$ and $c_D = \frac{2*8}{\mathrm{Re}_p}$,

whereas, for a rigid sphere: $\kappa \to \infty$ and $c_D = \frac{3*8}{\mathrm{Re}_p}$.

Therefore: $c_D(bubble) = \frac{2}{3} c_D(rigid\ sphere)$

or $St(bubble) = \frac{3}{2} St(rigid\ sphere)$.

For a water drop in air, for instance: $\kappa \approx 55$ so that $\frac{c_D}{c_D(\ rigid\ sphere)} = 99.40\%$: the error involved is less than 1%. The influence of the viscosity ratio will not be taken into account in the simulations.

On the other hand, the influence of the particle Reynolds number on the drag will be treated the same way it is treated in the case of rigid spheres. Note that, in practice, the drag on bubbles or drops is increased due to their deformation and to the presence of surfactants at their interface.

### 2.6.2 The modified Stokes number as the relevant parameter

For bubbles, the relevant parameter is no longer the Stokes number but the modified Stokes number: $St' = \delta * St$. Indeed, in the equation of motion (see equations 2.22 section 2.4.1), the coefficient in front of the acceleration term is $(1+\frac{\delta}{2})$ is much bigger than 1 in the case of bubbles. Correspondingly, the drag term is weaker than in the case of rigid spheres. To account for this, it is appropriate to divide each term of the equation by $\frac{\delta}{2}$. The drag term parameter becomes $St' = \delta * St$.

### 2.6.3 Sensitivity to the acceleration of the fluid

Bubbles are very sensitive to the acceleration of the fluid (i.e. to the pressure term), whereas it has no effect on the motion of very heavy particles. This extra sensitivity to pressure effects plays a dominant role in the dynamics of bubbles. The pressure gradients are felt three times as much as in the case of fluid elements, causing the bubbles to accumulate in regions of low pressure.

Neglecting the history term and given that $\delta >> 1$, the equation of motion is indeed (in dimensional form):

$$\frac{\delta}{2}\frac{d\vec{v}_p}{dt} = \frac{2}{3}\frac{18\nu\delta}{d^2}\left[\vec{u}(\vec{x},t) - \vec{v}_p(t)\right]_{\vec{x}=\vec{x}_p(t)} - \delta\,\vec{g} + \delta\left[\frac{D\vec{u}}{Dt}\right]_{\vec{x}=\vec{x}_p(t)} + \frac{\delta}{2}\frac{d}{dt}\left[\vec{u}(\vec{x},t)\right]_{\vec{x}=\vec{x}_p(t)} \qquad \textbf{(2.33)}$$

so that

$$\frac{d\vec{v}_p}{dt} = \frac{4}{3}\frac{18\nu}{d^2}\left[\vec{u}(\vec{x},t) - \vec{v}_p(t)\right]_{\vec{x}=\vec{x}_p(t)} - 2\vec{g} + 2\left[\frac{D\vec{u}}{Dt}\right]_{\vec{x}=\vec{x}_p(t)} + \frac{d}{dt}\left[\vec{u}(\vec{x},t)\right]_{\vec{x}=\vec{x}_p(t)} \qquad \textbf{(2.34)}$$

and given that, for low particle Reynolds numbers: $\left[\frac{D\vec{u}}{Dt}\right] \approx \frac{d}{dt}\left[\vec{u}(\vec{x},t)\right]$, the equation reduces to:

$$\frac{d\vec{v}_p}{dt} = \frac{24\nu}{d^2}\left[\vec{u}(\vec{x},t) - \vec{v}_p(t)\right]_{\vec{x}=\vec{x}_p(t)} - 2\vec{g} + 3\left[\frac{D\vec{u}}{Dt}\right]_{\vec{x}=\vec{x}_p(t)} \qquad \textbf{(2.35)}$$

# 3 SIMPLE ANALYSIS OF LIGHT AND HEAVY PARTICLE MOTION IN THE 2D HORIZONTAL PLANE OF A PANCAKE VORTEX

## 3.1 Validity of the 2D approach

### 3.1.1 Significance of the 2D approach

Strictly speaking, the three-dimensional approach is the only correct approach to treat the problem. Indeed, unless the particle is neutrally buoyant and doesn't have any initial vertical velocity, it will either rise or fall. By doing so, the background velocity field in which it evolves changes, because the vortex does have a vertical structure. So, it's important to keep track of the vertical movement of the particle.

Nevertheless, we'll start by considering the dynamics of the particle in the horizontal planes of the vortex (mainly its symmetry plane), as if the movement was taking place at a constant elevation $z$, or at least assuming that the particle motion in the horizontal is decoupled from its vertical motion. This assumption is reasonable if the vertical motion is negligible compared to the thickness of the vortex, in the time interval considered.

Therefore, strictly speaking, the results presented below only apply to a vortex configuration where the horizontal component of the fluid velocity field is independent of the elevation. Doing so, we actually ignore the real three-dimensional structure of the pancake vortex, but we still deal with the horizontal fluid velocity that characterizes the pancake vortex.

### 3.1.2 Possibility of a quasi 2D motion

#### 3.1.2.1 Residence time of a particle

A particle that is not neutrally buoyant will either fall or rise. Therefore there is a limited time interval during which the vortex can affect the particle in order to enhance or delay settling or to create non-uniformities in the particle concentration field. To get an idea of the magnitude of this time interval, one can compute the residence time of a particle (i.e. the time a particle stays in the vortex structure).

In the present study, the residence time (called settling time $\tau_S$ in the case of heavy particles) is simply related to the steady forcing by gravity. It is defined as the amount of time it takes a particle falling/rising with its terminal velocity to go through the pancake like vortex. The total width of the vortex is $w = 2\lambda$ ($\lambda$ designating the thickness of the vortex: see section 2.2.1). The settling time is given by:

$$\tau_S = \frac{w}{U_{term}}. \tag{3.1}$$

The terminal velocity $U_{term}$ is the velocity a particle would achieve if it were falling/rising under the action of buoyancy and drag, in a still fluid. It is obtained in a non-dimensional form by setting the particle acceleration to zero in the equation for the vertical motion:

$$(1+\frac{\delta}{2})\ddot{z} = -\frac{1}{St}\dot{z} - \frac{(1-\delta)}{Fr^2} \tag{3.2}$$

$$\ddot{z} = 0 \quad \Rightarrow \quad \dot{z} = -(1-\delta)\frac{St}{Fr^2} \tag{3.3}$$

Hence: $$U^*_{term} = |1-\delta|\frac{St}{Fr^2} \tag{3.4}$$

In dimensional form:

$$U_{term} = U|1-\delta|\frac{St}{Fr^2} \quad \text{or} \quad U_{term} = |1-\delta|\frac{\rho_p d^2 g}{18\mu} \tag{3.5}$$

Therefore: $$\tau_S = \frac{w Fr^2}{U|1-\delta|St} \quad \text{or} \quad \tau_S = \frac{1}{|1-\delta|}\frac{18\mu w}{\rho_p d^2 g}. \tag{3.6}$$

Note: the calculation of the terminal velocity would be more complicated for high particle Reynolds numbers.

### 3.1.2.2 Conditions for a quasi 2D motion

**Role of the parameters $Fr$, $St$ and $\delta$**

Preliminary remark: Since the drag term is proportional to $\frac{1}{d^2}$ and the terminal velocity to $d^2$, the smaller the particle, the closer its trajectory will be to the two-dimensional motion of the fluid particles.

The two-dimensional approximation will be valid if, in the time interval considered, the movement of the particle in the vertical is negligible compared to its horizontal motion. Under reasonable initial conditions, we expect the horizontal velocity of the particle to be of the same order as the characteristic velocity of the fluid motion: $U$. So, the vertical displacement will be negligible if $U_{term} << U$.

Because $U_{term} = U|1-\delta|\frac{St}{Fr^2}$,

$U_{term} << U$ is equivalent to:

$$\frac{|1-\delta|St}{Fr^2} << 1. \qquad (3.7)$$

It's interesting to note that all of the three key parameters ($Fr$, $St$ and $\delta$) play an important role here. Grossly speaking, the horizontal motion will be all the more prevailing as:

- the particle is close to neutral buoyancy ($\delta = 1$)
- it has a small Stokes number
- it has a large Froude number.

Under those conditions, the vertical motion of a particle is negligible compared to the vertical extension (thickness) of the vortex, so that the velocity profile of the vortex in which it evolves does not change much. The two-dimensional approach is justified in that case. To be more precise: given that the sensitivity of the velocity profile of the vortex with respect to the elevation depends on the elevation itself, how much the particle is allowed to move in the vertical will also depend on the chosen elevation. The further from the horizontal plane of symmetry, the more restricted the vertical motion has to be for the two-dimensional approach to still be valid.

If it is assumed that a particle is released on the horizontal plane of symmetry and is allowed a maximum displacement $\Delta z = 0.1\lambda$ in the vertical, the corresponding variation in velocity is:

$$\frac{c(z=0)-c(z=0.1\times\lambda)}{c(z=0)} = 1-\exp(-\frac{(0.1\times\Lambda)^2}{2\Lambda^2}) \approx 0.5\%$$

To ensure that the displacement in the vertical is less than $\Delta z$, and given that the vertical velocity is smaller than $U_{term}$, it is sufficient to impose that the time interval $[0;T]$ on which the particle's movement is tracked satisfies:

$$U_{term} T \le \Delta z \quad \text{i.e.} \quad T \le T_{\sup} = \frac{\Delta z}{U_{\sup}}$$

$$T_{\sup} = \frac{\Delta z}{w} \tau_S = \frac{Fr^2}{|1-\delta| St} \frac{\Delta z}{U} = \frac{1}{|1-\delta|} \frac{18 \mu \Delta z}{\rho_P d^2 g}.$$

On the other hand, the time interval should be large enough to allow the particle to actually move in the horizontal plane. In other words, it should be at least larger than the characteristic time of the fluid motion:

$$T > T_{\inf} = \frac{L}{U}.$$

The non-dimensional time limits are:

$$T^*_{\inf} = \frac{T_{\inf}}{\Omega^{-1}} = T_{\inf} \frac{U}{L} = 1 .$$

and

$$T^*_{\sup} = \frac{T_{\sup}}{\Omega^{-1}} = T_{\sup} \frac{U}{L} = \frac{Fr^2}{|1-\delta|.St} \frac{\Delta z}{L} .$$

In other words, the vertical displacement of the particle will be reasonably small and the its horizontal movement reasonably significant if:

$$T_{\inf} < T < T_{\sup}$$

which requires that:

$$T_{\inf} < T_{\sup}, \quad \text{i.e.} \quad \frac{(1-\delta) d^2}{\delta} \frac{g}{18 \nu U \Delta z} < 1 .$$

For the two sets of experimental values previously considered, the Froude number is:

- Set #1: $Fr = \frac{U}{\sqrt{gL}} \approx 0.04$.
- Set #2: $Fr = \frac{U}{\sqrt{gL}} \approx 6$.

the inequality $T_{inf} < T_{sup}$ reads:

- For set #1: $\frac{(1-\delta)d^2}{\delta} < 9.5*10^{-10} \approx 10^{-9}$.
- For set #2: $\frac{(1-\delta)d^2}{\delta} < 2.7*10^{-6}$.

With particles of diameter $d = 30\mu m$, it implies:

- For set #1: $\frac{(1-\delta)}{\delta} < 1 \Rightarrow \delta > \frac{1}{2}$:

  the particle density should be less than twice that of the fluid (water).

- For set #2: $\frac{(1-\delta)}{\delta} < 3027.5 \Rightarrow \delta > 3.3*10^{-4}$:

  the particle density should be less than 3000 that of the fluid (air).

In practice, those restrictions are less dramatic, especially when dealing with flows of higher Froude number. Also, the vertical velocity of the particle has been over-estimated here. Indeed, the small-scale turbulence processes have been ignored, as well as the possibility of having a particle with an irregular shape or a rough surface. The associated friction forces have not been taken into account, so the actual fall or rise velocity of many particles of interest (marine snow and flocs for example) is slower than $U_{term}$. Therefore, the two-dimensional approach is expected to be valid for a broader range of parameters. For this reason, the two-dimensional motion of all kinds of particles (regardless of their density or their Stokes number) will be investigated, keeping in mind that, strictly speaking, the results obtained are valid only in the case of a fluid velocity field independent of the elevation – which corresponds to a vortex having an infinite vertical extension.

## 3.2 Equations of motion in 2D

Gravity is assumed to be perpendicular to the horizontal planes of the vortex (therefore, it does not intervene in the equation for the horizontal motion).

### 3.2.1 General case

-in cylindrical coordinates

$$\begin{cases} (1+\frac{\delta}{2})\frac{\ddot{r}}{r} = -\frac{1}{St}\frac{\dot{r}}{r} - \frac{c}{4}\delta\dot{\theta}\exp(-r^2) - (\frac{c}{2})^2\delta\exp(-2r^2) + (1+\frac{\delta}{2})\dot{\theta}^2 \\ (1+\frac{\delta}{2})\frac{d}{dt}(r^2\dot{\theta}) = \frac{1}{St}(\frac{c}{2}r^2\exp(-r^2) - r^2\dot{\theta}) + \frac{c}{4}\delta(1-2r^2)r\dot{r}\exp(-r^2) \end{cases} \quad \textbf{(3.8)}$$

-in Cartesian coordinates (x, y, z):

$$\begin{cases} (1+\frac{\delta}{2})\ddot{x} = \frac{1}{St}(-\frac{c}{2}y\exp(-r^2) - \dot{x}) - (\frac{c}{2})^2\delta x\exp(-2r^2) + (\frac{c}{2})\delta(x\dot{x}y + \dot{y}y^2 - \frac{\dot{y}}{2})\exp(-r^2) \\ (1+\frac{\delta}{2})\ddot{y} = \frac{1}{St}(\frac{c}{2}x\exp(-r^2) - \dot{y}) - (\frac{c}{2})^2\delta y\exp(-2r^2) - (\frac{c}{2})\delta(xy\dot{y} + \dot{x}x^2 - \frac{\dot{x}}{2})\exp(-r^2) \end{cases} \quad \textbf{(3.9)}$$

c normally depends on the chosen elevation (see section 2.2.2) but is a constant in the 2D approach. Assuming the particle remains in the horizontal plane $z = 0$, c is in fact equal to 1.

### 3.2.2 Simplifications in the case of very heavy particles

The particles are defined as heavy if $\delta < 1$, and very heavy if $\delta << 1$. In the limit case of very heavy particles ($\delta << 1$), the equations of motion become:

$$\begin{cases} \frac{\ddot{r}}{r} = -\frac{1}{St}\frac{\dot{r}}{r} + \dot{\theta}^2 & \textbf{(3.10)} \\ \frac{d}{dt}(r^2\dot{\theta}) = \frac{1}{St}(\frac{c}{2}r^2\exp(-r^2) - r^2\dot{\theta}) & \textbf{(3.11)} \end{cases}$$

or, in Cartesian coordinates:

$$\begin{cases} \ddot{x} = \frac{1}{St}(-\frac{c}{2}y\exp(-r^2) - \dot{x}) & \textbf{(3.12)} \\ \ddot{y} = \frac{1}{St}(\frac{c}{2}x\exp(-r^2) - \dot{y}) & \textbf{(3.13)} \end{cases}$$

## 3.3 Implementation in Matlab

After rewriting the system as a first order ODE, it is solved for a given set of parameters (including the Stokes number, the density ratio and the initial conditions). The solver adjusts the time step so that the error tolerance is satisfied.

Note: all the results are expressed in terms of dimensionless quantities.

### 3.3.1 Choosing the solver: stiff or nonstiff problem?

Matlab provides a variety of initial value ODE (Ordinary Differential Equation) problem solvers. The solver ode45, a one-step solver based on an explicit Runge-Kutta (4,5) formula, the Dormand-Prince pair, is generally recommended for nonstiff differential equations (differential equations are said to be nonstiff when the different time scales involved in the problem are of the same order). Solving the equations of motions with ode45 turned out to be computationally intense, in particular for particles with small Stokes numbers. On the other hand, when the stiff differential equations solver ode15s is used instead (a multi-step, variable order solver based on the numerical differentiation formulas (NDFs)), the resolution time is greatly improved. This suggests that the problem is actually stiff for low Stokes numbers. Even though a stiff solver needs to do more computations at each time step, it takes longer time steps than a nonstiff solver when used on a stiff problem, so that it actually solves the problem faster. (To be more precise, the stiff solver uses a variable time step: small while the fast time scale is important and then larger when it becomes insignificant.)

To assess the stiffness of the equations, the eigenvalues of the Jacobian matrix of the system are calculated. The problem is non-stiff as long as none of the eigenvalues of the Jacobian is large and negative (compared to the other eigenvalues). Because the system is non-linear, the Jacobian matrix is not a constant but a function of the variables $(x, y, \dot{x}, \dot{y})$, so that the only thing we can do is to examine the eigenvalues at different time steps, for a given simulation. It is observed that, as the Stokes number decreases, the Jacobian matrix has a pair of negative and large eigenvalues. As a consequence, even though it appears that both stiff and non-stiff solvers give the same numerical answer, the stiff solver ode15s will be preferably used.

### 3.3.2 Error tolerance

As previously discussed, the stiff solver uses a variable time step: small while the fast time time scale is important and then larger when it becomes insignificant. Beginning at the initial time with initial conditions, it steps through the time interval, computing a solution at each time step. If the solution for a time step satisfies the solver's error tolerance criteria, it is a successful step. Otherwise, it is a failed attempt; the solver shrinks the step size and tries again. Because the time step can be longer than with a nonstiff solver, the accuracy delivered might not be as good. To improve the accuracy, tighter relative and absolute error tolerances are imposed: a relative error tolerance of $10^{-9}$ and an absolute error tolerance of $10^{-12}$ are used, unless stated otherwise. This roughly means that all solution components will be correct up to 9 digits, except those smaller than threshold $10^{-12}$. It implies in particular that the correctness of the solution is not as good whenever the position x or y or the velocity u or v is smaller than $10^{-12}$. If that were the case too often, that would mean that the scaling of the solution is not suitable for the problem.

### 3.3.3 Parameters of the simulation

The parameters of the problem are

- the Stokes number $St$
- the density ratio $\delta$
- the initial conditions:

1) the location $(x_0, y_0)$ of the particle at $t = 0$: four initial positions will be mainly considered: A (0,0) corresponding to the vortex centre; B $(1/\sqrt{2}, 0)$ corresponding to the distance at which the azimuthal velocity $u_\theta$ is maximum; C (1,0) corresponding to the distance at which the vorticity $\omega_z$ changes sign; D $(\sqrt{2}, 0)$ corresponding to the distance at which the vorticity $\omega_z$ is minimum (see Figure 3.1).

2) the velocity $(u_0, v_0)$ of the particle at $t = 0$: only two different initial velocities will be investigated: the case where the particle is released from rest $(u0, v0) = (0,0)$ and the case where its velocity is equal to local velocity of the unperturbed fluid: $\vec{v}_p(t = 0) = \vec{u}(\vec{x}_p(t = 0))$.

For convenience, we'll use the following format to represent the set of parameters used in the simulation: $[St - \delta - \vec{x}_p(t = 0) - \vec{v}_p(t = 0)]$, where $\vec{v}_p(t = 0)$ will either be noted as $\vec{0}$ or $\vec{u}$, $\vec{x}_p(t = 0)$ as A, B, C or D (the exact coordinates will be indicated otherwise). For instance: $[0.1 - 1.5 - C - \vec{u}]$ means that the particle is characterized by a Stokes number of $0.1$, a density ratio of $1.5$, and is released at the location $(x0, y0) = (1,0)$ with the local velocity of the fluid. In addition, T will indicate the time span of the simulation.

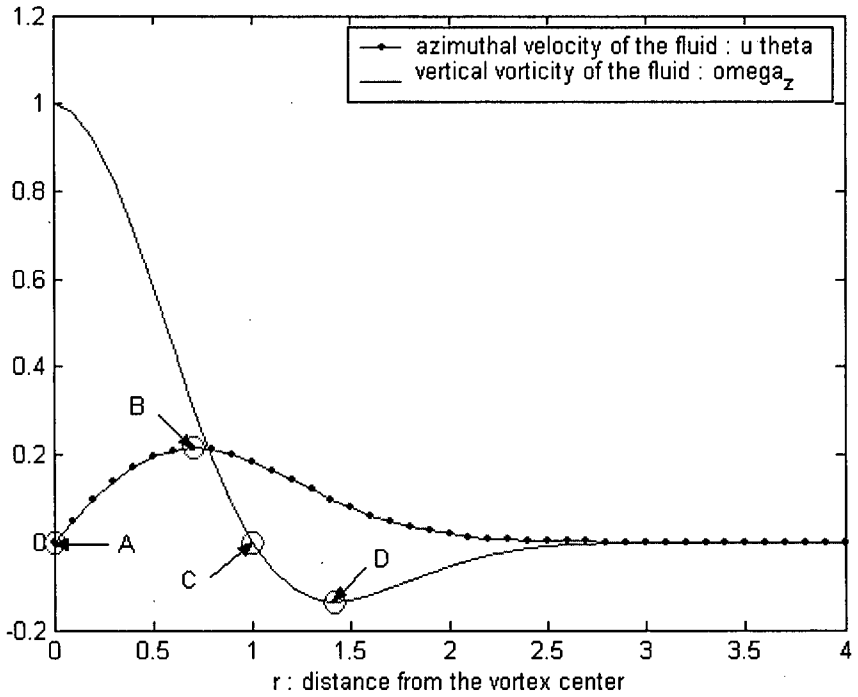


**Figure 3.1** Fluid velocity and vorticity profiles in the horizontal. The four recognizable points are: A ($r = 0$): centre of the vortex; B ($r = 1/\sqrt{2}$) distance at which $u_\theta$ is maximum; C ($r = 1$): distance at which $\omega_z$ changes sign; D ($r = \sqrt{2}$) : distance at which $\omega_z$ is minimum

## 3.4 Equilibrium point and its stability

A point $(r, \theta, z)$ is called a fixed point or an equilibrium point if the velocity and the acceleration of the particle at that particular location are zero.

### 3.4.1 Case of very heavy particles

As shown by the equations of motion (Equations 3.12 and 3.13), the only equilibrium point is at the vortex centre ($x = y = 0$). Also, $\dot{r} = 0$ admits no other solution than $\dot{\theta} = 0$, so there's no stable limit circle. To know about the stability of the centre, the equations are linearized around the vortex centre according to: $\exp(-r^2) \approx 1$ for $r << 1$:

$$\begin{cases} \ddot{x} = \frac{1}{St}(-\frac{c}{2}y - \dot{x}) & \textbf{(3.14)} \\ \ddot{y} = \frac{1}{St}(\frac{c}{2}x - \dot{y}) & \textbf{(3.15)} \end{cases}$$

In complex coordinates, the system becomes:

$$\ddot{Z} + a\dot{Z} - ia\frac{c}{2}Z = 0 \qquad \textbf{(3.16)}$$

with $Z = x + iy$ and $a = \frac{1}{St} \in R^{+*}$ (strictly positive real number)

The eigenvalues are:

$$\lambda_{1,2} = -\frac{a}{2} \pm \frac{1}{2}\sqrt{a^2 + 2iac} \qquad \textbf{(3.17)}$$

A simple geometrical argument can prove that: $\mathrm{Re}(\sqrt{a^2 + 2iac}) > a$, so that one eigenvalue is strictly positive. As a consequence, the vortex centre is unstable for heavy particles, regardless of the Stokes number: the centrifugal force overcomes the inward drag.

### 3.4.2 General case

Again, by considering the system in Cartesian coordinates (Equation 3.9), it appears that the only equilibrium point is the vortex centre. The linearization of the system gives:

$$\begin{cases} (1+\frac{\delta}{2})\ddot{x} = \frac{1}{St}(-\frac{c}{2}y - \dot{x}) - (\frac{c}{2})^2\delta x - (\frac{c}{2})\delta(\frac{\dot{y}}{2}) & \textbf{(3.18)} \\ (1+\frac{\delta}{2})\ddot{y} = \frac{1}{St}(\frac{c}{2}x - \dot{y}) - (\frac{c}{2})^2\delta y + (\frac{c}{2})\delta(\frac{\dot{x}}{2}) & \textbf{(3.19)} \end{cases}$$

In complex coordinates, the system becomes:

$$\alpha\ddot{Z} + \beta\dot{Z} + \gamma Z = 0$$

with $\alpha = 1+\frac{\delta}{2}$, $\beta = a - i\frac{c}{4}\delta$, $\gamma = (\frac{c}{2})(\frac{c}{2}\delta - ia)$ and $a = \frac{1}{St}$.

The complex eigenvalues are:

$$\lambda_{1,2} = \frac{-\beta \pm \sqrt{\beta^2 - 4\alpha\gamma}}{2\alpha} \qquad \textbf{(3.20)}$$

which is proportional to:

$$-a + i(\frac{c}{4}\delta) \pm \sqrt{a^2 - 4\left\{(\frac{c^2}{4}\delta + \frac{9}{64}c^2\delta^2) - i(\frac{ac}{2}(1+\frac{\delta}{4}))\right\}} \qquad \textbf{(3.21)}$$

The solution is of general form: $Z = c_1 e^{\lambda_1 t} + c_2 e^{\lambda_2 t}$

The second term represents an initial transient, whereas the first term reflects the long-term behaviour.

One eigenvalue has always a strictly negative real part. The other one has a strictly negative real part if and only if:

$$\left[\frac{ac}{2}(1+\frac{\delta}{4})\right]^2 < a^2(\frac{c^2}{4}\delta+\frac{9}{64}c^2\delta^2) \qquad \textbf{(3.22)}$$

i.e. $\delta^2+\delta-2>0$. **(3.23)**

The roots are –2 and 1. Given that $\delta$ is a positive parameter, the only solution is $\delta>1$. Therefore, the vortex centre is:

- a stable fixed point for light particles ($\delta>1$)
- an unstable fixed point for heavy particles ($\delta<1$)
- a neutrally stable fixed point for neutrally buoyant particles ($\delta=1$).

If the particle was to evolve in the core of the vortex only (solid body rotation vortex), the distance of the particle from the vortex centre would decay exponentially in the case of light particles, whereas it would grow exponentially in the case of heavy particles.

Note: If the system that uses $\frac{Du}{Dt}$ instead of $\frac{du}{dt}$ in the added mass term is considered instead (see Appendix A), the same conclusion is found.

Simulations show indeed that the centre of the vortex is an equilibrium point for any set of parameters $(St,\delta...)$ since a particle released at the centre without any initial velocity remains at the centre. Figure 3.2 illustrates what happens when a heavy particle and a light particle are released close to the centre (at the cross position $(x0;y0)=(0.1;0)$) and with the initial velocity equal to the local fluid velocity.

- The heavy particle does not come back to the centre: the equilibrium point is unstable.
- The light particle comes back to the centre: the equilibrium point is stable.

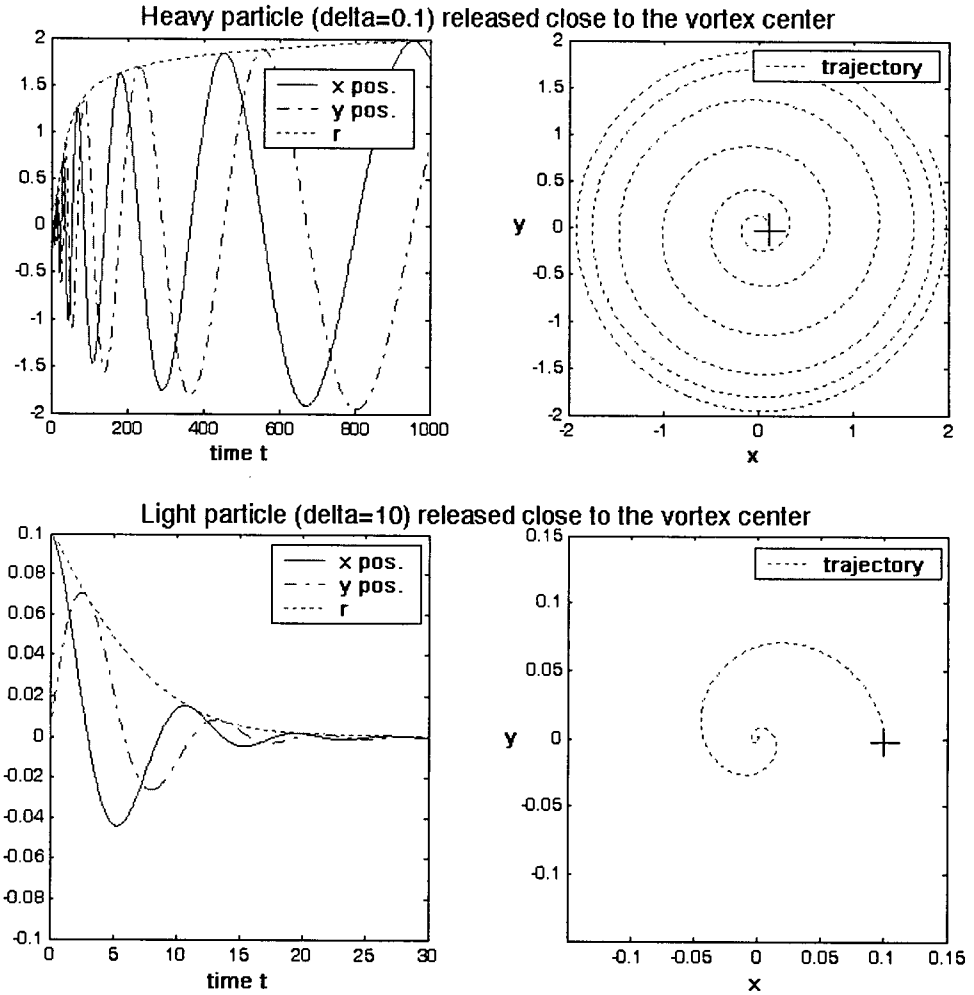


**Figure 3.2** Coordinates (x, y and r) and trajectory of a heavy particle (2 upper graphs) and a light particle (2 lower graphs) after they are released at the cross position, close to the vortex centre. The corresponding parameters are:

$$[St-\delta-\vec{x}_p(t=0)-\vec{v}_p(t=0)]=[1-0.1-(0.1;0)-\vec{u}],T=1000.$$

and $$[St-\delta-\vec{x}_p(t=0)-\vec{v}_p(t=0)]=[1-10-(0.1;0)-\vec{u}],\ T=30.$$

## 3.5 Influence of the density ratio

### 3.5.1 Light particles versus heavy particles

Simulations also show that, whatever their initial position is:

- heavy particles always tend to go away from the vortex centre
- light particles go towards the vortex centre

This is in agreement with the fact that heavy particles are ejected due mainly to the centrifugal effect, and light particles go towards the vortex centre, where the pressure is the lowest.

### 3.5.2 Case of light particles with a large Stokes number

A large Stokes number means that the inertia of the particle is important. Therefore, light particles will probably tend to overshoot while getting closer to the centre. That is indeed what we observe. Figure 3.3 illustrates the trajectory of a light particle having a density ratio of 100 and a Stokes number of 1, whereas in Figure 3.4 the density ratio is still equal to 100 but the Stokes number is now equal to 100. The trajectories obtained differ significantly. In the first case, the oscillation is about one point: the vortex centre, and the overshoot is very small. In the second case, the oscillation is more complex, the overshoot is more important.

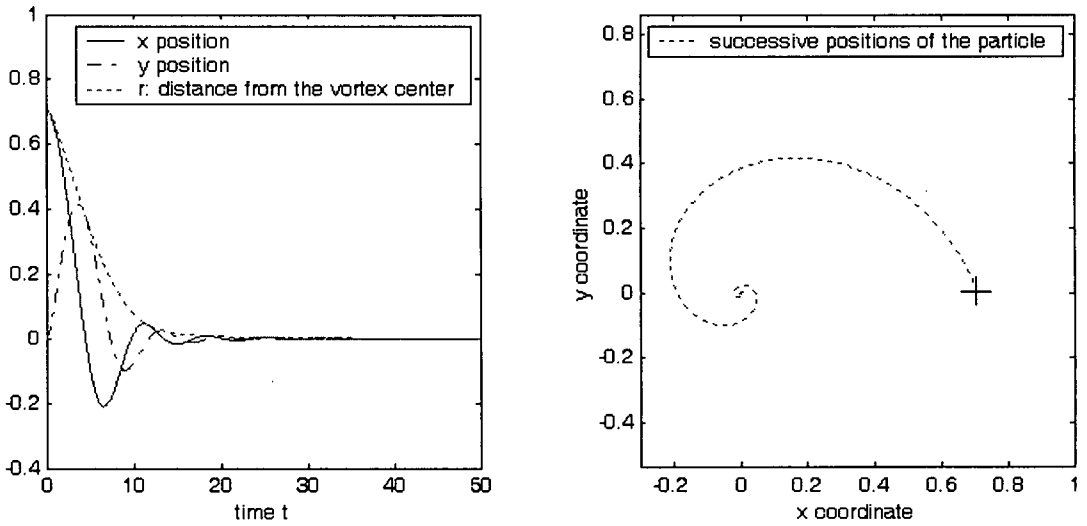


**Figure 3.3** Coordinates (x, y and r) and trajectory of a light particle with a small Stokes number: $[St-\delta-\vec{x}_p(t=0)-\vec{v}_p(t=0)]=[1-100-B-\vec{0}]$, $T=50$.

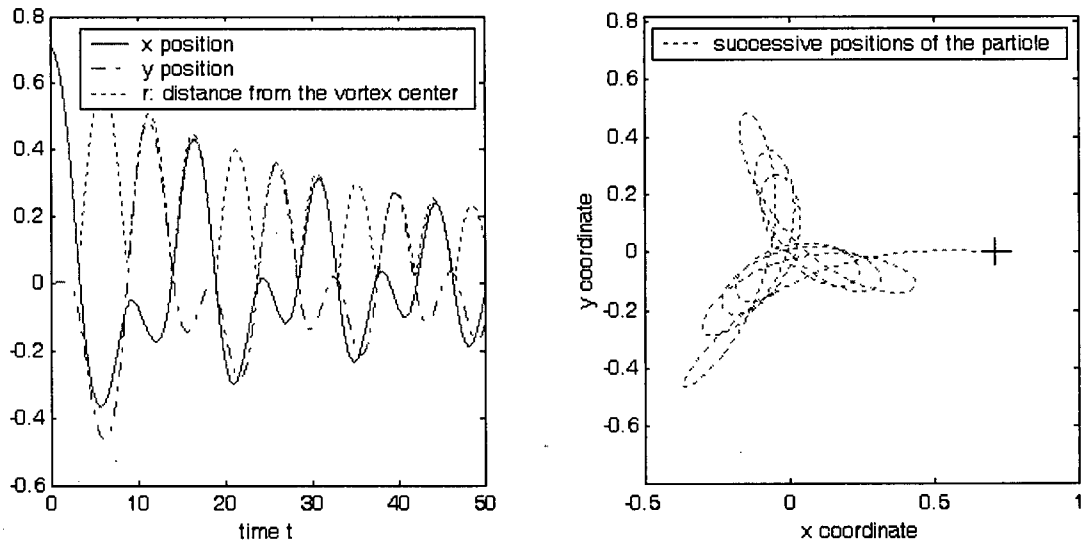


**Figure 3.4** Coordinates (x, y and r) and trajectory of a light particle with a large Stokes number: $[St-\delta-\vec{x}_p(t=0)-\vec{v}_p(t=0)]=[100-100-B-\vec{0}]$, $T=50$.

On the other hand, a heavy particle with a large Stokes number is expected not to be substantially affected by the vortex, at least for some time (see chapter 4).

### 3.5.3 Ability of neutrally buoyant particles to track fluid particles

We now come back to the non-linearized system, (with $\frac{Du}{Dt}$ instead of $\frac{du}{dt}$ in the added mass term). If it is assumed that the particle follows a circle: $r = r_0$, the radial equation gives:

$$\frac{3}{2}(\frac{c}{2})^2 \delta \exp(-2r_0^2) = (1+\frac{\delta}{2})\dot{\theta}^2 \qquad \textbf{(3.24)}$$

so that $$\dot{\theta} = \pm\sqrt{\frac{3\delta}{2+\delta}}\,\dot{\theta}_{fluid}, \text{ with } \dot{\theta}_{fluid} = \frac{c}{2}\exp(-r^2). \qquad \textbf{(3.25)}$$

Only the positive value of the rotation rate makes sense physically, though.

On the other hand, the azimuthal equation gives:

$$\dot{\theta} = \dot{\theta}_{fluid}. \qquad \textbf{(3.26)}$$

Therefore, the two equations agree only in the case of neutrally buoyant particles ($\delta = 1$). From this, two conclusions can be drawn. First: that, contrary to neutrally buoyant particles, buoyant and sinking particles cannot follow a circular trajectory. Second: that neutrally buoyant particles that follow a circular trajectory will actually track the fluid particles. In fact, this is the case as soon as the initial velocity matches that of the fluid. Indeed, if, at $t = 0$, $\dot{r} = 0$ and $\dot{\theta} = \dot{\theta}_{fluid}$, the radial force acting on it is identically zero, as shown by the radial equation of the system (the original one or the one that uses $\frac{Du}{Dt}$ instead of $\frac{du}{dt}$ in the added mass term) and the particle will follow a circular trajectory. A neutrally buoyant particle is now released with a zero initial velocity (Figure 3.5). The particle quickly goes on a circular trajectory, even though its initial velocity doesn't match the local fluid velocity. Its angular velocity also quickly adjusts to that of the surrounding fluid. This shows that neutrally buoyant particles are able to track fluid particles.

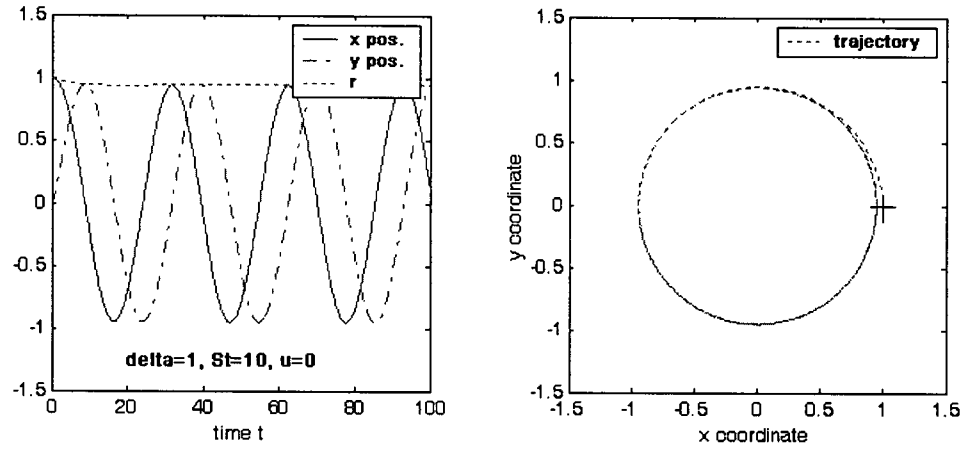


**Figure 3.5** Coordinates (x, y and r) and trajectory of a neutrally buoyant particle after it is released with zero initial velocity with the following parameters:
$[St-\delta-\vec{x}_p(t=0)-\vec{v}_p(t=0)]=[10-1-(1;0)-\vec{0}], T=100$.

In fact, particles with a very small Stokes number (i.e. very small particles) also end up tracking the fluid flow (i.e. go around a circle at the same rotation rate as that of the fluid).

## 3.6 Influence of the initial velocity

The effect of the initial velocity is supposed to depend on St and $\delta$:

- the smaller St is, the smaller the effect of the initial condition is (because the particle relaxation time – time it takes it to adjust to the fluid velocity – is small)

- the lighter the particles, the more they are affected by the initial conditions (because they are particularly sensitive to the acceleration of the fluid)

Comparative simulations illustrate how the influence of the initial velocity on the particle trajectory varies with respect to the parameters St and $\delta$ (Figure 3.6). Particles are released from the position $\vec{x}_p(t=0)=(1;0)$. The graphs on the left show the particle trajectory after it is released with zero initial velocity. On the right, the particle is released with the local fluid velocity.

- The first two rows of graphs correspond to the case of a heavy particle ($\delta = 0.1$) with St=10 and St=100 respectively. The trajectory is perturbed only for the large value of St.
- The latter two rows of graphs correspond to the case of a light particle ($\delta = 100$) with St=10 and St=100 respectively. The trajectory is more perturbed than for the heavy particle, and all the more when the Stokes number is big.

Figure 3.7 shows that, for the last combination of parameters considered ($\delta = 100$, St=100), the difference in trajectory is related to a difference in the amplitude of the oscillation of r (the distance from the vortex centre).

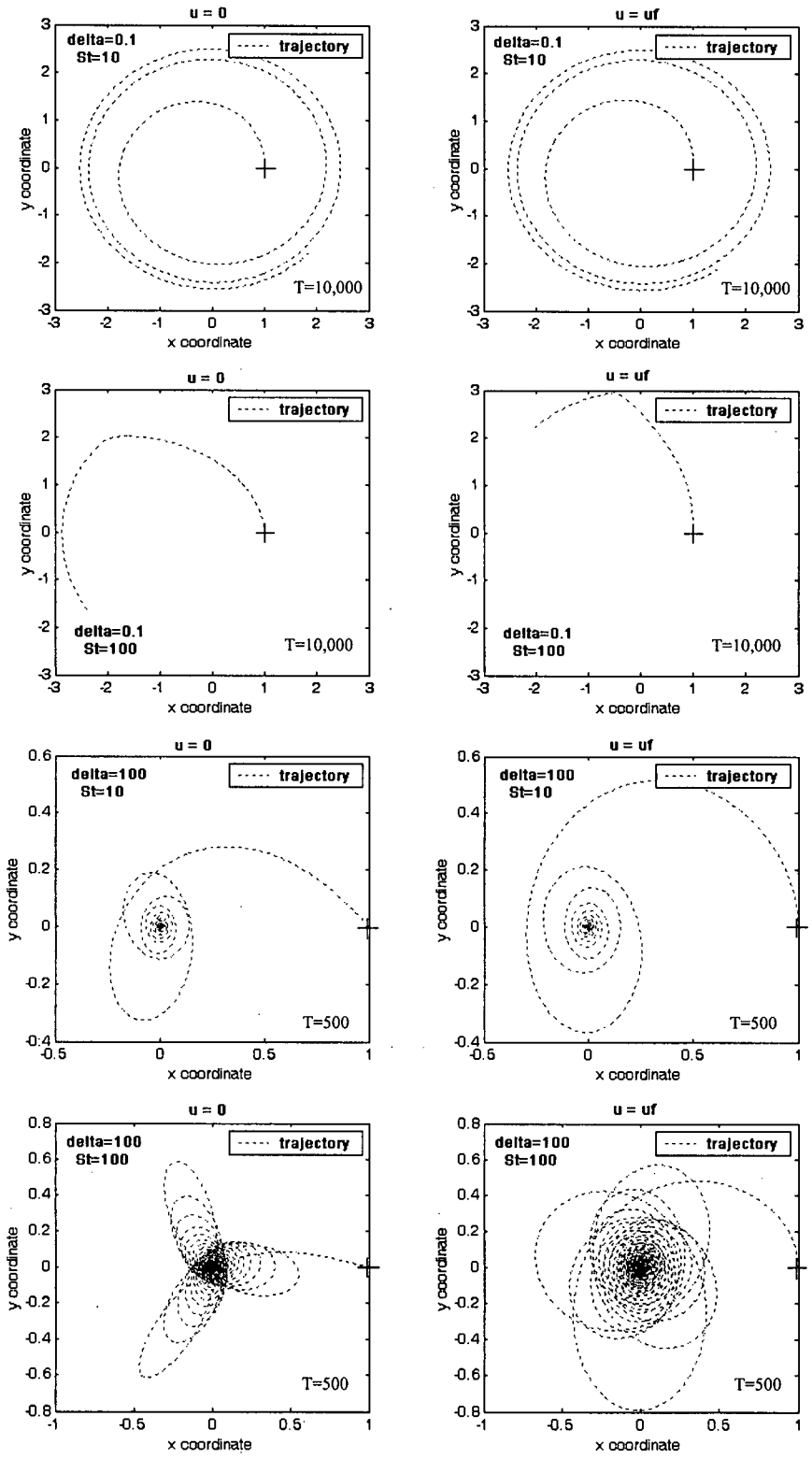


**Figure 3.6** Trajectories of particles released from $\vec{x}_p(t=0)=(1;0)$, with zero initial velocity (left) or with the local velocity (right), for different combinations of parameters.

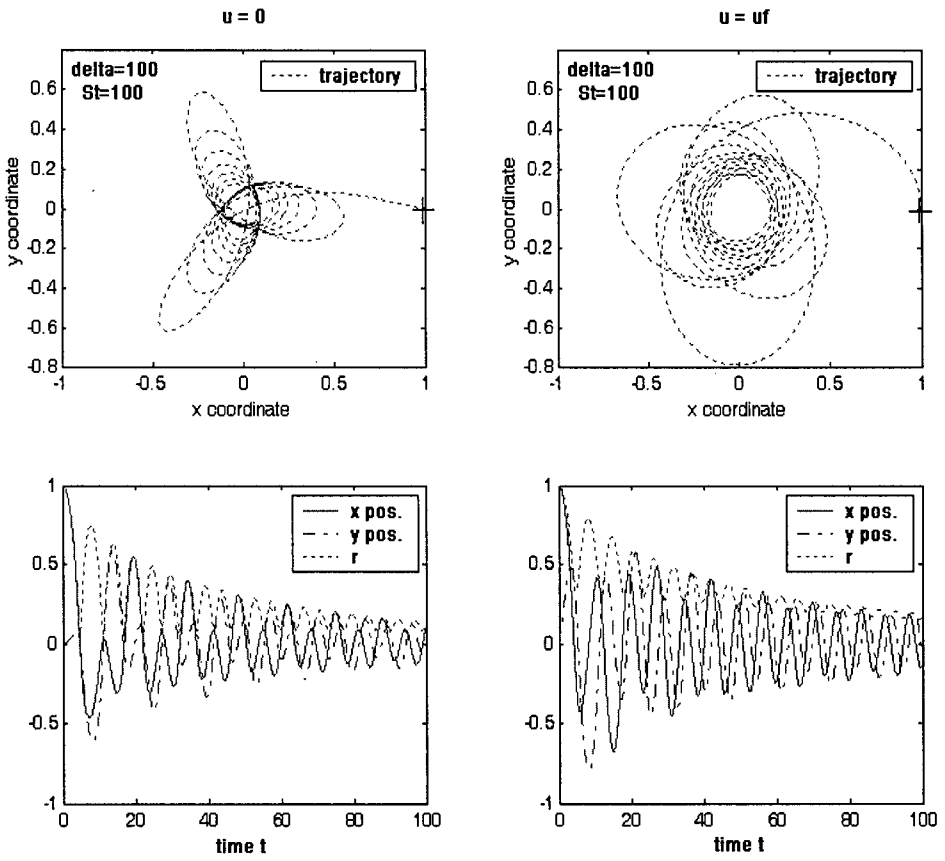


**Figure 3.7** Trajectories (top) and coordinates (bottom) of a light particle with a large Stokes number released with zero initial velocity (left) and with the local initial velocity (right).

In the rest of the thesis (Chapter 4 to Chapter 7), heavy particles with density ratio $\delta = 4*10^{-4}$ and Stokes number $St = 0.1$, $St = 1$ and $St = 10$ respectively are considered. For such heavy particles, the particle trajectory is not really affected by the value of the initial velocity (the particle could either be released from rest or with the local fluid velocity). Nevertheless, note that particles will be released with the local fluid velocity in the two-dimensional study (Chapters 4 and 5), since we are not so much interested in the initial stage for the two-dimensional study, and that they are released with a zero initial horizontal velocity in the three-dimensional study, since it is believed to be the closest to the real problem of particle settling through a pancake vortex.

# 4. DYNAMICS OF HEAVY PARTICLES IN THE 2D HORIZONTAL PLANE OF A PANCAKE VORTEX

From now on, heavy particles with density ratio $\delta = 4*10^{-4}$ and Stokes number $St = 0.1$, $St = 1$ and $St = 10$ respectively are considered. These characteristics are derived from the laboratory investigation of the particle dispersion by the coherent vortex structures present in the wake of a bluff-body, by Yang (1993). In his study, he used solid spherical glass beads in air.

The ratio of the particle diameter to the flow characteristic length scale (which has to be specified in the computer program to evaluate the particle Reynolds number) is, by choice:

$$\frac{d}{L} = 2*\sqrt{St}*10^{-3}. \qquad \textbf{(4.1)}$$

(Equation 4.1 respects the assumptions of the Maxey-Riley equation and the fact that the diameter varies as the square root of the Stokes number).

What we know or suspect:

- the particles will be ejected from the vortex centre because they are heavy
- heavy particles concentration may increase considerably at the edges of large-scale vortices (Tang et al. - 1992): this has to be verified and quantified

Simulations show that the particles always move away from the vortex centre, and that the ejection rate decreases as they are ejected. But a more detailed analysis is necessary to quantify the ejection rate, understand what forces are involved, and see what the overall result is when the flow is seeded with a large number of particles. This is the point of Chapters 4 and 5.

**Note 1**

Some of the facts presented in this section have already been investigated by Raju and Meiburg (1997), who studied the core region and the outer region of the vortex separately. The interesting aspect of the present study, which integrates the core region and the outer region in a single velocity profile, is therefore to see how the patterns observed for particles in the outer region differ from the ones observed for particles which have evolved in the core region before entering the outer region. Some results obtained by Druzhinin (1994) are also used or verified. In particular, a wave propagating phenomenon will be visualized in the concentration field, the existence of which has been argued by Druzhinin (1994).

**Note 2**

Particles are released with the local fluid velocity (see section 3.6 for comments about the role of the initial velocity).

## 4.1 The ejection rate ($\frac{\dot{r}}{r}$ or $\dot{r}$): general trend

The term 'vortex core' will refer to the central region of the vortex where the fluid velocity can be approximated by a solid body rotation (because of the viscosity of the fluid). The radial position $r = 1/\sqrt{2}$ will be considered as the upper limit of the core region. The region outside the core will be referred to as the outer region (see Figure 4.1).

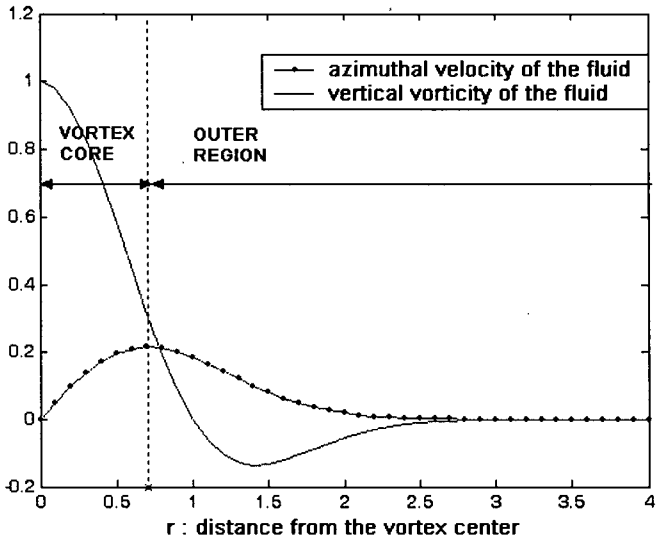


**Figure 4.1** Fluid vorticity and velocity profiles in the horizontal, with the distinction between the vortex core region and the outer region.

A heavy particle is now released very close to the vortex centre (Figure 4.2). The radial velocity (dr/dt) is computed as the particle is getting ejected. Three different Stokes number are considered: 0.1, 1 and 10.

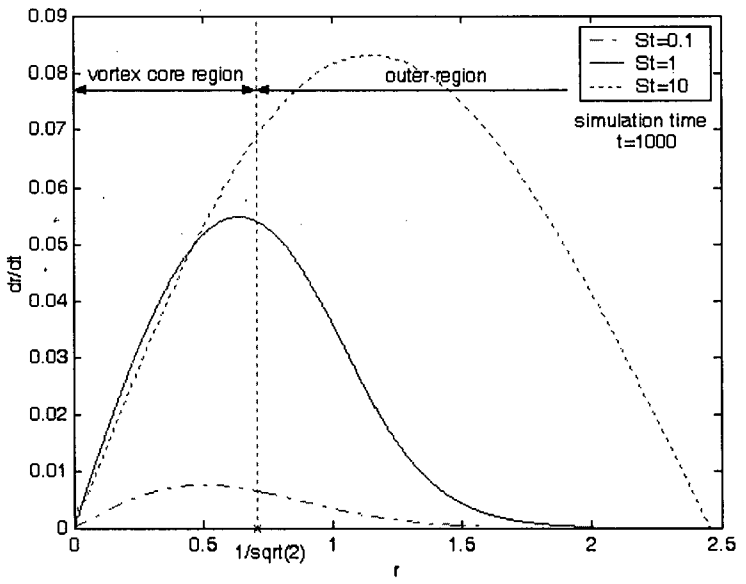


**Figure 4.2** Radial velocity of the particle with respect to its radial displacement ($r$). The particle is released at $(x0; y0) = (0.01; 0)$ i.e. very close to the vortex centre, with a different Stokes number each time.

The line drawn indicates the upper limit of the vortex core region. Roughly speaking, the **core region** is associated with an **increase of the radial velocity**, whereas the **outer region** is associated with a **decrease of this radial velocity**. Also, a particle with a smaller Stokes number reacts quicker to the change in the velocity profile.

## 4.2 Forces involved in the radial direction

As mentioned in section 3.2.2, for very small values of the density ratio, the main forces are due to inertia and drag. The simplified equations written in the Cartesian coordinates are:

$$\ddot{x} = \frac{1}{St}(-\frac{c}{2} y \exp(-r^2) - \dot{x}) \tag{4.2}$$

$$\ddot{y} = \frac{1}{St}(\frac{c}{2} x \exp(-r^2) - \dot{y}) \tag{4.3}$$

The full equation for the radial displacement is:

$$(1+\frac{\delta}{2})\ddot{r} = -\frac{1}{St}\dot{r} + (1+\frac{\delta}{2}) r \dot{\theta}^2 - \frac{c}{4}\delta r \dot{\theta} \exp(-r^2) - (\frac{c}{2})^2 \delta r \exp(-2r^2) \tag{4.4}$$

(in its simplified version: $$\frac{\ddot{r}}{r} = -\frac{1}{St}\frac{\dot{r}}{r} + \dot{\theta}^2 \tag{4.5}$$

the equation for the azimuthal direction being:

$$(1+\frac{\delta}{2})\frac{d}{dt}(r^2\dot{\theta}) = \frac{1}{St}(\frac{c}{2} r^2 \exp(-r^2) - r^2\dot{\theta}) + \frac{c}{4}\delta(1-2r^2) r \dot{r} \exp(-r^2)\ ) \tag{4.6}$$

The left hand side of Equation 4.4 and the last term of the right hand side are the inertial term (radial acceleration plus centrifugal term), the first term on the right hand side is the drag term, and the other terms are negligible and come from pressure gradient force and virtual mass.

For simplification, the left hand side is called 'the acceleration term', the Stokes drag 'the drag term' and the rest of the terms 'the centrifugal term'.

$$[(1+\frac{\delta}{2})\ddot{r}] = [-\frac{1}{St}\dot{r}] + [(1+\frac{\delta}{2})r\dot{\theta}^2 - \frac{c}{4}\delta r\dot{\theta}\exp(-r^2) - (\frac{c}{2})^2\delta r\exp(-2r^2)]$$

acceleration drag centrifugal term **(4.7)**

So, how do the forces involved evolve as the particle is getting ejected?

If we neglect the effect the pressure gradient force and of the virtual mass, the only term which the fluid velocity profile impacts directly on is the azimuthal drag term, and therefore the rotation rate of the particle and the centrifugal term of the radial equation. It is all the more the case that the Stokes number is small, since a larger drag means that the particle responds better to the fluid velocity. In the **core region**, where the azimuthal fluid velocity increases as the particle is ejected, the rotation rate of the particle is expected to **increase** (because of the drag term), and the **centrifugal term** with it. On the other hand, in the **outer region** of the vortex, the rotation rate is expected to **decrease**, as well as the **centrifugal term**.

Figure 4.3 gives the absolute values of the forces mentioned above, for a Stokes number $St = 0.1$, $St = 1$ and $St = 10$, and for a particle released successively in the core region and in the outer region. It is observed that the centrifugal force can increase while the particle is in the core region, that it decreases as the particle evolves in the outer region, and that it's all the more true when the particle has a small Stokes number. It is worth noting that, as the Stokes number gets larger, one does not see a monotonic increase of the centrifugal force, but rather a decrease followed by an increase.

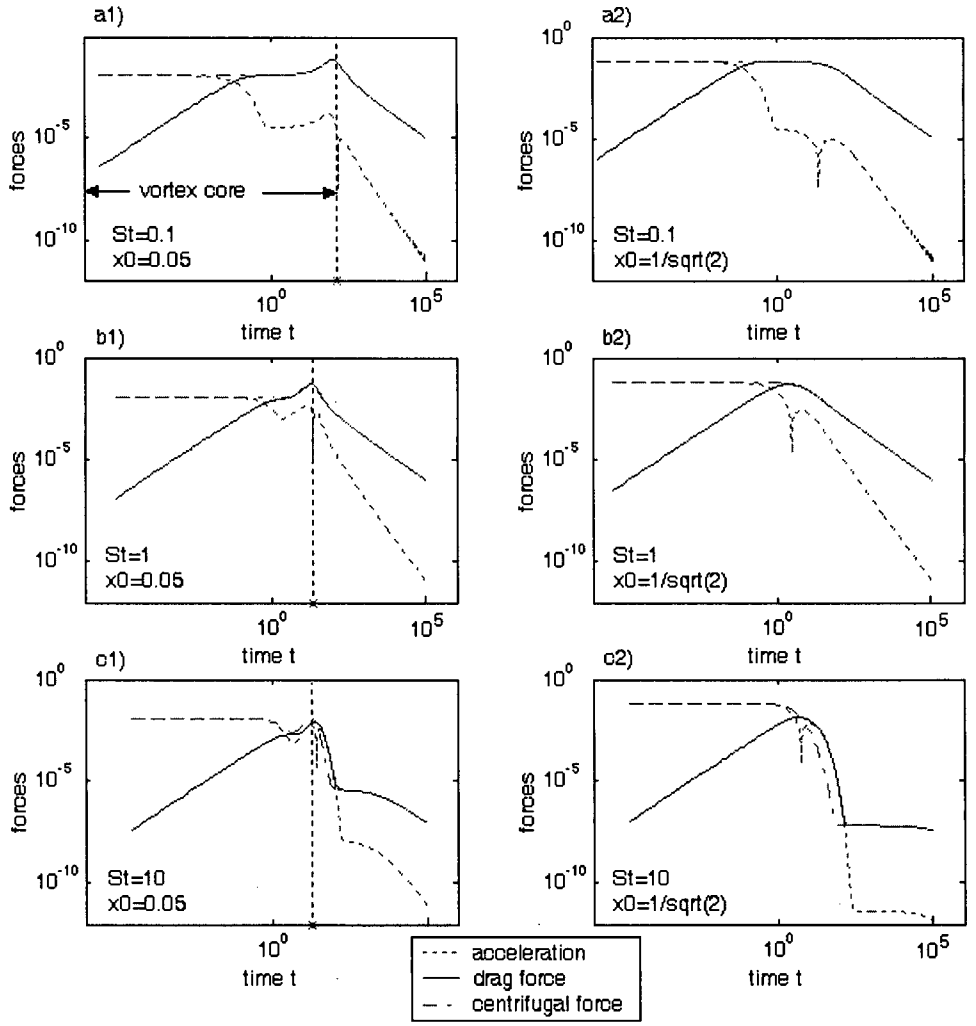


**Figure 4.3** Logarithmic plots of the absolute values of the 'acceleration', the 'drag force' and the 'centrifugal force', with respect to time. On the left: particle released close to the centre (evolving first in the core region). On the right: particle released on the lower limit of the outer region (and therefore evolving exclusively in the outer region)

Figure 4.3 also illustrates that for a Stokes number less than one, there is an initial balance between the 'acceleration force' and the 'centrifugal force' (the drag force indeed is zero since the initial velocity of the particle is set to be equal to the local fluid velocity). This initial balance is quickly replaced by a balance between drag and centrifugal forces (the solid line being superimposed on the dash dot line). On the other hand, for a Stokes number of 10, the initial and

final balances are the same but there is an intermediate regime in which the acceleration term and the drag term are in balance. The transition between the intermediate regime and the final regime is sharp.

Thus, fundamental qualitative differences exist between the cases $St = 0.1$ and $St = 1$ on the one hand, and the case $St = 10$ on the other hand. In addition, the bigger the Stokes number is, the weaker the influence of the vortex on the particle, and therefore the longer the intermediate regime is (indeed, the centrifugal term directly reflects the influence of the vortex on the particle and it would be zero in the absence of a vortex). Figure 4.4 shows an enlargement of graph c1) of Figure 4.3, for a better illustration.

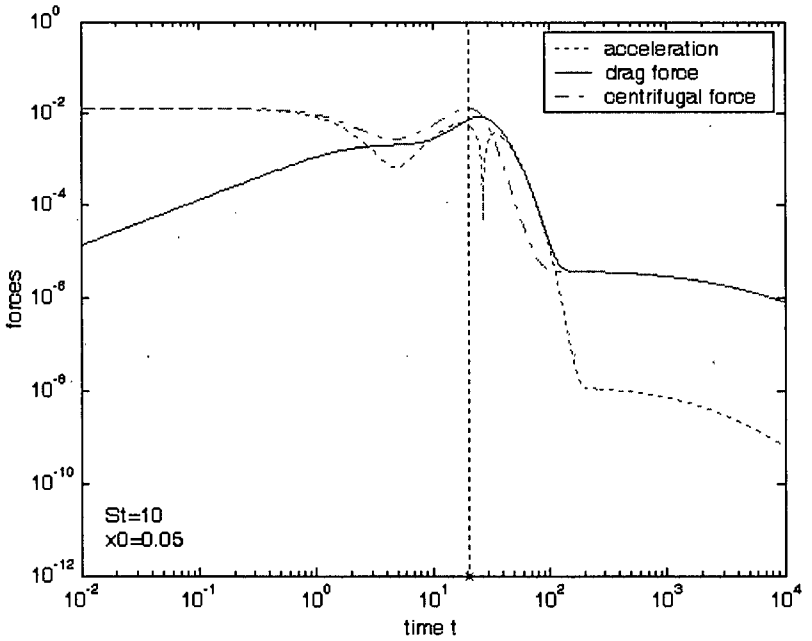


**Figure 4.4** Absolute values of the 'acceleration', the 'drag force' and the 'centrifugal force', with respect to time, for a particle with St=10 released close to the vortex centre.

**Summary**

In the case of a very heavy particle, the inertia (acceleration and centrifugal terms) and the drag are the only important forces. In the initial stage, the acceleration force balances the centrifugal force, whereas in the final stage, the drag balances the centrifugal force. An intermediate regime where drag balances the acceleration force exists for particles having a sufficiently large Stokes number. The intermediate regime corresponds to the regime where the particle is 'not affected' by the presence of the vortex.

## 4.3 Analytical results for a small Stokes number ($St < 1$)

For small values of the Stokes number ($St < 1$), Druzhinin (1994) derived the general form of the equation for the radial velocity for a particle having a Stokes number small compared to unity, in a two-dimensional axisymmetrical vortex of velocity $u_\theta$ as:

$$\dot{r} = St\left(\frac{u_\theta^2}{r}\right). \tag{4.8}$$

Since:
$$u_\theta = \frac{r}{2}\exp(-r^2) \tag{4.9}$$

we get:
$$\dot{r} = \frac{St}{4} r \exp(-2r^2) \tag{4.10}$$

so that:
$$\ddot{r} = \frac{St}{4}\dot{r}(1-4r^2)\exp(-2r^2) \tag{4.11}$$

Therefore
$$\ddot{r} = f(r) \tag{4.12}$$

where
$$f(r) = \left(\frac{St}{4}\right)^2 r(1-4r^2)\exp(-4r^2). \tag{4.13}$$

We can predict in particular that for small Stokes numbers, the radial acceleration is positive for $r < 0.5$, is zero for $r = 0.5$ and negative for $r > 0.5$. This is in agreement with what is observed (see Figure 4.2). Of course, it would be nice too to derive an analytical expression of the radial acceleration for the case of a larger Stokes number, but that is much more difficult.

## 4.4 Particle dynamics in the core region

As illustrated in Figure 4.2, the radial velocity varies linearly with the distance form the vortex centre in the core region. The ratio (dr/dt)/r -which represents the ejection rate- is a constant. This constant seems to be highest for St=1. Figure 4.5 illustrates this effect on particles having a Stokes number equal to 0.01, 0.1, 1, 10 and 100 respectively, which are released close to the centre, at $(x0; y0) = (0.01; 0)$, with the local fluid velocity. A plateau region is observed on the graph for the ejection rate. It indicates that the ratio (dr/dt)/r can be approximated by a constant most of the time the particle is in the core region (after the transient has died away).

**Note about the initial ejection rate**

It's worth noting that the larger the magnitude of the Stokes number is, the larger the initial ejection rate will be. The initial ejection rate will not be considered in this section.

**Note about the St=100 case**

The case St=100 is not significantly different from the other cases even though the particle seems not to be affected by the vortex. Due to its strong inertia, the particle is ejected far from the vortex centre, but then its radial velocity quickly decays: the particle finally goes on a circular trajectory. The particle's motion is very slow at that stage, since the fluid velocity itself is very small at such a large distance from the vortex centre. So, strictly speaking, there is no case for which one can

say the particle is ejected 'out of the vortex'. It makes sense since the vortex does not have a clear extent in the horizontal direction (there is no radial position for which the azimuthal fluid velocity is strictly equal to zero).

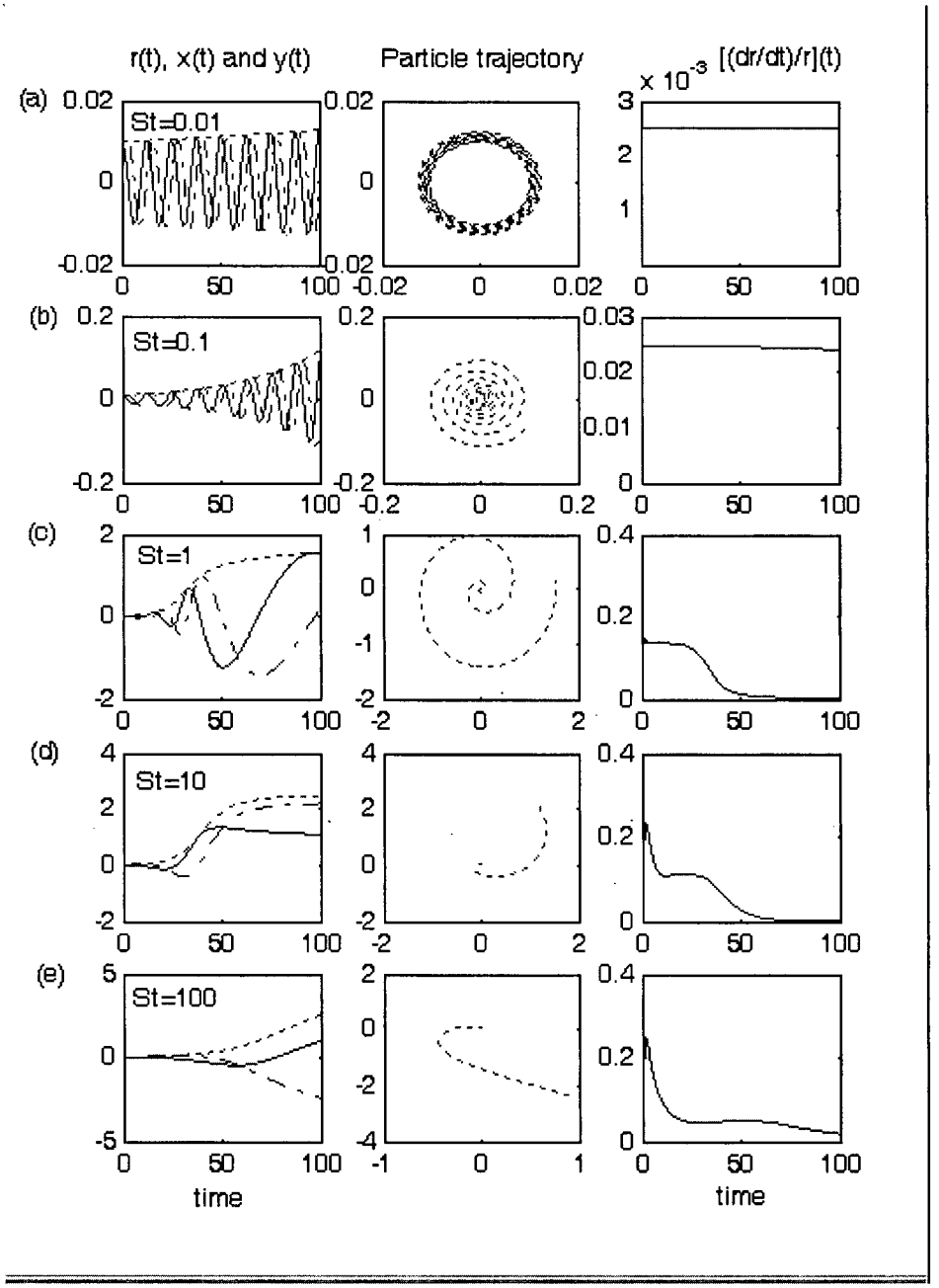


**Figure 4.5** Left: distance from the vortex centre r, Cartesian x and y coordinates, with respect to time. Centre: trajectory of the particle (x position versus y position). Right: ejection rate (dr/dt)/r with respect to time. (a) St=0.01, (b) St=0.1, (c) St=1, (d) St=10, (e) St=100. Particles released at $(x0; y0) = (0.01;0)$, with the local fluid velocity

**Case of a small Stokes number**

For small values of the Stokes number ($St < 1$), as previously discussed, Druzhinin (1994) derived the general form of the equation for the radial velocity, for a particle evolving in a two-dimensional axisymmetrical vortex:

In the vortex core region: $$u_\theta = \frac{r}{2}\exp(-r^2) \approx \frac{r}{2} \qquad \textbf{(4.14)}$$

So that, according to Druzhinin's calculations, the ejection rate can be approximated by :

$$\frac{\dot{r}}{r} = \frac{St}{4} \qquad \textbf{(4.15)}$$

The ejection rate as computed by Equation 4.15 is very close to the one obtained in the simulations with a Stokes number St=0.01 and St=0.1 (Figure 4.5). Equation 4.15 therefore is a good approximation for the ejection rate of particles having a small diameter.

**The ejection is optimal for an intermediate Stokes number**

When the values of the ejection rate in the plateau region of the simulations are compared (Figure 4.5 and Table 4.1), it appears that the ejection rate grows significantly as the Stokes number increases from small values to intermediate values, and slowly decays when the Stokes number is further increased. The ejection rate in the core region of the vortex is therefore optimal for an intermediate value of the Stokes number. This is clearly visualized in Figure 4.6.

| St | 0.01 | 0.1 | 1 | 10 | 100 |
|---|---|---|---|---|---|
| Ejection rate (approximation) | 2.5*10^(-3) | 2.5*10^(-2) | 1.4*10^(-1) | 1.1*10^(-1) | 5*10^(-2) |

**Table 4.1** Ejection rate in the core region for different Stokes numbers.

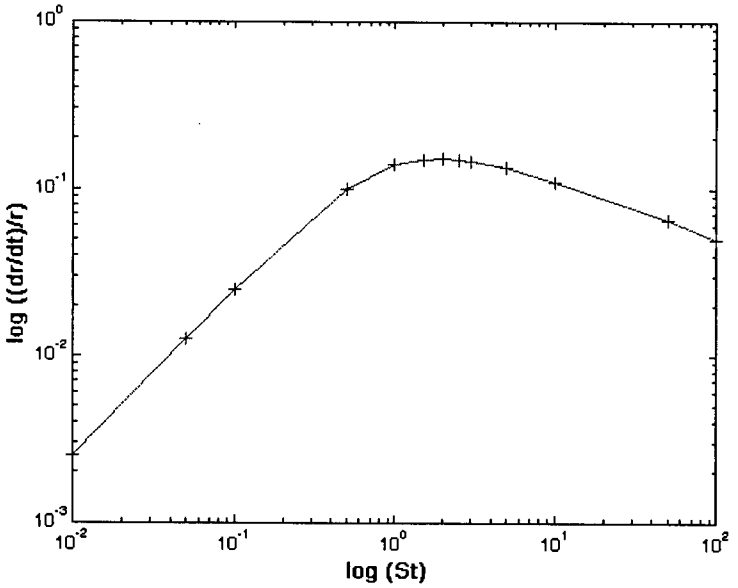


**Figure 4.6** Logarithmic plot of the ejection rate in the vortex core region, with respect to the Stokes number, as observed on simulations. (From data points corresponding to St = 0.01, 0.05, 0.1, 0.5, 1, 1..5, 2, 2.5, 3 5, 10, 50, 100.)

**Link with the linear analysis of the equations of motion**

The ejection/entrapment trend in the core region of the vortex can be evaluated by linearizing the equations of motion around the vortex centre. The linearization leads to equations of motion that are identical to the ones obtained by Raju & Meiburg (1997) when solving the case of a solid body rotation. This is not surprising since the velocity field of the pancake vortex linearized around the vortex center is equivalent to a solid-body rotation:

$$u_\theta = \frac{c}{2} r \exp(-r^2) \approx c\frac{r}{2} \qquad \text{for } r << 1. \tag{4.16}$$

The solution is of the form:

$$Z = c_1 e^{\lambda_1 t} + c_2 e^{\lambda_2 t} \tag{4.17}$$

The asymptotic ejection/entrapment rate is given by the real part of the largest eigenvalue: $\mathrm{Re}(\lambda_1)$, whereas its imaginary part corresponds to the asymptotic rotation rate of the particle.

Both rates depend on $St$, $\delta$ and $c$, and there is a value of the Stokes number for which the ejection/entrapment is optimal.

For reference, the exact expression of the real and imaginary parts of $\lambda_1$ are:

$$\mathrm{Re}(\lambda_1) = -\frac{a}{(2+\delta)} + \frac{1}{(2+\delta)}\frac{1}{\sqrt{2}}\left((a^2 - c^2\delta - \frac{9}{16}c^2\delta^2) + \sqrt{(a^2 - c^2\delta - \frac{9}{16}c^2\delta^2)^2 + 4a^2c^2(1+\frac{\delta}{4})^2}\right)^{\frac{1}{2}}$$

**(4.18)**

$$\mathrm{Im}(\lambda_1) = \frac{c\delta}{(8+4\delta)} + \frac{1}{(2+\delta)}\frac{1}{\sqrt{2}}\left(-(a^2 - c^2\delta - \frac{9}{16}c^2\delta^2) + \sqrt{(a^2 - c^2\delta - \frac{9}{16}c^2\delta^2)^2 + 4a^2c^2(1+\frac{\delta}{4})^2}\right)^{\frac{1}{2}}$$

**(4.19)**

For reference, the exact expression of the real and imaginary parts of $\lambda_2$ are:

$$\mathrm{Re}(\lambda_2) = -\frac{a}{(2+\delta)} - \frac{1}{(2+\delta)}\frac{1}{\sqrt{2}}\left((a^2 - c^2\delta - \frac{9}{16}c^2\delta^2) + \sqrt{(a^2 - c^2\delta - \frac{9}{16}c^2\delta^2)^2 + 4a^2c^2(1+\frac{\delta}{4})^2}\right)^{\frac{1}{2}}$$

**(4.20)**

$$\mathrm{Im}(\lambda_2) = \frac{c\delta}{(8+4\delta)} - \frac{1}{(2+\delta)}\frac{1}{\sqrt{2}}\left(-(a^2 - c^2\delta - \frac{9}{16}c^2\delta^2) + \sqrt{(a^2 - c^2\delta - \frac{9}{16}c^2\delta^2)^2 + 4a^2c^2(1+\frac{\delta}{4})^2}\right)^{\frac{1}{2}}$$

**(4.21)**

The contour plot of $\mathrm{Re}(\lambda_1)$ illustrates that for light particles ($\delta > 1$, $\delta$ being fixed), there is a value of the Stokes number for which the entrapment rate is maximized (Figure 4.7). On the other hand, for heavy particles ($\delta < 1$), and for a given density ratio delta, there is a Stokes number for which the ejection rate is maximized. This Stokes number is of intermediate value (~1).

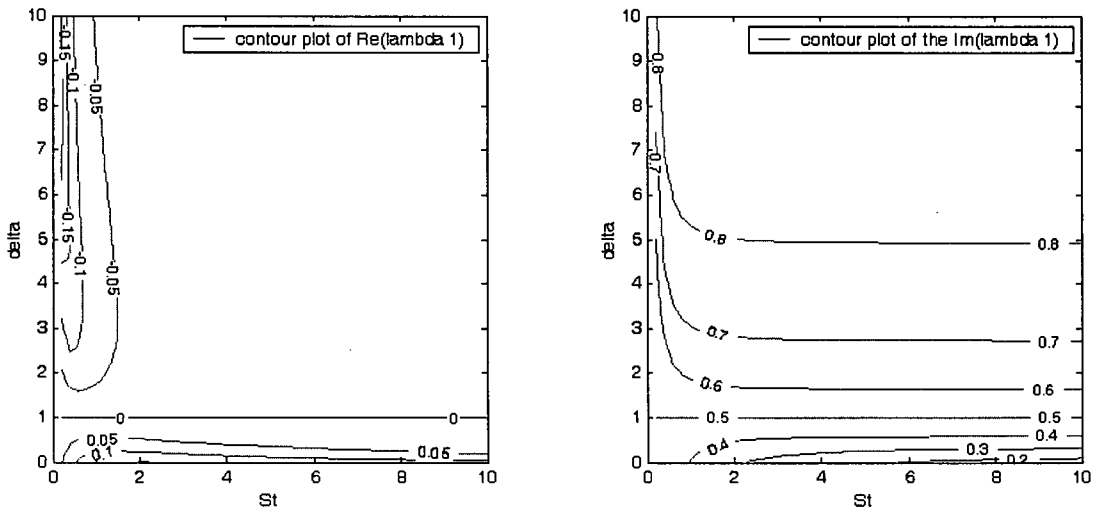


**Figure 4.7** Contour plot of the real and imaginary parts of the eigenvalues $\lambda_1$ and $\lambda_2$.

Moreover, for a very small value of the density ratio $\delta$, as the Stokes number is increased, lots of contour lines of the ejection rate are crossed till we get to an intermediate value of the Stokes number (St~1), implying a 'rapid growth' of the ejection rate. On the other hand, less contour lines are crossed when the Stokes number is further increased from an intermediate to a large value, implying a 'slow' decay of the ejection rate. Thus, the linear analysis is able to predict the evolution of the ejection rate observed in the simulation (Figure 4.6).

Nevertheless, the velocity field can be approximated by solid body rotation only as long as the particle remains close to the vortex centre. Because the calculated entrapment/ejection rates are asymptotic rates, they may or may not be reached depending on whether the particle is in this region for a long enough time. Simulations indicated that for the heavy particles considered, the ejection rate had time to reach a constant value, so that the analytical ejection rate given by $\mathrm{Re}(\lambda_1)$ is observed.

**Closer look at the ejection scenario: comparison between the St=1 and St=10 cases**

The cases St=1 and St=10 are now compared. The ejection rate in the plateau region is roughly 0.14 for the first case and 0.11 for the second. Obviously, the difference is significant but slight. So, how does that affect the particle trajectory?

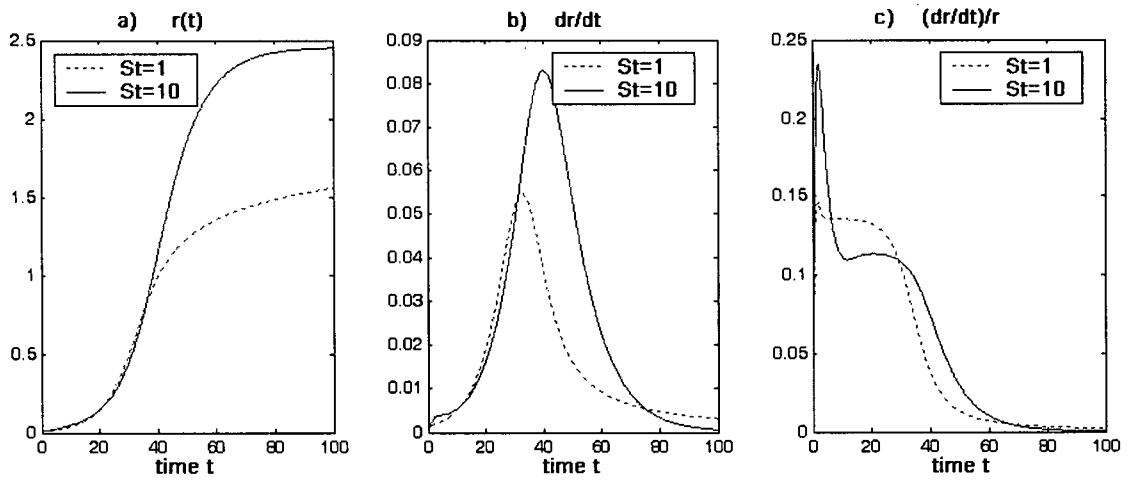


**Figure 4.8** a) Radial position, b) radial velocity and c) ejection rate, with respect to time, for 2 particles of Stokes number St=1 and St=10.

Figure 4.8 shows the radial position, velocity and ejection rate of two particles: one having a Stokes number of 1 and the other having a Stokes number of 10. They are released very close to the vortex centre, at the same initial position, with the local fluid velocity as their initial velocity.

As mentioned earlier, the radial velocity increases because of the solid-body rotation-like fluid velocity in the core region of the vortex, and decreases in the outer region of the vortex or in the 'transitional region' (depending on the Stokes number).

The St=1 particle reaches the upper-limit of the core region $r = 1/\sqrt{2}$ before the St=10 particle (at t=33.96, slightly before the other (t=34.47)). Therefore, in terms of the overall ejection performance, the St=1 particle achieves better ejection at those early times.

But, in fact, 4 stages can be distinguished.

1) Very early stage– $t<0.1$ – the 2 cases are undistinguishable

Initially $dr/dt=0$ so there is no drag in the radial direction. Since the Stokes number only affects the drag term in the equations of motion, and since the two particles are released in the same conditions (same initial position and velocity), the difference between the two cannot be observed.

2) Early stage – $0.1< t <10$ – stronger ejection for St=10 - doesn't last long.

The St=10 particle is ejected further at this stage. What happens is that the St=10 particle is still affected by the initial conditions, whereas the St=1 particle is able to adjust more quickly to the fluid velocity because of the stronger drag that applies on it. That is also apparent on the trajectory. The St=1 particle goes way more significantly on a circular trajectory, whereas the St=10 particle is going further from the vortex centre under the influence of its initial velocity vector.

3) Intermediate stage – $10 < t < 30$ – stronger ejection for St=1

As stressed previously, in the core region, after the initial transient has died away, the ejection rate is stronger for intermediate Stokes numbers. Even though the St=10 particle was initially ahead, the St=1 particle catches up, due to its larger ejection rate.

4) Late stage – $t > 30$ – ejection a lot stronger for St=10 – till it reaches large radius

The particles are now gone or almost gone from the core region. The St=1 particle is soon caught up. Indeed, in the outer region of the vortex, the ejection is stronger for increasing values of St (as will be discussed in the next section). But, as a result, the St=10 particle quickly reaches a region where the fluid velocity is very small. As a result, its radial velocity decreases. At some point, its

radial velocity even gets smaller than that of the St=1 particle, which, at that time (t~90), is still in a region where the fluid velocity is larger (i.e. the centrifugal effect is stronger). In other words, the St=1 particle 'is slowly ejected', whereas the St=10 particle is ejected initially more strongly, and then slows down, since it is 'already' at the 'edge' of the vortex.

As a result, the fact that there is an optimal ejection rate for intermediate Stokes numbers is expected not to have such a significant influence on the overall dispersion, because of what is happening later in the outer region.

**Possibility of accumulation in the vortex core region?**

It is interesting to investigate the possibility of accumulation because that would, in reality, lead to the possibility for particles to flocculate, which has great impact on the dispersion and is of relevance for many environment related problems.

Because: $\frac{\dot{r}}{r} = \mathrm{Re}(\lambda_1) > 0$, the radial velocity increases with the distance from the vortex centre, so the further the particle is from the vortex centre, the larger its radial velocity is. Therefore, **no accumulation or overtaking** is possible with particles having the **same characteristics** (same $\lambda_1$).

**Possibility of overtaking and accumulation for particles of different characteristics?**

Because the ejection rate depends on the particle characteristics, it is worth investigating the possibility of overtaking of a particle by another particle released closer to the centre but having a larger ejection rate. Three particles having Stokes numbers equal to, respectively: $St_1 = 0.1$, $St_2 = 1$ and $St_3 = 10$, and a density ratio $\delta = 4*10^{-4}$, are considered (Figure 4.9). Let $r0_1$,

$r0_2$, $r0_3$, $\lambda_1$, $\lambda_2$ and $\lambda_3$ be their initial position and ejection rates in the core region. Particle #2 has the largest ejection rate (intermediate Stokes number). It is released the closest to the centre:

$$r0_2 = 0.05 \quad \text{and} \quad r0_1 = r0_3 = 0.125$$

Assuming the simple law: $r(t) \approx r0\exp(\lambda t)$ can be applied (which is a crude approximation given that it neglects the influence of the initial conditions), overtaking of particle #1 by particle #2 and of particle #3 by particle #2 are supposed to happen at $t \approx \frac{\log(r0_1) - \log(r0_2)}{\lambda_2 - \lambda_1} \approx 7.33$ and $t \approx \frac{\log(r0_3) - \log(r0_2)}{\lambda_2 - \lambda_3} \approx 22.90$ respectively.

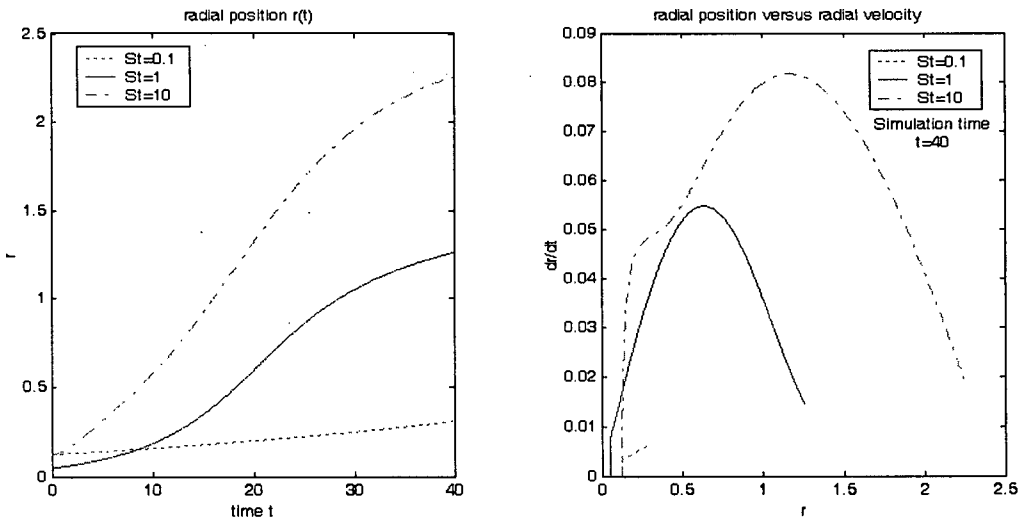


**Figure 4.9** Radial position with time (left) and radial velocity with respect to radial position, for three particles of Stokes number $St_1 = 0.1$, $St_2 = 1$ and $St_3 = 10$. The first and third particles are released at the radial position $r0_1 = r0_3 = 0.125$ and the second particle at $r0_2 = 0.05$.

Results presented in Figure 4.9 illustrate that particle #1 is overtaken by particle #2 at $t \approx 8.58$, which is consistent with the prediction, whereas particle #1 is not able to overtake particle #3, contrary to what simple predictions tell. This is due to the fact that the larger the Stokes number

is, the larger the initial ejection rate is. Moreover, particle #3 ($St_3 = 10$) is released further than particle #2, and therefore receives a stronger initial impulse (since its initial azimuthal velocity is set to be equal to the local fluid velocity and the fluid velocity increases with the distance from the vortex centre). The predictive calculation, which ignores the initial stage, is not able to accurately predict the radial displacement of particle #3.

The fact that two **particles of different characteristics** (either diameter or density) can get closer to each other while being ejected implies that particles will likely accumulate in an experiment involving a large number of them, resulting in some **inhomogeneities**.

**Brief assessment of the situation at the upper limit of the core region** ($r = 1/\sqrt{2}$)

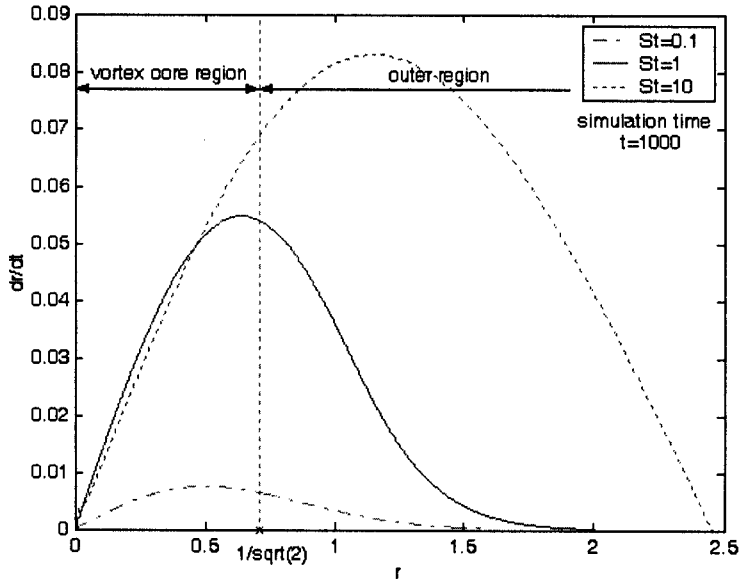


**Figure 4.10** Radial position versus radial velocity for 3 particles of Stokes number St=0,1, St=1 and St=10, released at the same position, close to the vortex centre at $(x0; y0) = (0.01; 0)$.

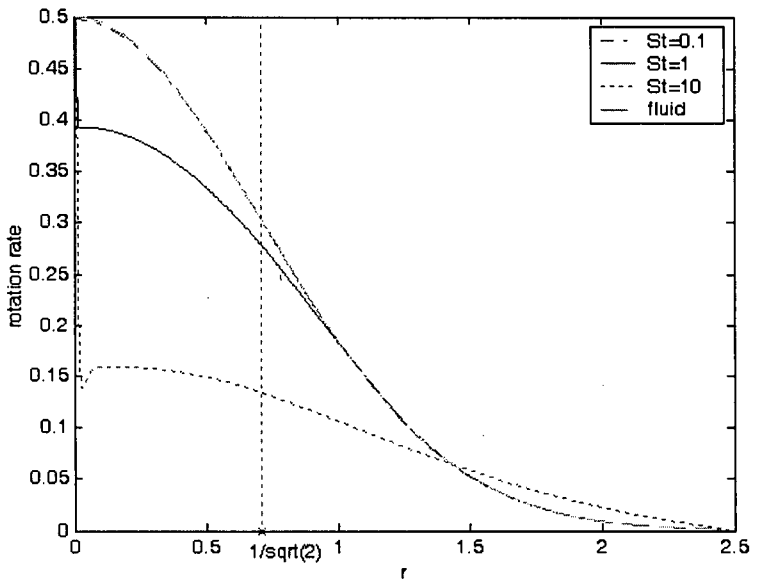


**Figure 4.11** Rotation rate with respect to the radial position for the same 3 particles as in the Figure 4.9.

As Figures 4.10 and 4.11 illustrate, at $r = 1/\sqrt{2}$:

- the radial velocity of the particle increases with the Stokes number
- particles with small Stokes number have already felt that they are in the transitional region to the outer region: their radial velocity decreases
- the rotation rate decreases with the Stokes number (the bigger the particle, the slower the rotation) and is smaller than the fluid rotation rate, except for particles having a small Stokes number – in which case the rotation rate of the particles is equal to that of the fluid elements.Also, the St=10 particle surprisingly rotates faster than the fluid elements at some later stage.

**Conclusions – the core region of the vortex**

1) After the initial transient has died away, the radial velocity obeys the law: $\frac{\dot{r}}{r} = const(St, \delta) > 0$.

2) There is no accumulation of particles in the vortex core region with particles of the same characteristics.

3) The ejection rate is maximum for an intermediate Stokes number (St~1), but it is certainly not that significant for the later stages; the overall dispersion is expected to be more affected by what is happening later in the outer region.

4) There is a possibility of accumulation and creation of inhomogeneities in the core with a pool of particles having different diameters or density.

5) When reaching the upper-limit of the core region, the radial velocity has already started to decrease for particles with a Stokes number $St \leq 1$, since they can 'feel' they are in the transitional region; particles with a bigger Stokes number are less sensitive to the fluid flow and react later.

## 4.5 Particle dynamics in the outer region

This section deals with particles that are released at $r = 1/\sqrt{2}$ (referred to as point B in Figure 3.1 section 3.3.3), and therefore evolving exclusively in the outer region of the vortex.

### 4.5.1 Ejection rate

In the outer region, **the ejection is stronger for increasing values of the Stokes number** (Figure 4.2 section 4.1). Particles with a small Stokes number are slowly ejected, whereas particles with a large Stokes number are initially ejected a greater extent, but then they cannot evolve much anymore, since they are already at the 'edge' of the vortex.

Contrary to what was observed in the core region, the **radial velocity decreases** as the particle is ejected (apart from the very early stage where the particle starts from a zero radial velocity and is given an initial impulse of angular momentum). The decrease of the radial velocity is due to the fact that the azimuthal velocity of the fluid decreases with the radial distance, so the angular momentum of the particle obtained from the surrounding fluid tends to decrease as the particle is moving away from the vortex centre.

### 4.5.2 Possibility of accumulation (St=0.1/1) or overtaking (St=10)

As a consequence of the decrease of the radial velocity, a particle initially further from the vortex centre could be **overtaken** by a particle of the same characteristics initially located closer to the vortex centre and therefore having a bigger initial angular momentum.

To investigate the possibility of overtaking, the case of two particles of the same characteristics (density ratio $\delta = 4*10^{-4}$ and same Stokes number) is considered:. Particle #1 is released from $(x0; y0) = (1.0;0)$ and particle #2 from $(x0; y0) = (1.5;0)$.

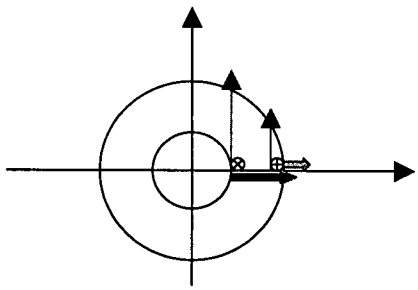

Will particle #1catch up particle #2?

The cases of three different Stokes numbers ($St = 0.1$, $St = 1$ and $St = 8$) are successively considered, on a long simulation time: t=10000 (Figure 4.12). The following is observed:

$St = 0.1$

Particle #1 has initially more momentum. Its radial displacement is slowly getting closer to that observed for particle #2, which it reaches asymptotically.

$St = 1$

As the Stokes number is increased, the inertia of the particles increases and the time it takes for particle #1 to reach the displacement of particle #2 decreases. For the intermediate Stokes number of one, their radial displacements are indistinguishable (except at a very early stage, of course).

$St = 8$

For bigger Stokes numbers, particle #1 overtakes particle #2 at a very early stage and is quickly ejected further. In other words, **overtaking** occurs.

Therefore

- For a pool of identical particles with a Stokes number smaller than one, we can expect accumulation of particles occurring at a certain radius.

- On the other hand, with a pool of particles with a Stokes number of 8, there might be overtaking, which, in turn, might **qualitatively change the dispersion** process.

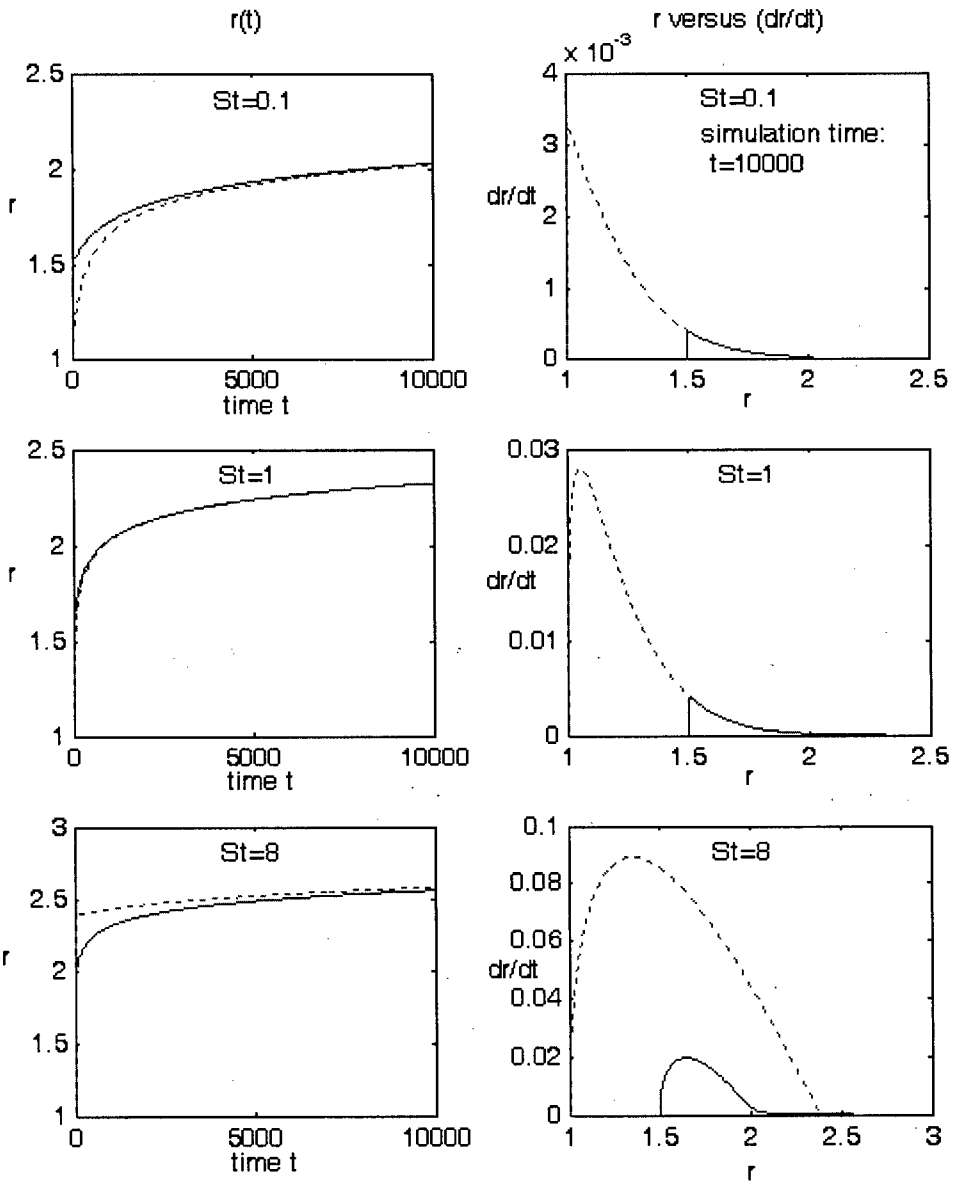


**Figure 4.12** On the left: distance from the vortex centre with time r(t); on the right: distance from the vortex centre (r) versus the radial velocity (dr/dt). From top to bottom: St=0,1; St=1; St=8.

### 4.5.3 Qualitative difference between St=0.1/1 and St=10

In section 4.5.2, it was found that there is a qualitative difference in the dynamics of the particles depending on whether their Stokes number is larger or smaller than one. This qualitative difference is also apparent in the graph of r(t) and has to be linked to the difference in the **balance of forces** that takes place **in the radial direction**, as discussed in section 4.2.

Figure 4.13 (a, b, c) illustrates the radial displacement with time, as well as the balance of forces, for a particle having a Stokes number of 0.1, 1 and 10 respectively. The radial displacement for St=10 is qualitatively different from that corresponding to the two other cases. It is the existence of **an intermediate regime** where **drag balances the centrifugal force** that introduces a qualitatively different law for r(t), and that **enables a particle to overtake a particle having the same characteristics**.

Note also that the radial velocity increases with the Stokes number. The larger the Stokes number is, the farther away from the vortex centre the particles accumulate.

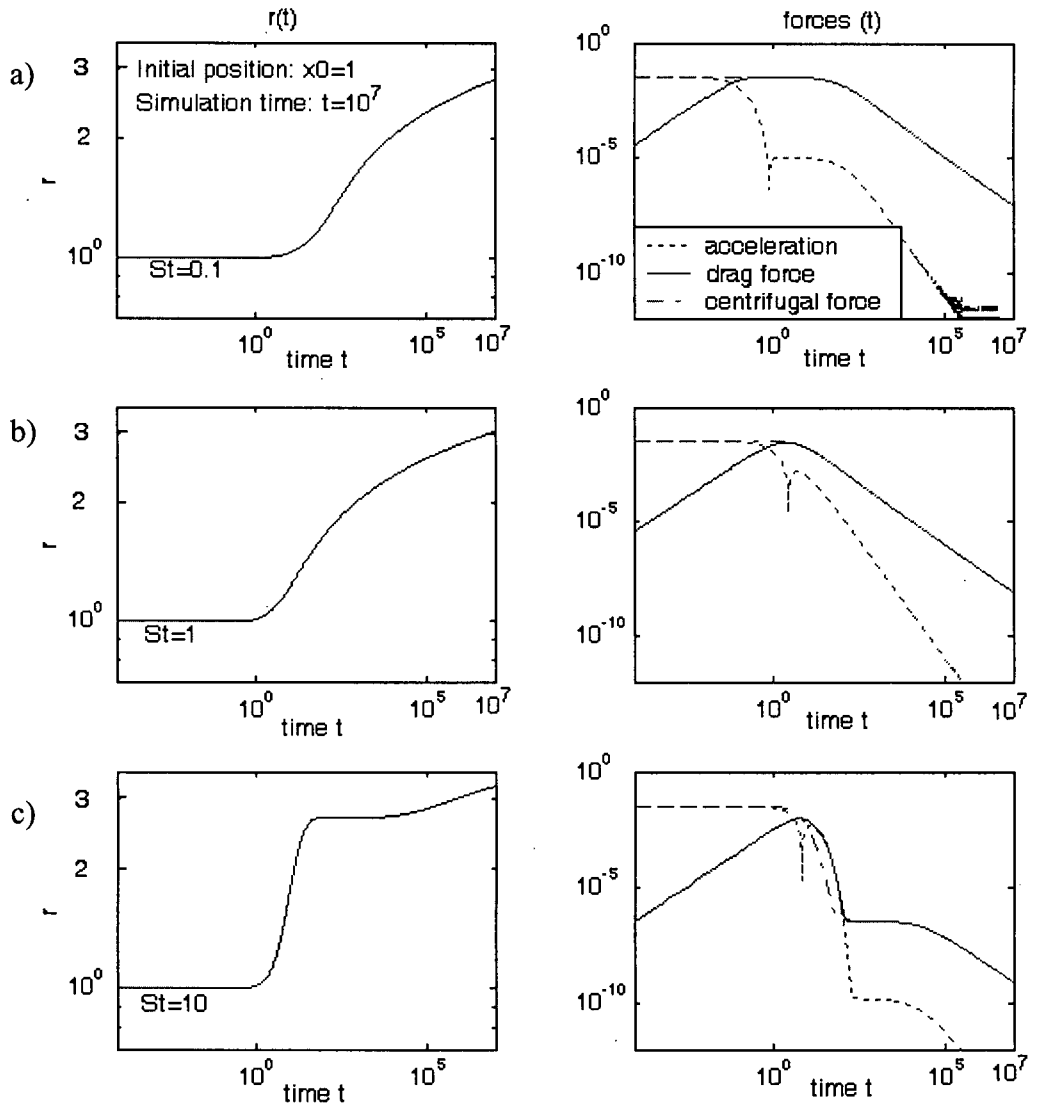


**Figure 4.13** Semi-logarithmic plot of the radial displacement with respect to time (left) and logarithmic plot of the absolute values of the forces involved in the radial direction (right): the 'acceleration', the 'drag force' and the 'centrifugal force'

$$[(1+\frac{\delta}{2})\ddot{r} = [-\frac{1}{St}\dot{r}] + [(1+\frac{\delta}{2})r\dot{\theta}^2 - \frac{c}{4}\delta r\dot{\theta}\exp(-r^2) - (\frac{c}{2})^2\delta r\exp(-2r^2)]$$

*acceleration* *drag* *centrifugal term*

a) St=0.1; b) St=1; c) St=10.

# 4. CONCENTRATION PROFILES IN THE HORIZONTAL PLANE OF A PANCAKE VORTEX

A large number of particles are seeded on a large area that goes beyond the vortex core region, on a regular grid (step $dx = dy$) of a disc of radius [0 3]. The initial distribution is thus homogeneous.

As with previous simulations, particles are released with the local fluid velocity. The concentration is calculated as the average number of particles per unit area for each annular region $dr$ (see Figure 5.1). It is non-dimensionalized by a reference level $c_0$, where $c_0$ is the uniform particle concentration existing at the beginning. The time evolution of the concentration profiles for $St = 0.1$, $St = 1$ and $St = 10$ successively will be examined in this chapter.

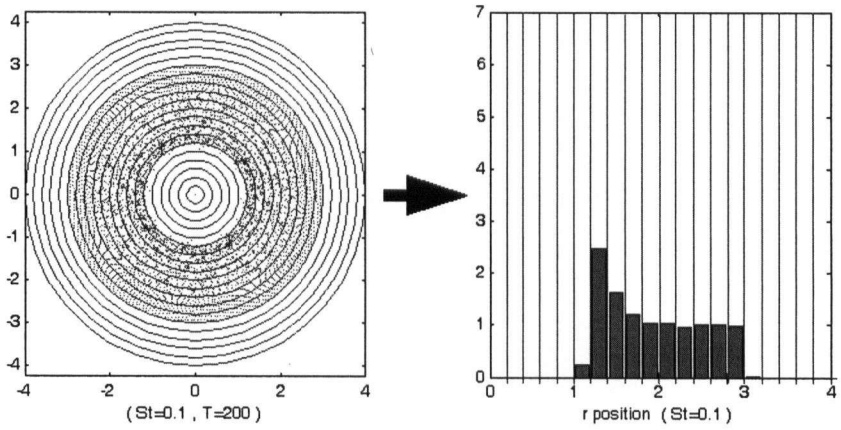


**Figure 5.1** Graph presenting how the concentration profiles are calculated. On the left: particle distribution pattern. On the right: concentration profile in the radial direction. The concentration is calculated for each annular region as the number of particles per unit area.

**Note**

The influence of the particles on the background fluid flow will be neglected, even though the concentration might get quite high in some regions of the flow field.

## 5.1 Snapshots of concentration profiles

In the following figures, snapshots of the dispersion patterns were obtained after seeding the fluid with 5026 particles (with a corresponding initial concentration $c_0 = 177$ particles per unit area). On the other hand, the concentration profiles, which require more particles to be accurate, were calculated for $5*10^7$ particles. Advantage was made of the axisymmetry of the problem by calculation the trajectories of only 4001 particles, initially located along a radius [0 4], and deducting from that the concentrations that would correspond to a case involving $5*10^7$ particles. (Solving the problem for $5*10^7$ particles directly would have been much too expensive computationally.) The corresponding particle concentration was calculated on annular regions of width $dr = 0.025$.

Snapshots are given for each three cases:

- St=0.1: at T=0, 10, 20, 50, 100, 200, 500 and 1000
- St=1: at T=6, 10, 20, 50, 100, 200, 500 and 1000
- St=10: at T=4, 6, 7, 8, 10, 20, 50, 100, 500 and 1000

Comments will follow (section 5.2).

# St=0.1

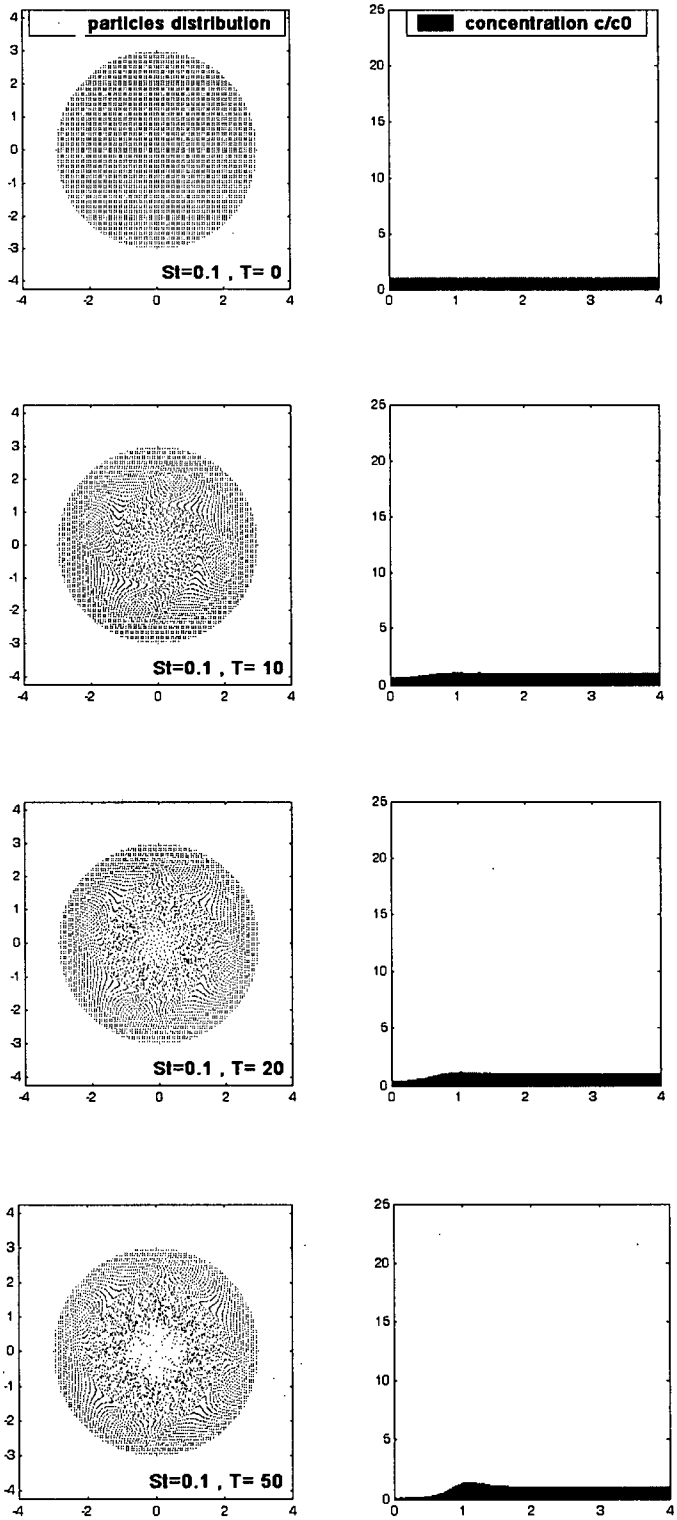
particles distribution
concentration c/c0
St=0.1 , T= 0
St=0.1 , T= 10
St=0.1 , T= 20
St=0.1 , T= 50

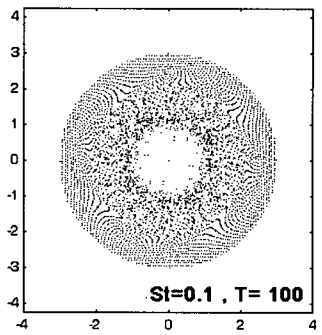
St=0.1 , T= 100

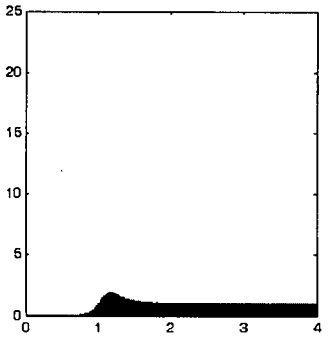

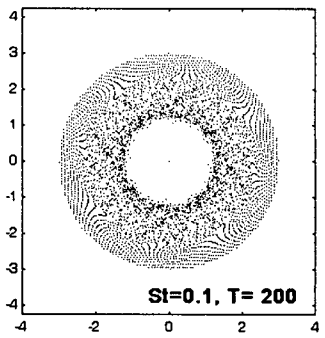
St=0.1, T= 200

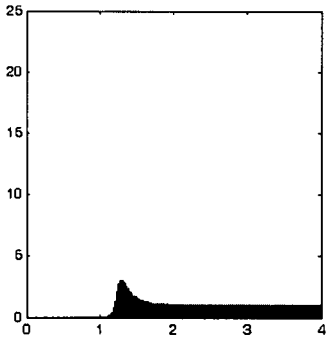

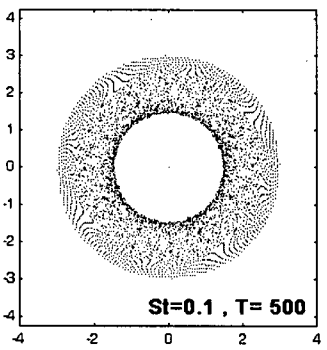
St=0.1 , T= 500

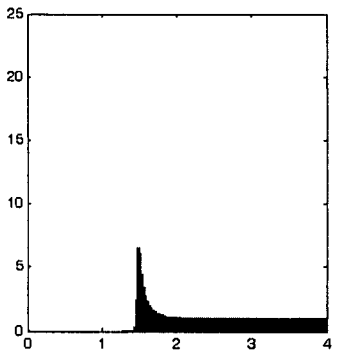

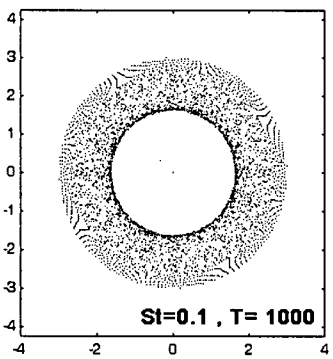
St=0.1 , T= 1000

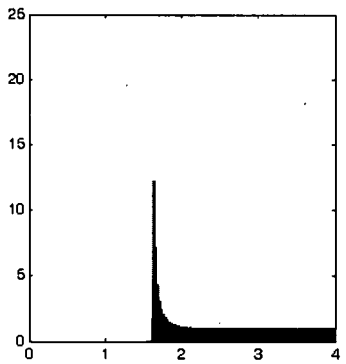

# St=1

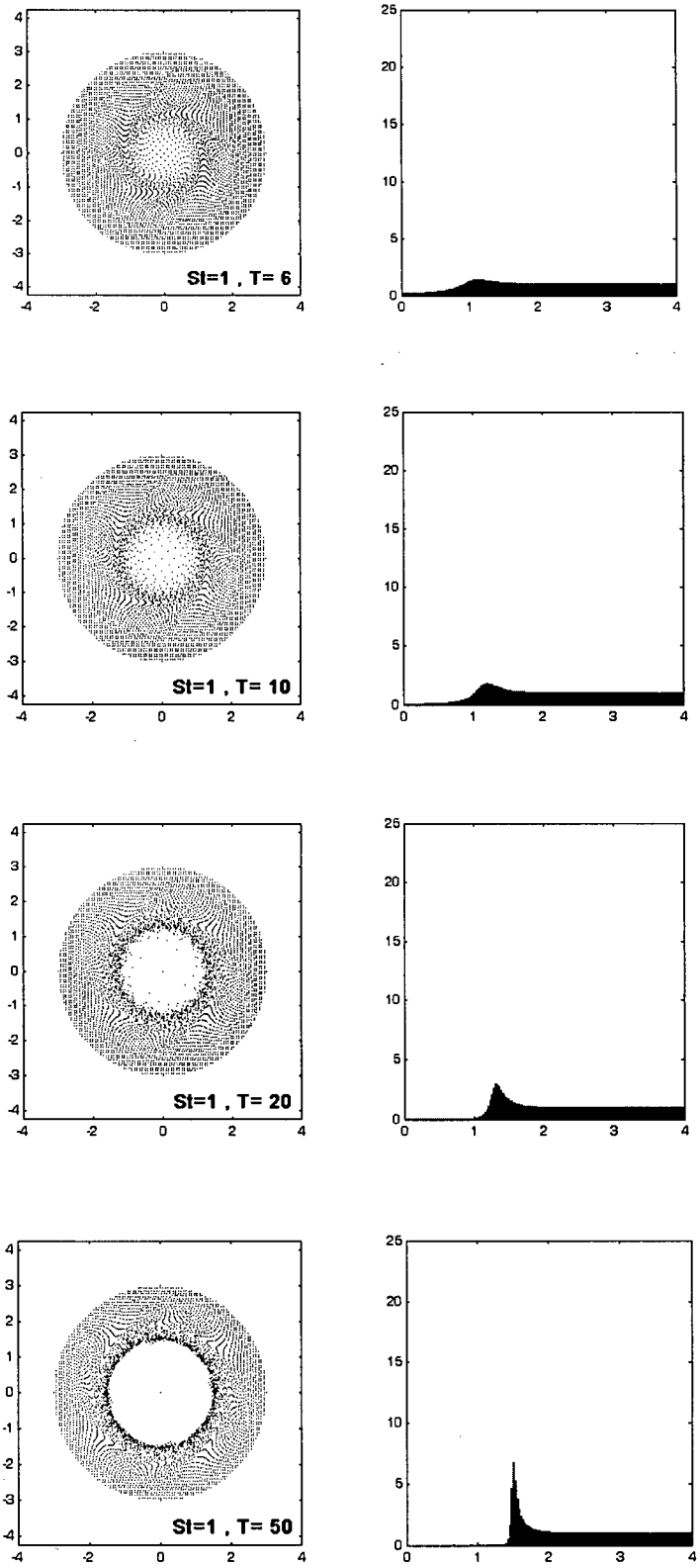

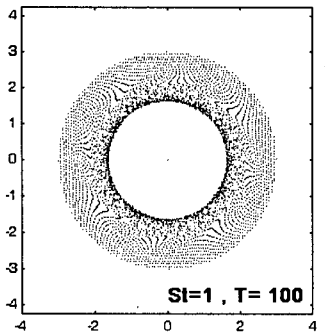
St=1 , T= 100

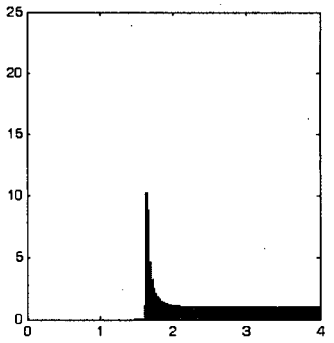

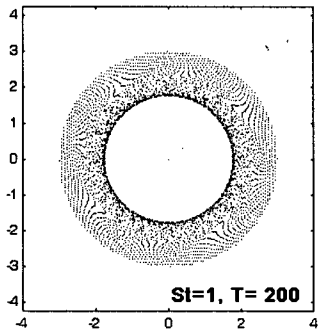
St=1, T= 200

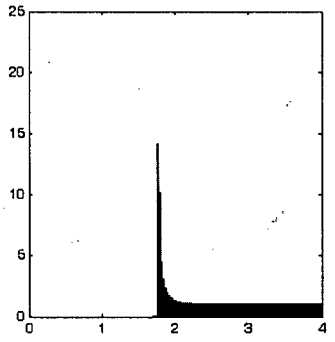

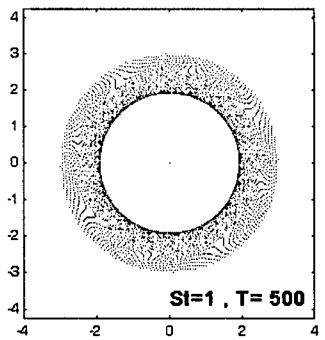
St=1 , T= 500

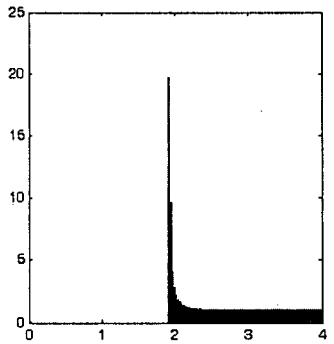

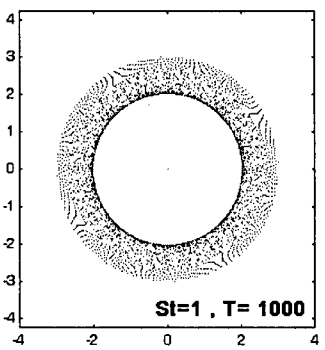
St=1 , T= 1000

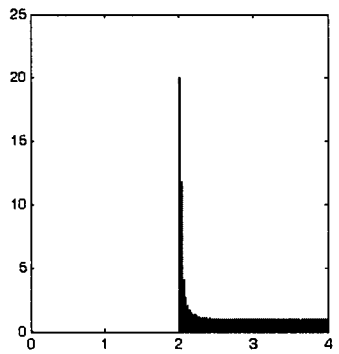

# St=10

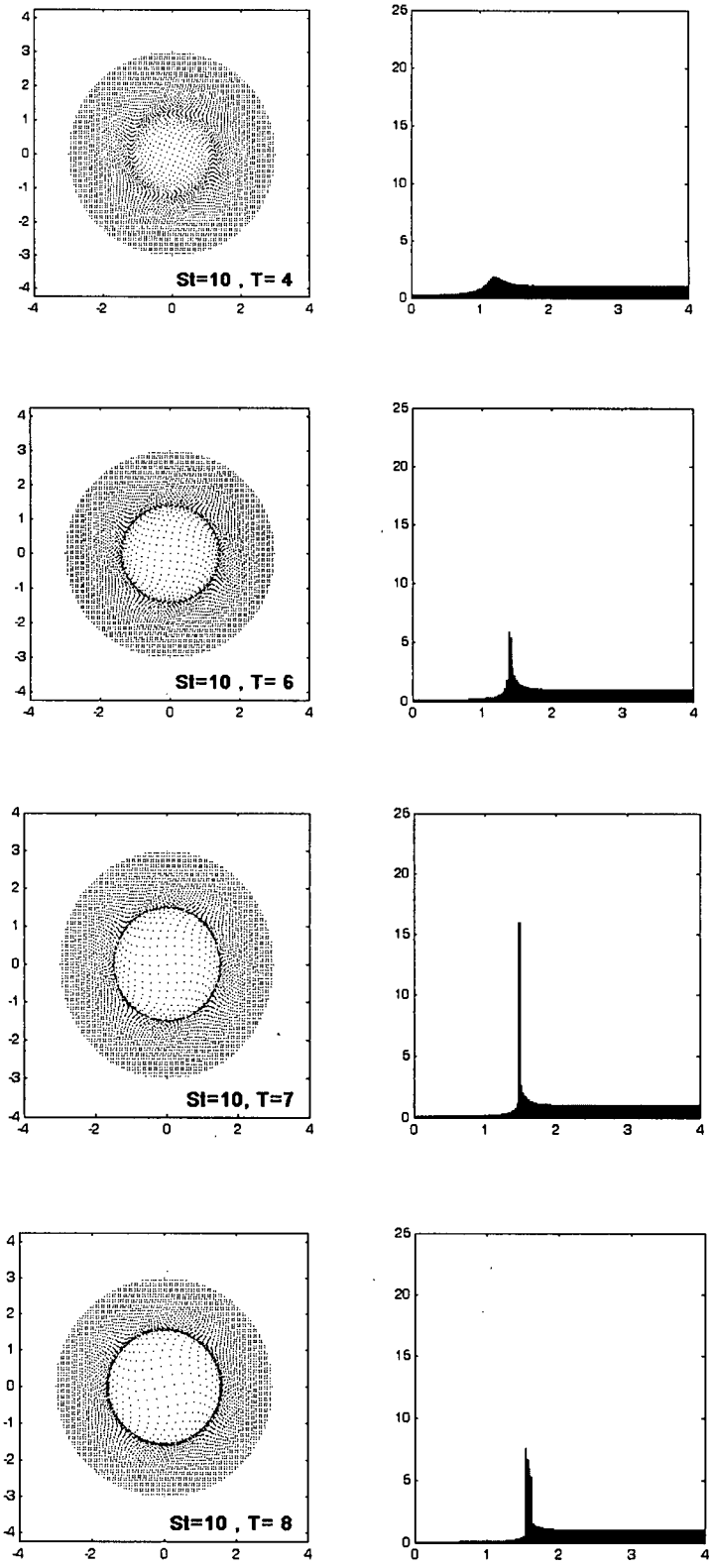

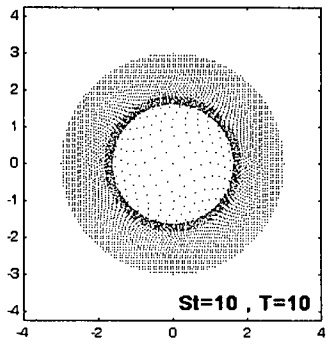
St=10 , T=10

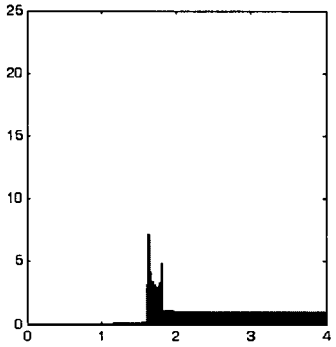

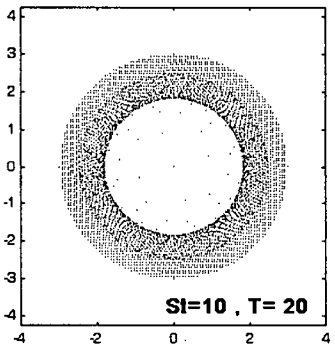
St=10 , T= 20

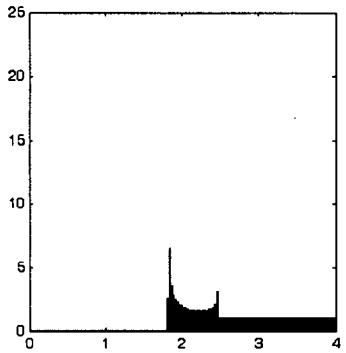

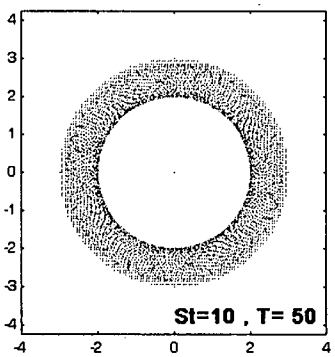
St=10 , T= 50

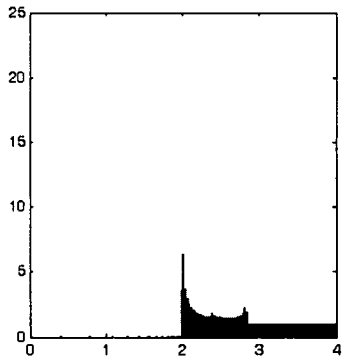

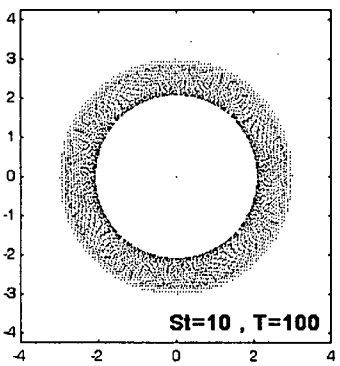
St=10 , T=100

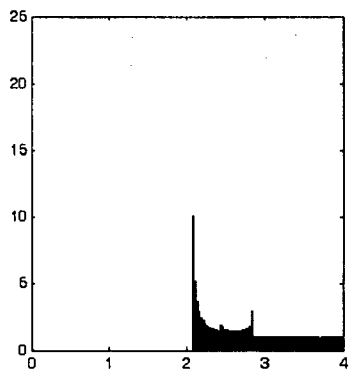

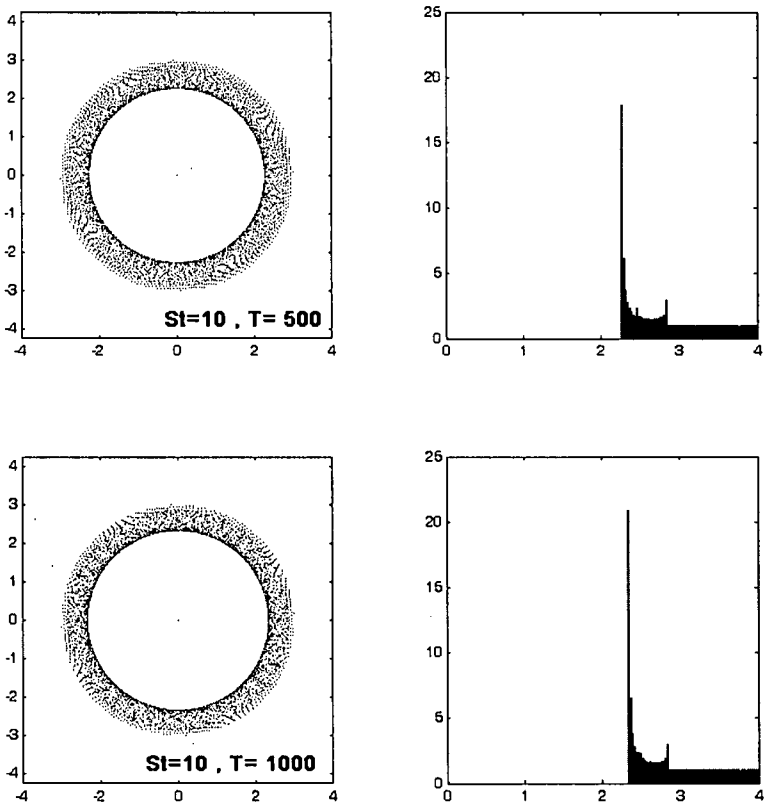


Comments and comparisons are provided in section 5.2.

Note about the case St=10.

Contrary to what is observed for the two cases St=0.1 and St=1, two fronts in the concentration profile are present for St=10, after time $T = 7$. The first peak (the closest to the vortex centre) has the same origin as the ones observed for St=0.1 and St=1. The second peak is due to the fact that particles initially located in the core region overtake particles which are initially further from the vortex centre, thus creating a second front of accumulation. At the time of the catch-up (around $T = 7$), the local particle concentration reaches an 'abnormally' high value. Just after the catch-up, the concentration at the first peak decreases as the second peak detaches itself from the first one. Then, it increases again due to the increase in particle accumulation with time.

## 5.2 Comments

**Overall time evolution of the concentration profiles**

For each Stokes number, the particle concentration decreases with time in the core region of the vortex but local accumulation of particles occurs in the outer region (as stressed in section 4, only in the outer region can particles of the same characteristics accumulate). A peak of concentration develops with time, grows and travels away from the vortex centre with the particles. It takes the form of a concentration wave whose crest is travelling to increasingly larger radii.

Note that this phenomenon would be different if the fluid velocity profile was different.

**Development and travelling of the peak of concentration**

The crest is initiated at approximately $r = 1$ for all three cases (Figure 5.2 and Figure 5.3). This result can be derived analytically for St=0.1 (see section 5.3).

Once the peak of concentration has appeared, it travels away from the vortex centre, at a faster rate as the Stokes number increases (Figure 5.3). As a consequence, **the larger the Stokes number is, the farther particles accumulate away from the vortex centre**. This is due to what happens in the early stage essentially (t<100), since the radial velocity of the crest is similar for all three cases at later times.

Note: If the flow were to be seeded with an inhomogeneous pool of particles in which those three Stokes numbers were present, we would observe the juxtaposition of the different peaks of concentration, each travelling away from the vortex centre at a different velocity. Note that the result would be different if the interactions between the particles were taken into account.

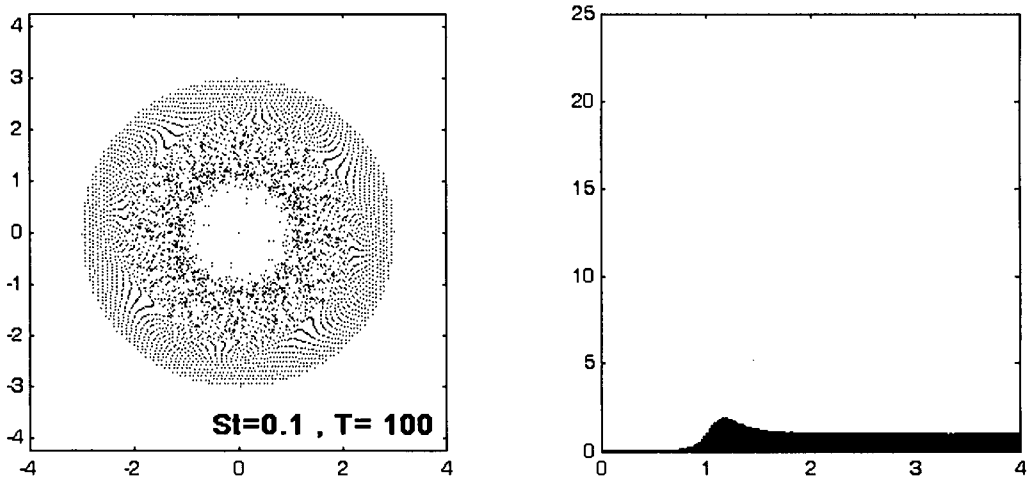


**Figure 5.2** Particle distribution (left) and concentration profile (right) for St=0.1 and T=100.

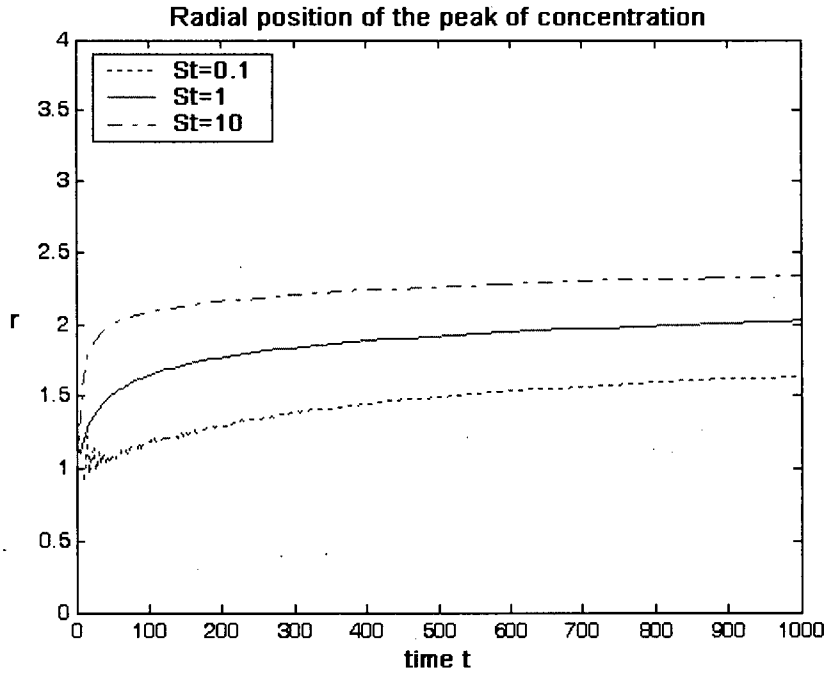


**Figure 5.3** Radial position (r) of the peak of concentration, with respect to time, for each three cases: St=0.1, St=1, St=10. Precision: dr=0.1. Corresponds to the case of $5.10^7$ particles seeded on the disc of radius [0 4].

**The accumulation is the most dramatic for St=1**

As illustrated by Figure 5.4, the concentration peak is the highest for an intermediate Stokes number (St=1), except during the initial stage of the simulation, when it is the highest for a large Stokes number (St=10). For a given time, the accumulation for St=0.1 is not as significant as for St=1 since the accumulation process takes longer for smaller Stokes numbers. Still, the accumulation is not the largest for St=10, since a second peak of concentration appears in that case, preventing optimal accumulation at one single radial position from the vortex centre. The reason why particles with a large Stokes number efficiently accumulate at early times is that, because of their large inertia, there is an intermediate regime where drag balances the radial acceleration (section 4.2), which allows them to quickly reach large radii and accumulate. The peak of concentration increases and then decreases very significantly around $T = 7$, when the catch-up happens.

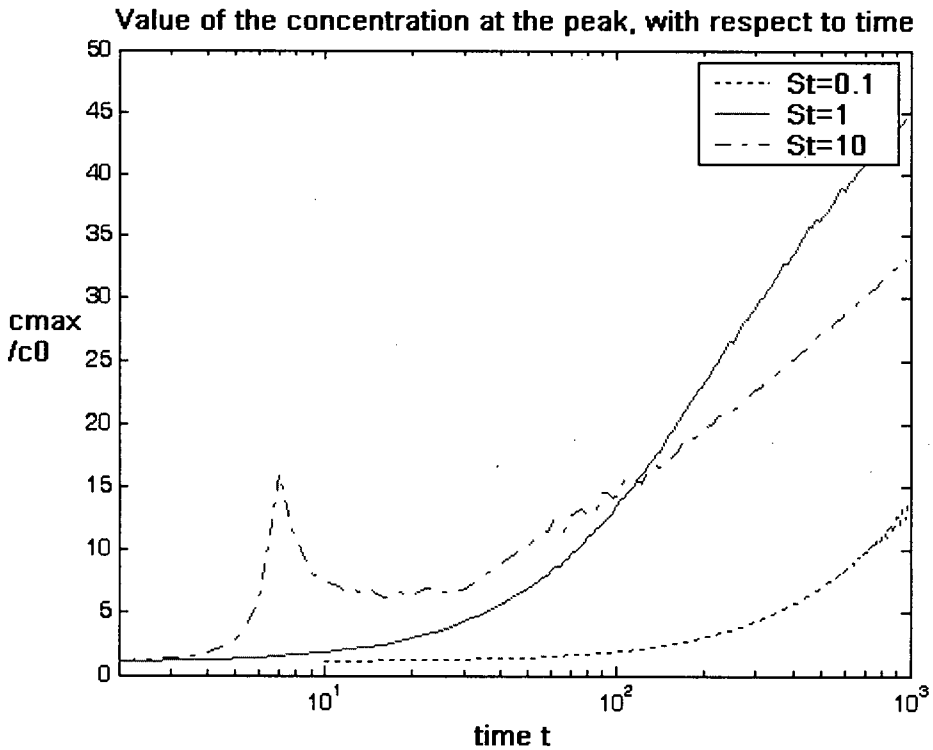


**Figure 5.4** Value of the concentration at the peak, with respect to time, for each three cases: St=0.1, St=1, St=10. Corresponds to the case of $5.10^7$ particles seeded on the disc of radius [0 4].

**Limitation of Figure 5.4**

Note that the values of the concentration given in Figure 5.4 depend on the choices made for the evaluation of the concentration (computed presently on annular regions of width dr=0.01). The point of Figure 5.4 is not so much in providing actual values of the peak of concentration but in providing a base for the comparison between the three cases: St=0.1, St=1 and St=10.

**Conclusion**

Apart from the early stage, inhomogeneities are the strongest for intermediate Stokes numbers.

**Similarities / dissimilarities between the cases** $St = 0.1$ **and** $St = 1$

The concentration profiles observed for $St = 0.1$ and $St = 1$ are similar, and show that it just takes 10 times longer for the $St = 0.1$ particles to achieve the same result (see Table 5.1 and Figure 5.5 for the comparison between the case $St = 0.1$, $T = 10^3$ with the case $St = 1$, $T = 10^2$).

| $c_{max}$ | $\eta$ | $T = 10^1$ | | $T = 10^2$ | | $T = 10^3$ | | $T = 10^4$ | | $T = 10^5$ | |
|---|---|---|---|---|---|---|---|---|---|---|---|
| $St = 0.1$ | | 1.08 | --- | 1.62 | 1.1 | **4.31** | **1.7** | **5.48** | **2.1** | **5.86** | **2.3** |
| $St = 1$ | | 1.62 | 1.3 | **4.31** | **1.7** | **5.48** | **2.1** | **5.86** | **2.3** | 5.76 | 2.5 |
| $St = 10$ | | 3.75 | 1.7 | 3.10 | 2.1 | 4.00 | 2.3 | 4.23 | 2.5 | 7.67 | 2.9 |

**Table 5.1** Maximum value of the concentration observed $c_{max}$ (i.e. height of the peak of concentration) and the corresponding radial position $\eta$, for St=0.1, 1, 10, at different times T. The corresponding simulations involved 1962 particles only, seeded on a regular

grid (of step $dx = dy = 0.12$, implying $c0 \approx 69.39$ particles per non-dimensionalized unit area) and the concentration given was calculated on rather broad annular regions $dr = 0.2$. Despite it is a rather rough computation, it still shows the qualitative features of the peak of concentration.

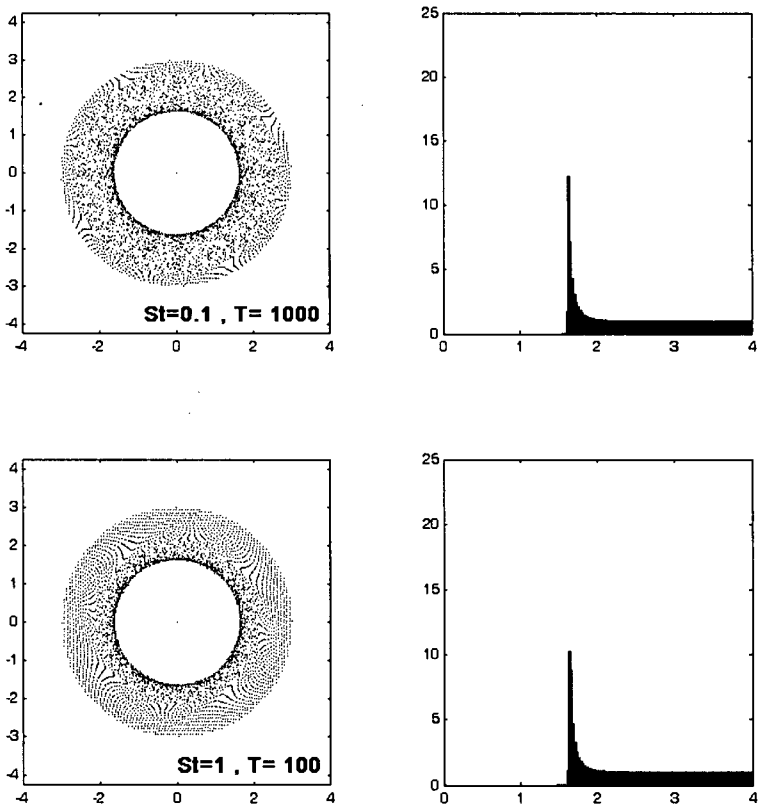


**Figure 5.5** Particle distribution (left) and concentration profile (right) for St=0.1 and T=1000 (top), and for St=1 and T=100 (bottom).

However, significant dissimilarities do exist between the two cases. The particle dynamics are not equivalent. Even though in both cases we end up with a core region devoid of particles, framed by a thin annular region where particles accumulate, in the case St=1 the exterior of this annular region is relatively undisturbed compared to the St=0.1 case (see Figure 5.5).

Also, in the stage that precedes the formation of the annular region of high particle concentration, the particles are substantially more dispersed in the case St=0.1 than in the case St=1 (Figure 5.6).

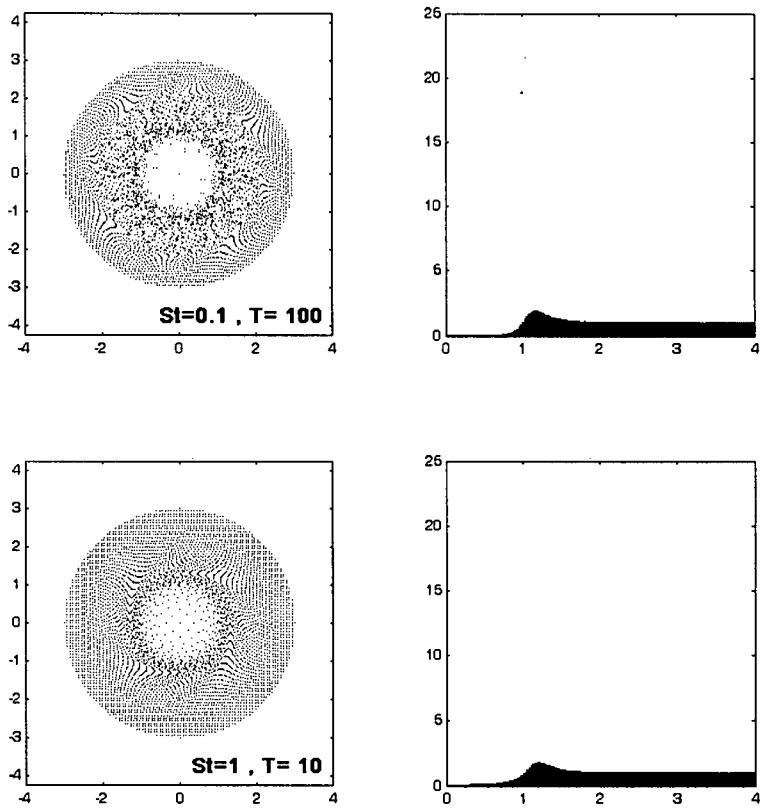


**Figure 5.6** Particle distribution (left) and concentration profile (right) for St=0.1 and T=100 (top), and for St=1 and T=10 (bottom).

These observations reinforce the idea that optimal accumulation occurs for St=1, and that the differences between St=0.1 and St=1 are not just a matter of time.

## Case St=10

The snapshots presented earlier (section 5.1) indicate that the St=10 case differs from cases with Stokes numbers smaller than 1. This is linked to that fact that only for sufficiently large Stokes number, an intermediate regime, where drag balances the radial acceleration term (inertial term),

exists. The 'catch up' that it gives rise to is visually noticeable. Particles located initially in the core region are expelled quickly in the outer region, instead of accumulating with the other particles on the annular region of high particle concentration. As a result, the patterns created are not as inhomogeneous as the ones obtained for cases where the catch-up is absent (i.e. where the Stokes number involved is smaller).

In figure 5.7, three different colours are used to visualize the 'catch up ' phenomenon. Particles located initially in the centre ($r \leq 1$) are in blue, those located in the intermediate ring ($1 < r \leq 2$) are in yellow, and those located in the outer ring ($2 < r \leq 3$) are in pink. The particles in the centre quickly form a blue ring that extends beyond the yellow particles.

**Main conclusion:**

Inhomogeneities are the strongest for intermediate Stokes number (St~1).

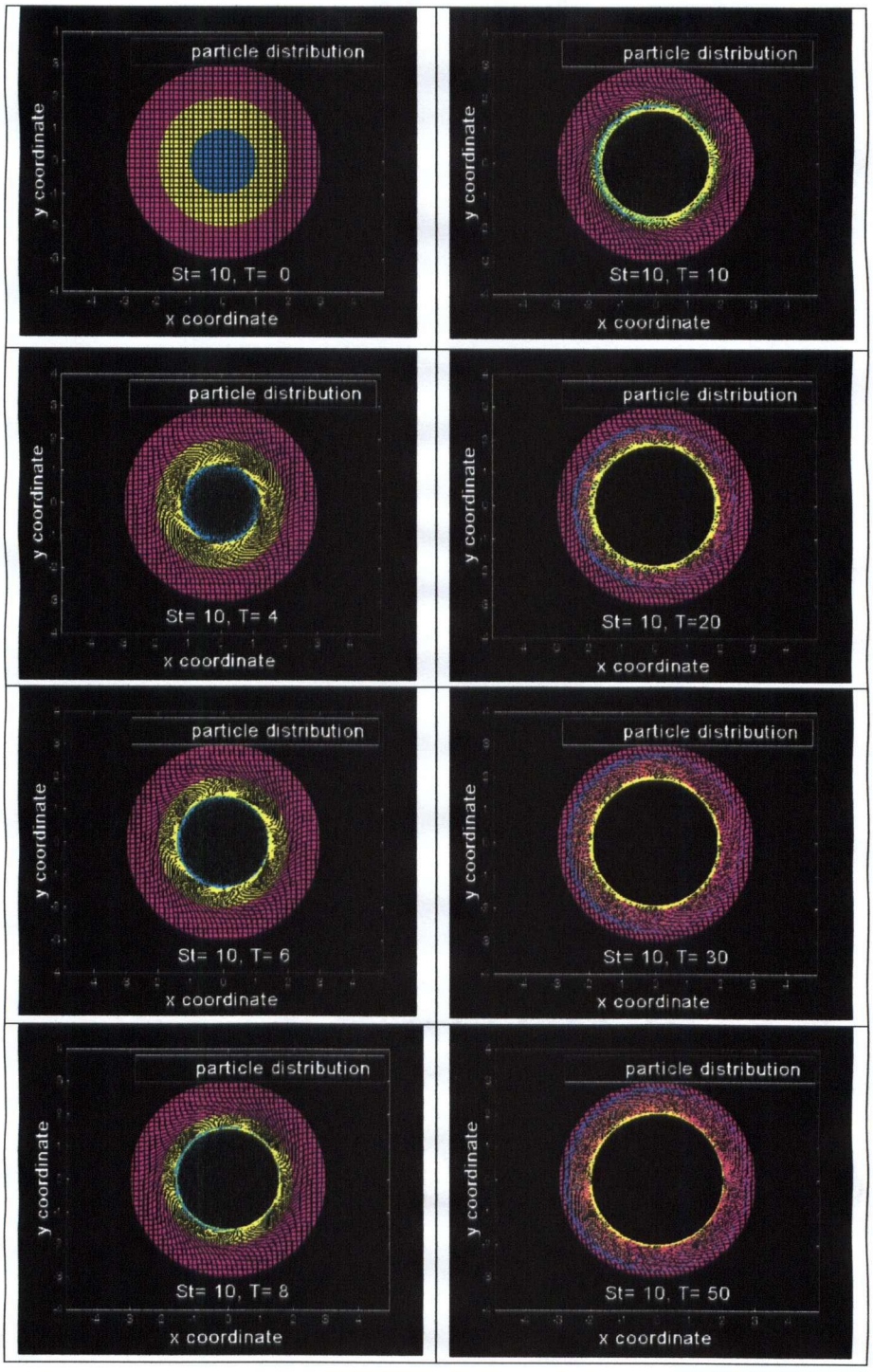


**Figure 5.7** Particle distribution for St=10, at T=0, 4, 6, 8, 10, 20, 30 and 50, for 32761 particles seeded uniformly on the disc $\mathbf{r} \leq \mathbf{3}$ at T=0. Particles are in blue if they were initially in the disc of radius 1, in yellow if they were in the annular region $1 < r \leq 2$, and in pink if they were in the annular region $2 < r \leq 3$. Those figures visualize the 'catch up' phenomenon.

## 5.3 Analytical results for small Stokes numbers ($St < 1$)

As presented earlier, Druzhinin (1994) derived some analytical results for particles having a Stokes number that is small compared to unity ($St < 1$). In particular, in the case of a sufficiently small concentration of particles (such that their influence on the carrier flow can be neglected), he notes that the evolution of the concentration field $c(r,t)$ is described by:

$$\frac{\partial c}{\partial t} + \frac{St}{r}\frac{\partial}{\partial r}(c u_\theta^2) = 0 \qquad \textbf{(5.1)}$$

with $$c(r, t=0) = c_0(r). \qquad \textbf{(5.2)}$$

This equation shows that the time scale for the increase or decrease of the concentration with time is $\Delta t \sim \frac{1}{St}(\frac{L}{U_0})^2$. In that respect, the process is getting **more efficient as $St$ is increased** (while remaining small compared to one).

Druzhinin gives the general form of the solution of this Cauchy problem as:

$$c(r,t) = c_0(r_0) * (\frac{u_\theta^2(r_0)}{u_\theta^2(r)}) \qquad \textbf{(5.3)}$$

the function $r_0(r,t)$ being implicitly defined by:

$$\int_{r_0}^{r} \frac{u\,du}{u_\theta^2(u)} = St * t \qquad \textbf{(5.4)}$$

Since the fluid velocity for the type of vortex addressed in the present study is:

$$u_\theta = \frac{r}{2}\exp(-r^2) \qquad \textbf{(5.5)}$$

the following equation is obtained:

$$\frac{\partial c}{\partial t} + \frac{St}{r}\frac{\partial}{\partial r}(c\frac{r^2}{4}\exp(-2r^2)) = 0 \qquad \textbf{(5.6)}$$

The solution is:

$$c(r,t) = c_0(r_0) * (\frac{r_0^2}{r^2})\exp(r^2 - {r_0}^2) \qquad \textbf{(5.7)}$$

with $r_0(r,t)$ being implicitly defined by:

$$\int_{r_0}^{r} \frac{\exp(2u^2)}{u} du = \frac{St}{4} t\,. \qquad \textbf{(5.8)}$$

In the following, it is assumed that the initial concentration is homogeneous. The time derivative of the concentration is then:

$$\frac{\partial c}{\partial t} = 2c_0 \frac{\partial r_0}{\partial t}\frac{r_0}{r^2}(1 - r_0^2)\,. \qquad \textbf{(5.9)}$$

From the expression of $r_0(r,t)$, it appears that $\frac{\partial r_0}{\partial t} < 0$ and that $r_0(r,t)$ is a strictly decreasing function of time such that $r_0(r, t=0) = r$.

Therefore:
$$\begin{cases} \frac{\partial c}{\partial t} > 0 & \text{for} \quad r_0 > 1 \\ \frac{\partial c}{\partial t} < 0 & \text{for} \quad r_0 < 1\,. \end{cases} \qquad \textbf{(5.10)}$$

Consequences:

Equation 5.10 means that the concentration of particles decreases with time everywhere within the region $r < 1$ (and not only in the core region $r < 1/\sqrt{2}$, as it could have been thought), and

that, at any location outside this region, the concentration initially increases with time and then decreases. The further from the vortex centre, the longer it takes for $r_0$ to 'cross' the value 1 and therefore for the concentration to start decreasing.

As mentioned by Druzhinin for a similar type of 2D vortex, these equations result in a traveling concentration wave starting from uniform particle concentration. This phenomenon was illustrated by Druzhinin (1994) in the cases of a circular flow ($u_\theta = \frac{r}{2(1+r^2)}$; $u_r = 0$) and of a Rankine vortex ($u_\theta = \frac{r}{2}$ if $r < 1$ and $u_\theta = \frac{1}{2r}$ if $r \geq 1$; $u_r = 0$). Note that both the particle inertia and the vortex structure are of significance for the generation of the concentration waves. It would be interesting to address the case of the Lamb-Oseen vortex ($u_\theta = \frac{1}{2\pi r}[1 - \exp(-\frac{r^2}{2\delta^2})]$, where $\delta$ stands for the core size and is determined by the balance of strain and viscous diffusion) or of a co-rotating pair of point vortices in a future study, for instance.

In the case addressed by the present study, it is expected that the crest will develop at $t = 0$ at the $r$ location where the temporal increase of the concentration is maximal, i.e. at $r$ such that

$$\frac{\partial}{\partial r}(\frac{\partial c}{\partial t})(r, t = 0) = 0. \qquad \textbf{(5.11)}$$

$$\frac{\partial}{\partial r}(\frac{\partial c}{\partial t})(r, t = 0) = \frac{\partial}{\partial r}(\frac{\partial c}{\partial t}(r, t = 0)) = \frac{\partial}{\partial r}(-\frac{St}{r}\frac{\partial}{\partial r}(\frac{c_0}{4} r^2 \exp(-2r^2)))$$

$$= \frac{\partial}{\partial r}(-\frac{St}{2} c_0 (1 - 2r^2)\exp(-2r^2))$$

$$= 4 St\, c_0\, r(1 - r^2) \qquad \textbf{(5.12)}$$

which is zero at $r = 1$.

Therefore, the crest of the concentration wave initially develops on the circle $r = 1$. This is in agreement with the simulations for $St = 0.1$ (see snapshots section 5.1).

The fact that it is at the same position $r = 1$ that the initial temporal increase in concentration is maximal $(\frac{\partial}{\partial r}(\frac{\partial c}{\partial t}) = 0)$ and that it is the edge of the region where concentration decreases $(\frac{\partial c}{\partial t} < 0$ for $r_0 < 1$ and $\frac{\partial c}{\partial t} > 0$ for $r_0 > 1)$ suggests that **a steep front** develops initially at $r = 1$.

**Summary**

For small Stokes numbers ($St < 1$):

- A traveling concentration wave starting from uniformly particle concentration develops in the 2d field. The crest initially appears at $r = 1$.

- The time scale on which the concentration varies is inversely proportional to the Stokes number, so that formation of the traveling wave is more efficient as the Stokes number is increased. But this argument is valid only for sufficiently small Stokes number.

Given that particles having a large Stokes number (therefore a large inertia) are not as much influenced by the vortex, we can predict that there is an **intermediate value of the Stokes number for which the process (and the creation of inhomogeneities) is the strongest.**

## 5.4 Concentration profiles: conclusions

- When particles are initially seeded homogeneously, the particle concentration decreases with time in the core region of the vortex but local accumulation of particles occurs in the outer region, taking the form of a concentration wave whose crest is travelling to increasingly larger radii. This phenomenon depends both on the particle inertia (Stokes number) and on the fluid velocity profile.

- In the present study, for small Stokes numbers, the crest initially develops at a radius $r = 1$.

- For intermediate times ($T = 10^2$, $T = 10^3$ and $T = 10^4$), the concentration peak is the highest in the case St=1.

- A closer look at the particle distributions shows that inhomogeneities are the strongest for intermediate values of the Stokes number.

**Notes**

1) The magnitude of the concentration peak grows with time. However, it should be noted that, as the concentration gets locally high, some other effects such as the action of the particles on the flow itself should be considered.

2) On the annular region where particles accumulate, flocculation may be expected to occur. For instance, two particles colliding could agglomerate into one bigger particle. The Stokes number

corresponding to this larger agglomerated particle would be larger than the initial Stokes number for the two initial particles. As a result, the dispersion process would be more complex.

## 5.5 Extrapolation for the 3D case

The 3D case considers a flow that is seeded with a homogeneous pattern of particles that are allowed to settle down through a pancake vortex. The presence of the vortex will create some inhomogeneities, the characteristics of which we can roughly predict given the results of the two-dimensional study and knowing the settling velocity of the particles (section 3.1.2.1) For the particles considered since chapter 4, the time it takes them to settle through the vortex is of order $O(1000)$ for St=0.1, of order $O(100)$ for St=1 and of order $O(10)$ for St=10. Therefore, the radial position of the peak of concentration and its magnitude can roughly be evaluated from Figure 5.8 and Figure 5.9.

The final radial position of the concentration peak that will appear as a consequence of the presence of the vortex is expected to be around 1.6 or 1.7 for all three cases. Likewise, the maximum concentration involved is of the same magnitude in all three cases. Therefore, **we do not predict a high sensitivity to the Stokes number for the dispersion patterns created by the vortex during particle settling**. The St=10 case should be a little different qualitatively though, since particles in that case are in the early phase where overtaking occurs, as discussed in section 4.5.2, 4.5.3 and 5.2. Results of the actual 3D simulations are presented in section 6.2.3. It includes a comparison with the present predictions.

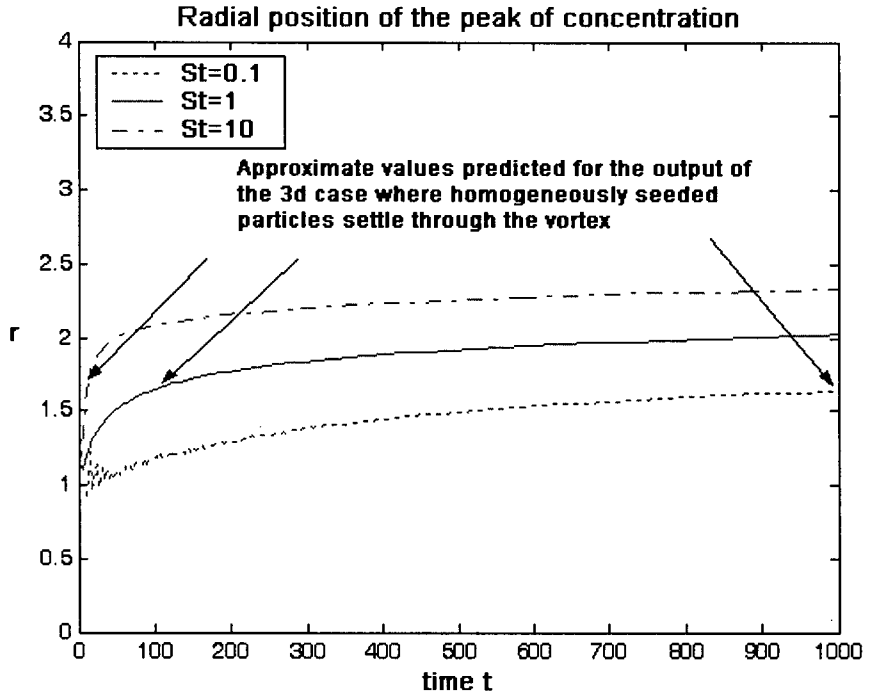


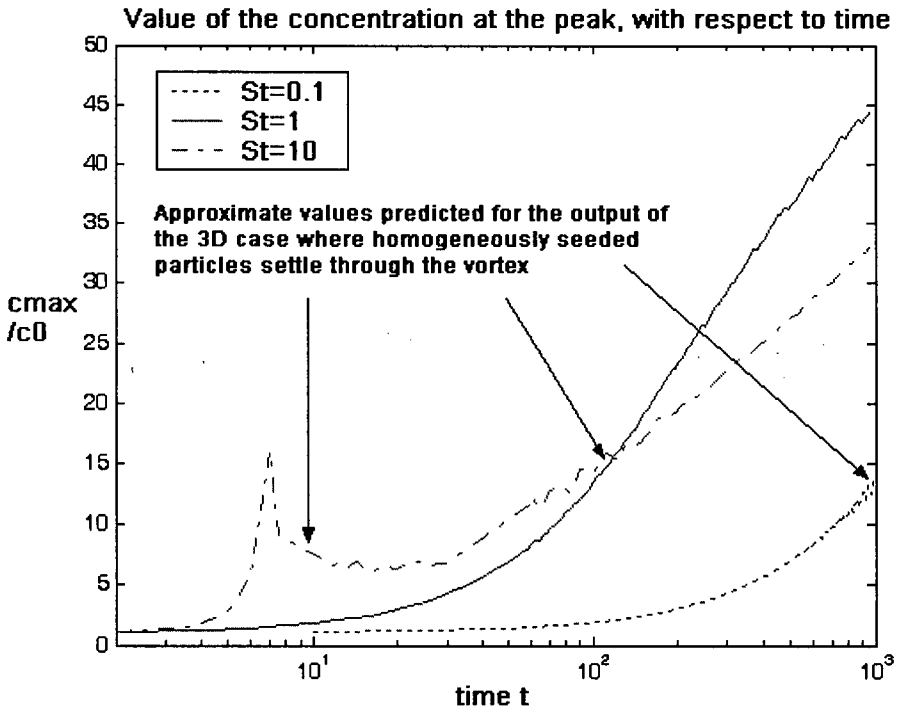


**Figures 5.8 and 5.9** Approximate predictions of the radial position of the concentration peak and of the maximum concentration involved, when a homogeneous pattern of particles is let to settle down freely through the vortex.

# 6. THE 3D STUDY

## 6.1 Role of the gravity on the dispersion

In a still fluid seeded with a homogeneous pool of particles, gravity cannot create concentration gradients, because it uniformly accelerates all the particles without creating any velocity differences among them. Therefore, it is not necessary to study the effect of gravity itself. However, gravity can affect the appearance of concentration inhomogeneities through interactions with the effects of a vortex.

When gravity has a component in the horizontal plane, its interactions with the velocity field of the vortex give rise to an interesting particle dynamics. When gravity does not have any component in the horizontal plane, it merely affects the vertical motion of the particles, on which the vortex has no effect since a pancake vortex has no vertical velocity component: $u_z = 0$. In that case, why don't we just forget about the vertical motion?

However, the vertical motion must be still considered since the background velocity field in which the particle evolves changes as it rises or falls. The vortex has a vertical structure. In particular, a particle can escape from the vortex. So, it's important to keep track of the vertical movement of the particle, in the general case, unless the motion is quasi two-dimensional.

## 6.2 Sinking of a planar distribution of particles through a pancake vortex

### 6.2.1 Description of the 'experiment'

The settling of a planar distribution of a homogeneous pool of particles initially seeded above the pancake vortex is now investigated.

In the previous chapter, the particle dynamics in the horizontal plane of symmetry of the vortex was considered, assuming the motion was two-dimensional. In Chapter 6, the dependence of the fluid velocity profile on the elevation is taken into account (through the variable 'c'):

$$u_\theta(r,z) = c\frac{r}{2}\exp(-r^2) \quad \text{with} \quad c(z) = \exp(-\frac{z^2}{2\Lambda^2}),\ c \in R^{+*}.$$

Unless stated otherwise, a vortex of thickness $\Lambda = 0.3$ will be considered. The symmetry plane of the pancake vortex corresponds to the elevation z=0. Particles are released above the pancake vortex, in the plane $z_0 = 1$, where the velocity induced by the vortex is still very small. Indeed, for a thickness $\Lambda = 0.3$, the maximum velocity at $z_0 = 1$ is $8.29*10^{-4}$, i.e. of order $O(10^{-3})$. On the other hand, the maximum velocity at z=0 is $2.14*10^{-1}$, i.e. of order $O(10^{-1})$. Because all of the particles have the same Stokes number, they experience the same buoyancy force and therefore settle at the same vertical velocity. All of the particles are released with zero initial horizontal velocity - contrary to the precedent chapter - so that initial conditions have the possibility to influence the particles motion, but with a vertical velocity equal to the settling velocity. This is believed to be the closest to the real problem of the settling of particles through a pancake-like vortex.

**Neglect of the history term**

The history term modifies the short-term behaviour of the particle, especially if it is released from rest. Indeed, the history term represents the sensitivity of the drag to acceleration, so if acceleration is important, the history term might play a role. Nevertheless, it can be neglected in the present study (see section 2.4.2 and Appendix B for explanations).

### 6.2.2 Parameters at stake

The velocity profile is given. The vortex thickness ($\Lambda = 0.3$) will be allowed to vary only in section 6.2.5. The density ratio is fixed (as it has been since Chapter 4): $\delta = 4*10^{-4}$. So there are 2 parameters to consider: the Stokes number (St), and the settling velocity. If particles settle quickly, they will not substantially be affected by the vortex. On the other hand, if they settle very slowly, the vortex will have time to perturb the particle settling.

The settling velocity was calculated in section 3.1.2.1 as:

$$U_{term} = U|1-\delta|\frac{St}{Fr^2}.$$

As with previous simulations, the experimental values from Yang's experiment (1993) will be used. The Froude number is equal to 8. For each Stokes number, the (non-dimensional) settling velocity and the time it takes for particles to settle at this velocity from the elevation $z = 1$ to the elevation $z = -1$ is:

St=0.1 → $U_{term} = 1.56 * 10^{-3}$ $T = 1280.51$: order $O(1000)$

St=1 → $U_{term} = 1.56 * 10^{-2}$ $T = 128.051$: order $O(100)$

St=10 → $U_{term} = 1.56 * 10^{-1}$ $T = 12.8051$: order $O(10)$

### 6.2.3 Results

The following simulations involve 5025 particles initially located on a grid of step $dx = dy = 0.075$ on the disc of radius 3 (as for the visualizations for the 2d study). Particles are given enough time to settle from z=1 to approximately z=-10. Figure 6.1 gives both the snapshots of the particle distribution during the settling and the final planar distribution at the exit of the vortex ($z = -10$).

Figures 6.2 through 6.5 present a more detailed analysis of the evolution of the concentration profile during settling.

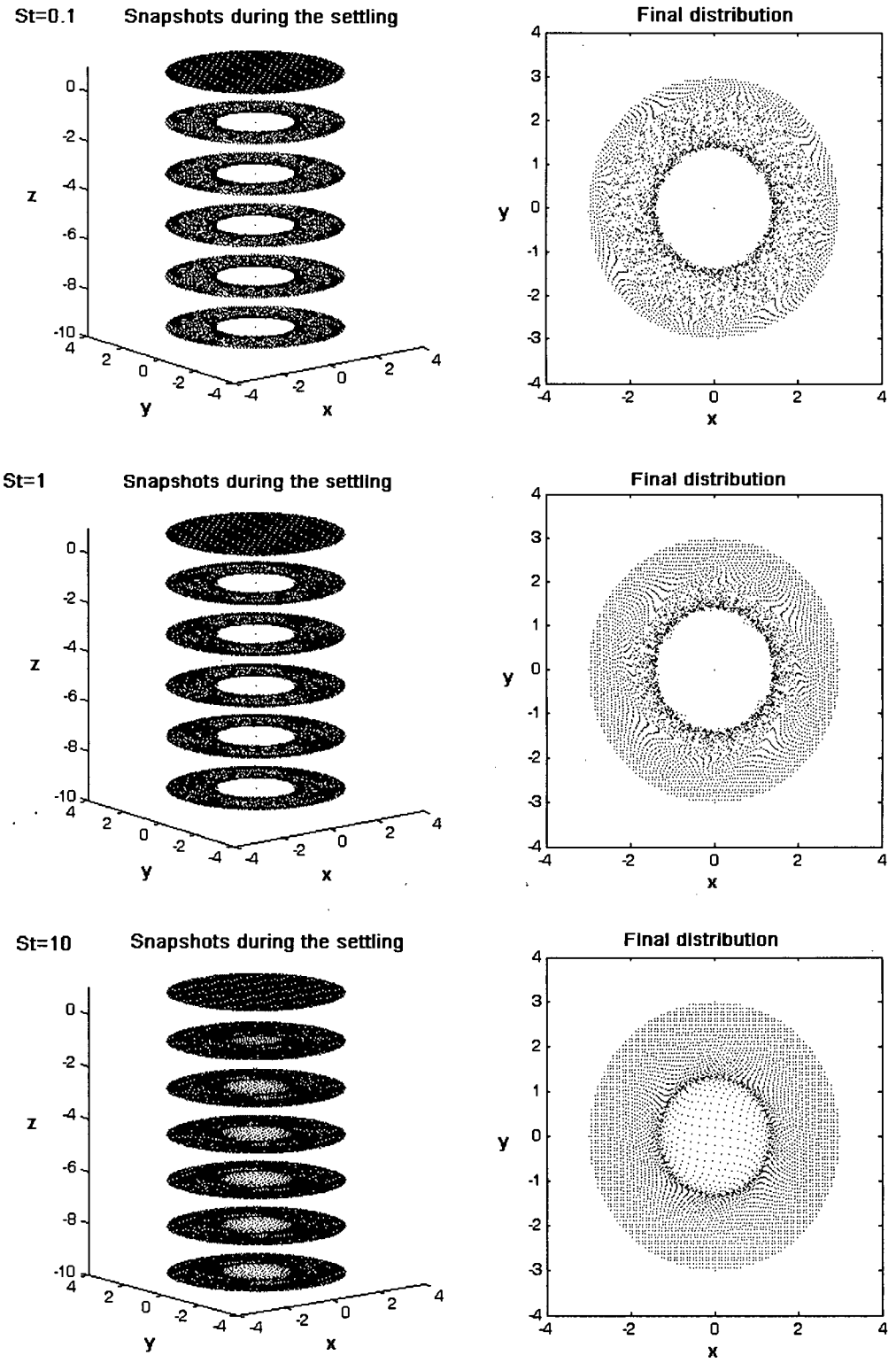


**Figure 6.1** Settling of particles through a pancake vortex. From top to bottom: St=0.1 (T=2500), St=1 (T=250) and St=10 (T=25). Left: snapshots of the particle distribution during the settling; right: final planar distribution at the exit of the vortex ( $z = -10$ ).

In agreement with the predictions of section 5.5, the planar distribution of the particles at the exit of the pancake vortex is almost identical for the cases St=0.1 and St=1: the vortex core is completely free of particles up to the approximate radial position r=1.2 for St=0.1 and r=1.1 for St=1 (Figure 6.2). Particles have mainly accumulated at r=1.415 for St=0.1 and r=1.425 for St=1 (Figure 6.2 and Figure 6.3).

It is interesting to note that this radial position corresponds to the distance ($r = \sqrt{2}$) at which the vorticity $\omega_z$ is minimum in the horizontal planes of the pancake vortex (see Figure 3.1). But there is no general rule to derive from this given that the influence of the thickness of the vortex ($\Lambda$) has not been taken into account. The fact that particles accumulate at this specific distance from the vortex centre is probably only true for the particular case considered ($\Lambda = 0.3$).

On the other hand, for St=10, the particles have not had the time to be fully expelled from the vortex core (Figure 6.2). Although a ring of accumulated particles has had the time to form, it is not as dramatic as that for Stokes numbers of 0.1 or 1. Figures 6.4 and 6.5 also illustrate that whereas the planar distribution of the St=0.1 and St=1 particles remains identical after the particles have passed the level $z = -1$, it is not the case for the St=10 particles. The St=10 particles are still under the influence of the vortex when they reach the elevation $z \approx -3$. The peak of concentration keeps travelling away from the vortex centre and keeps growing, due to the large inertia of the particles, even though the velocity involved by the vortex at that point is very small (compare Figure 6.2 and 6.3). The vertical profiles obtained for particles being steadily seeded (section 6.2.4) will also show that the action of the vortex on the St=10 particles is long-lasting.

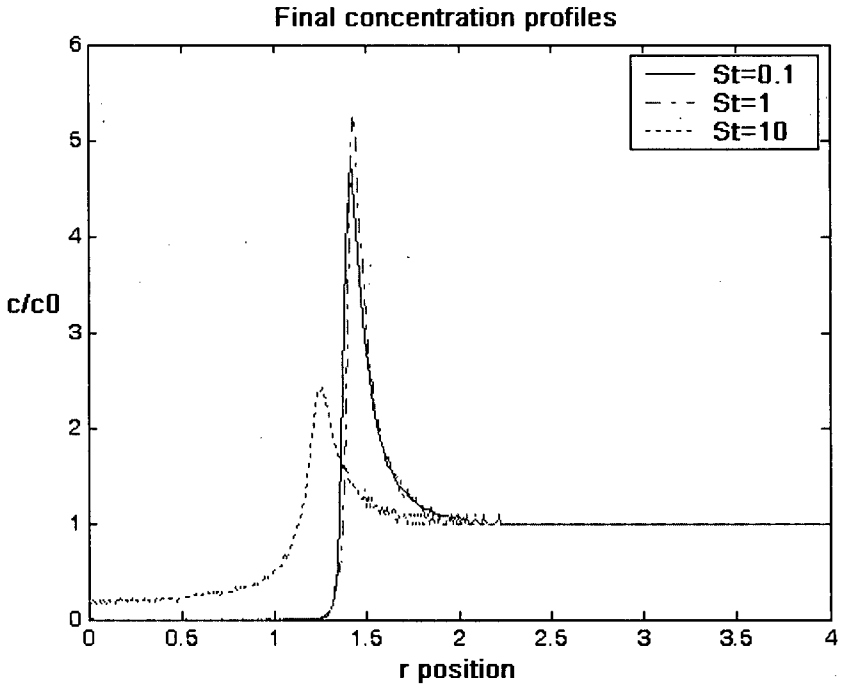


**Figure 6.2** Concentration profiles in the radial direction, at about $z \approx -3$, for each three cases: St=0.1 (T=2500), St=1 (T=250) and St=10 (T=25).

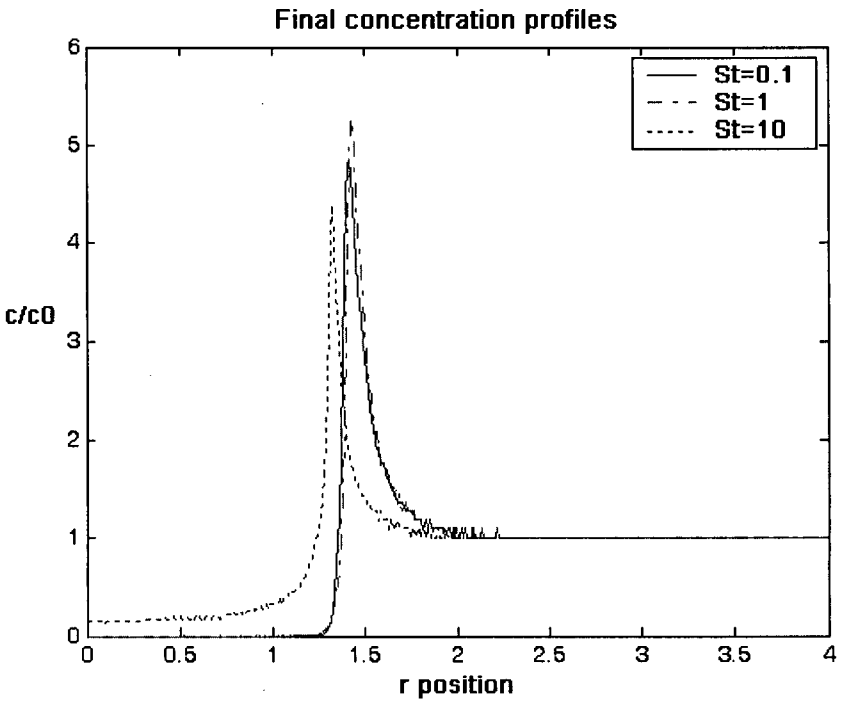


**Figure 6.3** Concentration profiles in the radial direction, at about $z \approx -10$, for each three cases: St=0.1 (T=8000), St=1 (T=800) and St=10 (T=80).

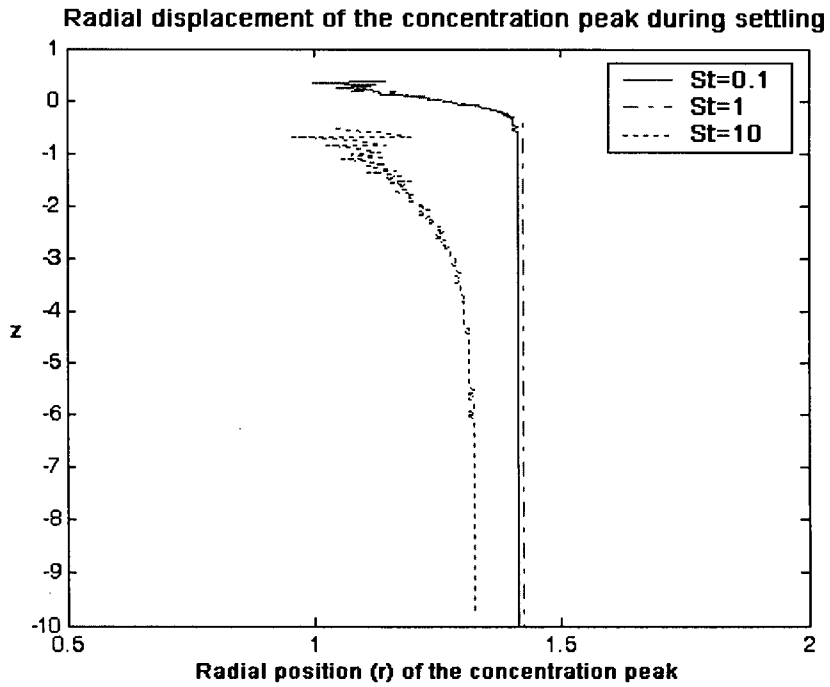


**Figure 6.4** Radial displacement of the concentration peak that forms during settling through the pancake vortex, with respect to the elevation z, for each three cases: St=0.1, St=1 and St=10.

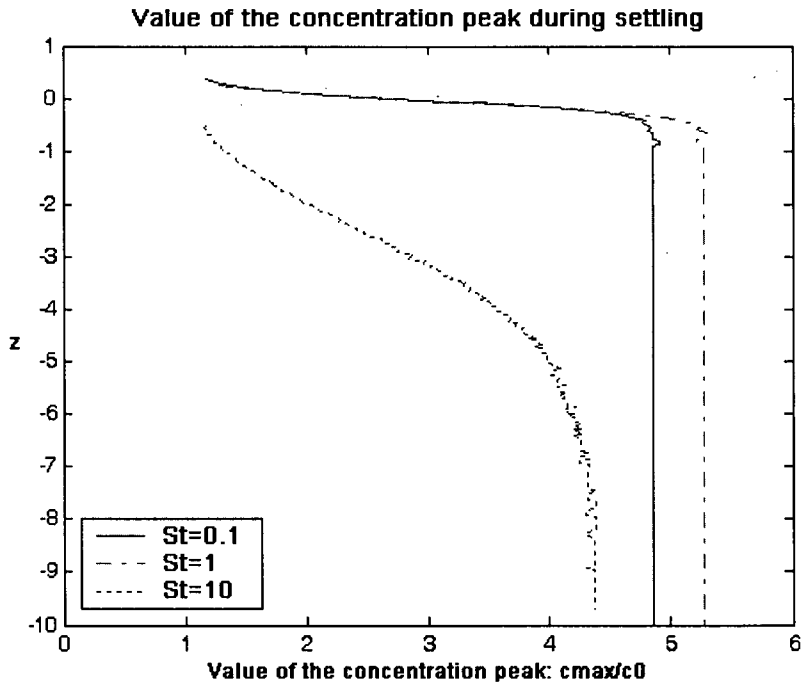


**Figure 6.5** Value of the concentration peak (cmax/c0) during settling, for each three cases: St=0.1, St=1 and St=10, with respect to the elevation z.

Note

For St=10, the second peak of concentration that appears in the 2D case as a result of a catch-up does not have the time to form in the 3D case. Nevertheless, it appears when the vortex is thicker (see section 6.2.5 for a vortex of thickness $\Lambda = 0.5$).

### 6.2.4 Extrapolation for particles being steadily seeded

The case where the flow is continuously seeded with particles at the elevation z=1 can be trivially deducted from the previous case (that of the settling of one planar distribution of particles only). Vertical profiles will be examined.

The vertical profiles

In Figure 6.6, two figures are presented for each Stokes number considered. The first one (left) gives the position of all particles located in the slice of width $|dy| \leq 0.01$. Although it would be nice to get more particles represented to get a more refined vertical profile, it is not possible to consider a too wide slide because of the optical errors it would imply (indeed, all particles are not in the same vertical plane but are represented as such on the graph). The problem also is that the result depends on the slice considered (the axisymmetry of the solution is ruined by the fact that particles are initially distributed on a rectangular grid: see Figures 6.7 and 6.8). Nevertheless, this first slice enables visualize that **the smaller the Stokes number is, the wider the lateral disturbed area is.**

The second figure (right) gives a more refined profile by juxtaposing the position of all particles located in the slide of width $|dy| \leq 0.1$, in the same vertical plane (only their distance from the vortex centre is considered). For St=0.1 and St=1, the vertical profile looks like an **inverted**

**funnel**. The **vortex acts as an umbrella with respect to the particle settling.** For St=10, the 'umbrella effect' is significantly weaker. Particles are able to go through the central region of the vortex. Also, particles keep being ejected even after exiting the vortex ( $z \sim -1$ ): the long-lasting influence of the vortex is due to the inertia of the particles.

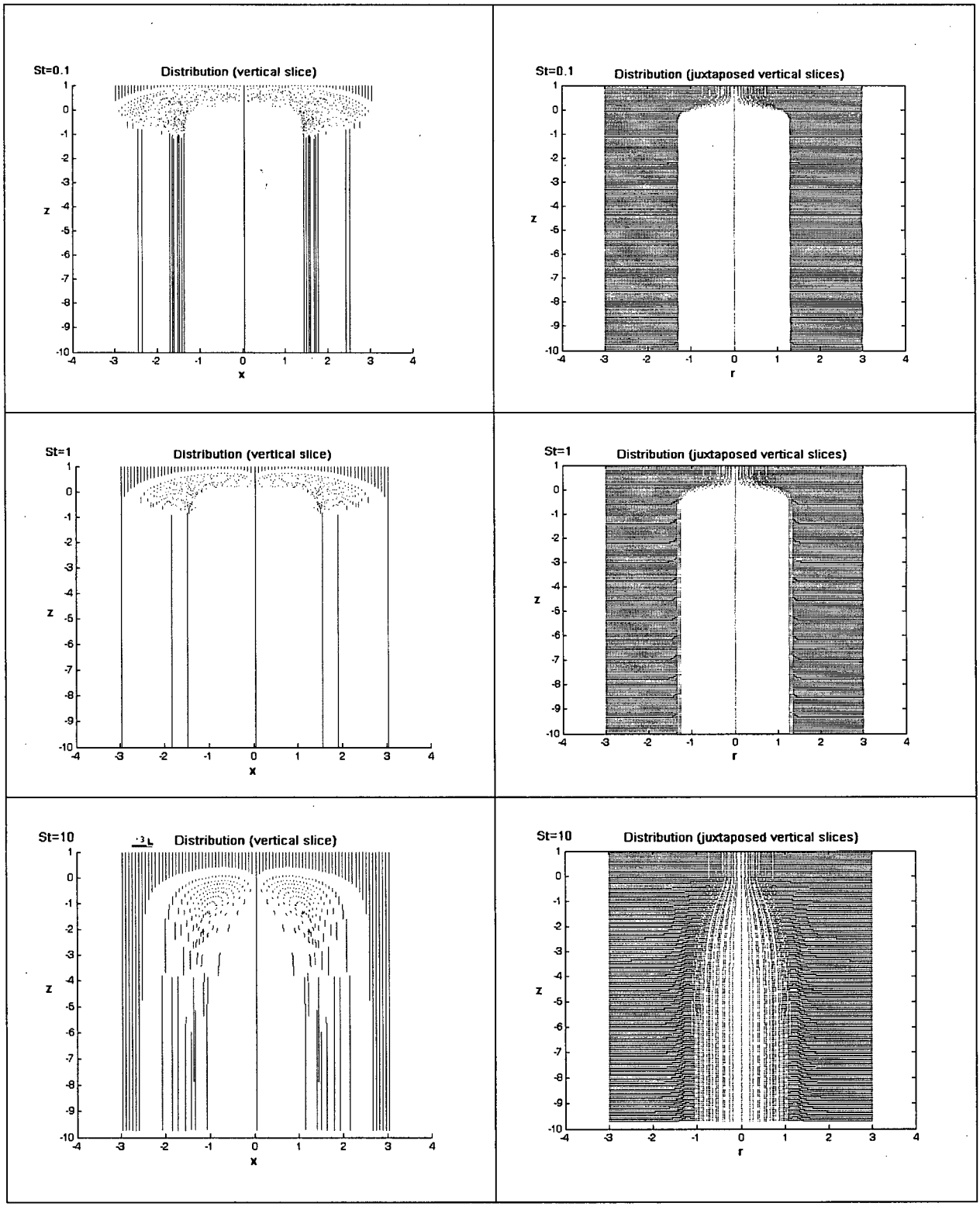


**Figure 6.6** Vertical profiles of the particle distribution during settling through a pancake vortex. From top to bottom: St=0.1, St=1, St=10. Left: result for a slice $|dy| \leq 0.01$. Right: profile obtained by juxtaposing the radial position of all particles located in the slide $|dy| \leq 0.1$.

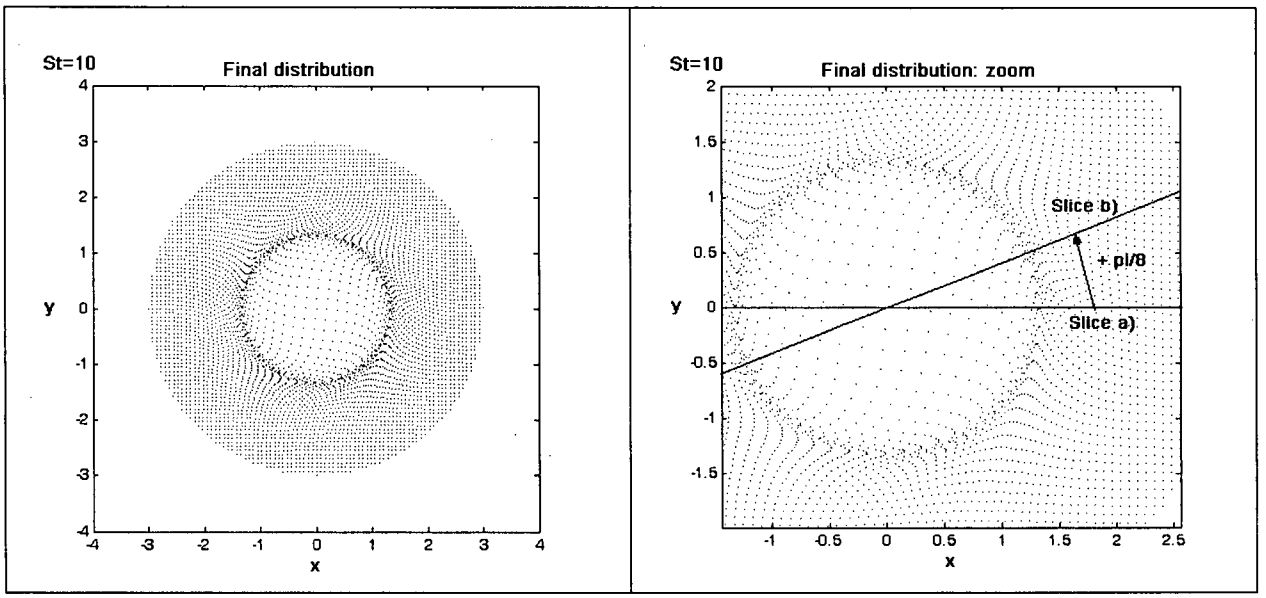


**Figure 6.7** On the left: final distribution of the particles in the horizontal plane for St=10. On the right: zoom that qualitatively shows to what extent two vertical slices a) and b) taken at different angles through the distribution can lead to different results. Slices a) and b) are not equivalent (see Figure 6.8) since the initial particle distribution is not perfectly axisymmetric.

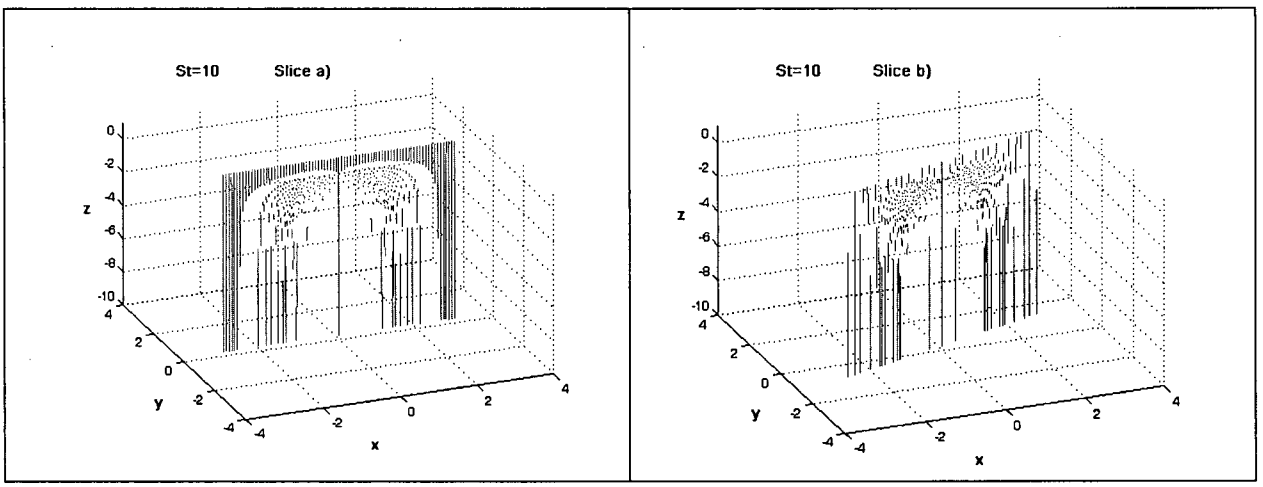


**Figure 6.8** Two vertical slices taken from the same experiment (St=10, see Figure 6.7). The difference in angle is pi/8. The fact that the two slices are not equivalent reminds us that the solution is not perfectly axisymmetric.

Role played by the Stokes number on the umbrella effect

As illustrated in Figure 6.6, the vertical profiles change dramatically when the value of the Stokes number switches from 1 to 10. Intermediate cases are presented in Figure 6.9. They show that St=1 is a threshold value beyond which the action of the pancake vortex as an umbrella for the particle dispersion weakens. The qualitative change of the vertical profiles that occurs at St=1 corresponds to a change in the particle dynamics, as explained in section 5.

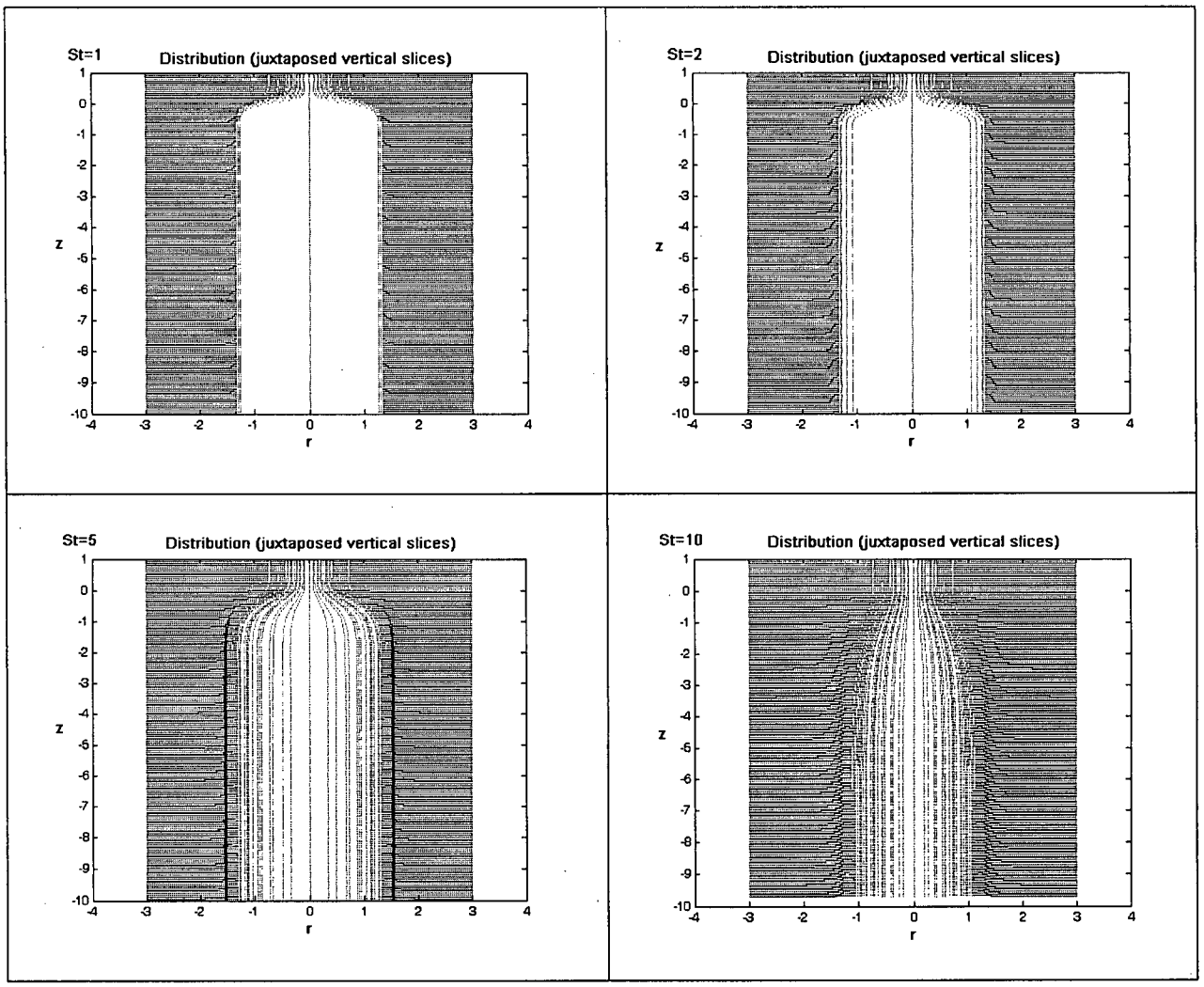


**Figure 6.9** Vertical profiles for St=1, St=2, St=5 and St=10.

### 6.2.5 Influence of the vortex thickness: $\Lambda$

Up to this point, the vortex thickness ($\Lambda = 0.3$) was not allowed to vary. In this subsection, the final concentration profiles of particles settling through a vortex of thickness $\Lambda = 0.2, 0.3, 0.4$ and $0.5$ respectively are examined (Figures 6.10 to 6.13).

(Particles are now released from a higher initial position (z=2 instead of z=1) to be sure that the vortex is let to act fully on the particles trajectories, even in the case of a vortex of thickness $\Lambda = 0.5$).

The concentration profiles illustrate that:

- in the case of a very flat vortex ($\Lambda = 0.2$), particles with a Stokes number of 10 end up being located closer to the vortex centre than the particles with a smaller Stokes number. This is the **opposite of what is usually expected**. Moreover, the particles with a Stokes number of 10 have not had the time to concentrate as much as the particles with a smaller Stokes number.
- As the vortex thickness increases, it is the particles with the largest Stokes number that tend to be located farther from the vortex axis centre. The peaks of concentration get more dramatic as well.
- The second peak of concentration that was observed in the 2D study (section 5) as a result of the overtaking phenomenon for particles having a Stokes number of 10 is present only if the vortex is thick enough ($\Lambda \geq 0.4$). When the vortex thickness is $\Lambda = 0.4$, the peak of concentration observed at the exit of the vortex for a Stokes number of 10 is exceptionally high. It is due to the overtaking phenomenon.

The 2D analysis has made it easy to interpret these different concentration profiles.

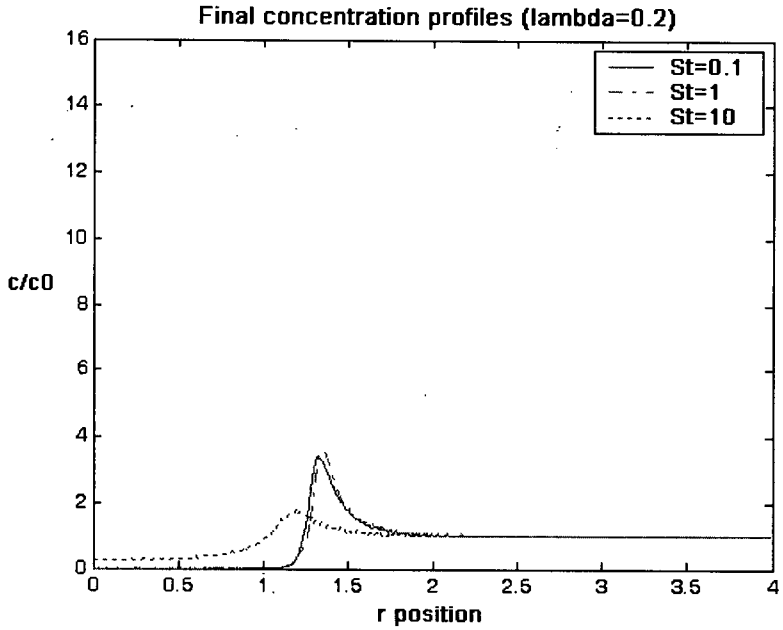


**Figure 6.10** Final concentration profiles (in the radial direction) after particles have settled through a pancake of thickness $\Lambda = 0.2$, for each three cases: St=0.1, St=1 and St=10.

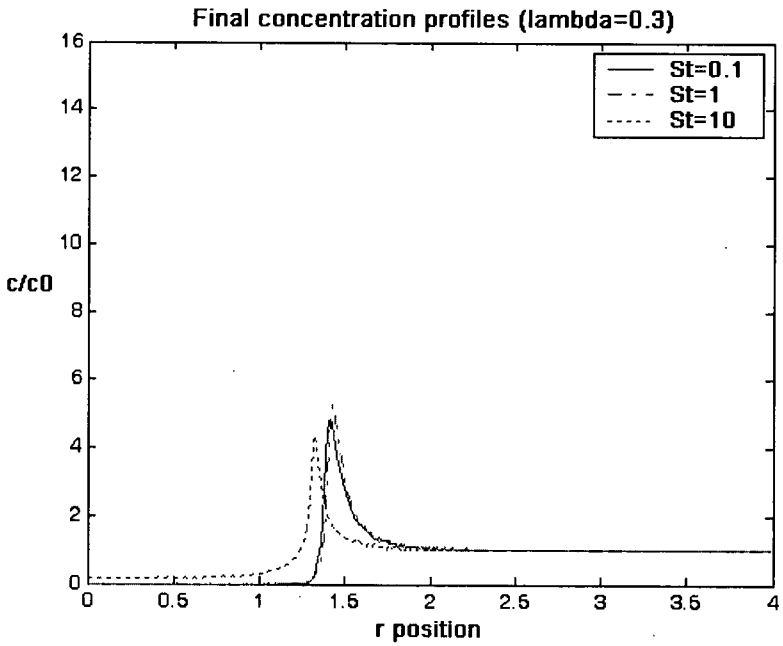


**Figure 6.11** Same as Figure 6.11 but with a vortex thickness $\Lambda = 0.3$.

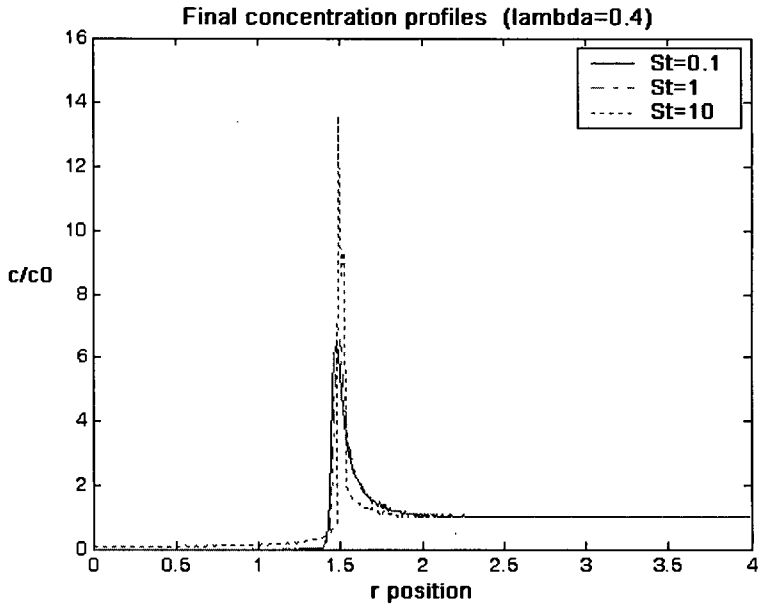


**Figure 6.12** Same as Figure 6.11 but with a vortex thickness $\Lambda = 0.4$.

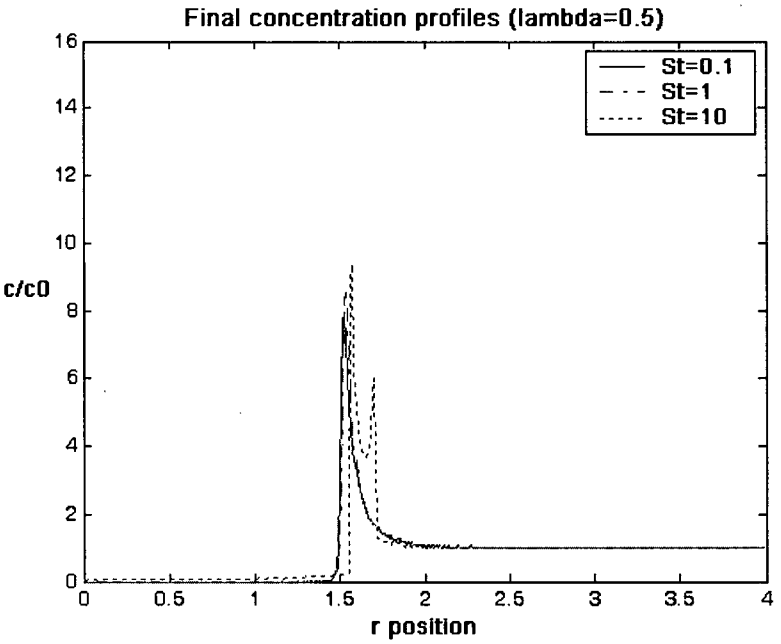


**Figure 6.13** Same as Figure 6.11 but with a vortex thickness $\Lambda = 0.5$.

# 7. DISCUSSION

This study can be considered as a first step toward an understanding of the role played by pancake vortices in particle dispersion. The study could be extended in different ways.

First, it would be of practical interest to address the case of particles having a smaller density (i.e. a larger density ratio $\delta$), while still having a relatively large Stokes number (so that the particle motion is substantially different from that of a fluid element). To be able to do so, one has to find a way to relax the assumptions of the Maxey-Riley (1983) equation.

Besides, it would be interesting to address the case of other vortex structures (Lamb-Oseen vortex, spiral vortex...) and compare the results for the propagation of the concentration wave. Note that the case of a Rankine vortex was addressed by Druzhinin (1994) in the case of small Stokes numbers.

Also, the study does not include the interactions between particles. However, those interactions are expected to play an important role in the regions of high particle concentration. In particular, flocculation would probably affect the dispersion process in reality. This issue is discussed in the following.

The flocculation of particles depends on the collisions between particles, caused by their relative motion. This relative motion may be caused by Brownian movement, by fluid movement giving rise to velocity gradients, or by particle motion due to an external force (e.g. gravity). Flocculation is important in many industrial processes such as pulp and paper, mining and water and wastewater treatment. The aggregates that would form as a result of collisions between particles would be characterized by a larger Stokes number than that of the primary particles. As such, they would move away from the vortex centre faster, and they would fall faster as well. Flocculation could result in a pool of particles exhibiting a continuous distribution of Stokes numbers.

The incorporation of the whole flocculation process in the numerical model is beyond the scope of this thesis. Nevertheless, it is possible to relate the likelihood of flocculation as a function of radius to the concentration profiles obtained in section 5 for the study of particles evolving in the 2D horizontal plane of the vortex. The case of the orthokinetic flocculation caused by the velocity gradient in the horizontal plane is considered (the particle settling will be neglected here).

## Likelihood of the orthokinetic flocculation

### Principle

The flocculation caused by velocity gradients is called orthokinetic flocculation. In the present study, the velocity gradient of the carrier fluid in the horizontal plane is responsible for relative motion of particles: a particle located at a point with high tangential velocity tends to move faster than one at a point with low velocity. If the particles are close enough together, their different velocities will eventually cause them to come into contact. The likelihood of orthokinetic flocculation will be addressed in the following.

### Assumptions

Rapid flocculation is assumed, i.e. there is no surface force repulsion between the particles, and every collision leads to aggregation. Also, flocculation is assumed to be relatively non-important: the collision rate is calculated as if no previous flocculation had happened. If the analysis proves that the rate of collision is significant under certain conditions, then it will give an idea of the conditions in which flocculation is expected to significantly change the results of the simulations.

**The rate of collision**

The derivation of the rate of collision in the 3D case by Ives (1977) is adapted to the 2D case. Two particles i and j are considered, j being treated as the collector. If their centre lies within a distance inferior to $R_{i,j} = r_i + r_j$ (where $r_i$ and $r_j$ are the radius of the particle i and j), the particles collide. The flow rate that comes to the j particle through the imaginary section of length $2R_{i,j}$ (Figure 7.1) is:

$$Q(r) = 2\int_0^R x(\frac{du}{dr}(r+x))dx \qquad \textbf{(7.1)}$$

with $R = R_{i,j} = r_i + r_j$

and $\frac{du}{dr}$ is the local velocity gradient in the radial direction.

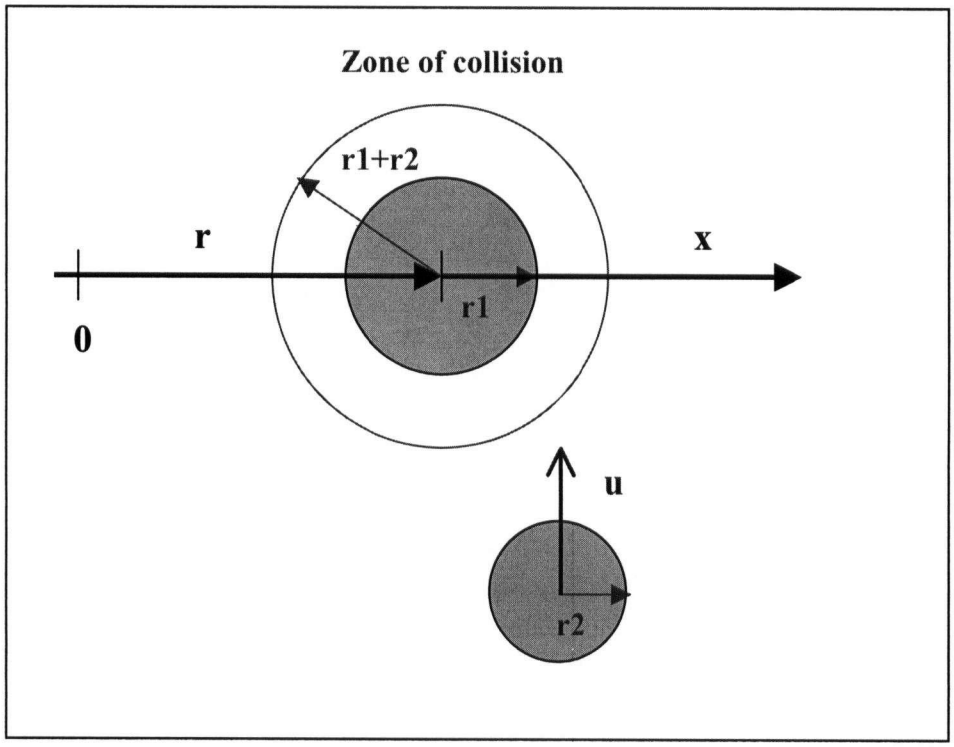


**Figure 7.1** Definition sketch for othokinetic flocculation in 2D.

$Q$ is the 2D flow rate, so for $c_i$ particles per unit area, the rate of collision of i-particles with the j-particle is:

$$c_i(r)Q(r) = 2c_i(r)\int_0^R x(\frac{du}{dr}(r+x))dx \qquad \textbf{(7.2)}$$

If there are $c_j$ particles per unit area, the rate of collision $\frac{dN_{i,j}}{dt}$ (number of collisions per unit area and per unit time) of i-particles with the j-particles is:

$$\frac{dN_{i,j}}{dt}(r) = 2c_i(r)c_j(r)\int_0^R x(\frac{du}{dr}(r+x))dx\,. \qquad \textbf{(7.3)}$$

Substituting the expression for $\frac{du}{dr}$ in the horizontal plane of symmetry of the vortex (Figure 7.2) and taking into account the time dependence of the concentration profiles gives:

$$\frac{dN_{i,j}}{dt}(r,t) = c_i(r,t)c_j(r,t)\int_0^R x\left|1-2(r+x)^2\right|\exp(-(r+x)^2)dx \qquad \textbf{(7.4)}$$

Note: all the variables are dimensionless in this expression. In particular, $x$ and $R$, which measure some lengths, are the ratios of the actual distances to the length scale of the vortex.

Then, given that the pool of particles is initially homogeneous, and assuming that the characteristics of the particles (diameter, number of particles) remain constant despite the flocculation phenomenon, the rate of collision is:

$$\frac{dN}{dt}(r,t) = c(r,t)^2\int_0^{d/L} x\left|1-2(r+x)^2\right|\exp(-(r+x)^2)dx\,. \qquad \textbf{(7.5)}$$

where $d$ is the particle diameter, and $c$ the local concentration of the particles, given by the concentration profiles (assuming that the initial concentration $c_0$ is known) (see section 5).

As in previous simulations: $\frac{d}{L} = 2*10^{-3}\sqrt{St}$ (see Chapter 4). Also, it is assumed that a total number of $P = 10000$ particles are initially released on the disc of radius [0 3] (the corresponding concentration is $c_0 = 353$ particles per unit area). Note that the collision rate varies as the initial concentration squared, and the results obtained will have to be modified if the initial concentration is given a different value (to get the value of collision rate for a number of particles $P'$ different from $P$, just multiply the given collision rate by $(P'/P)^2$).

**Results**

Equation 3 shows that the parameters that are of primary importance are:

- the particles concentration $c(r,t)$
- the velocity gradient $\frac{du}{dr}(r)$ (see Figure 7.2)
- and the diameter of the particle $d \propto \sqrt{St}$

The collision rate is proportional to $c^2(r,t)$, and approximately proportional to $d^2 \propto St$.

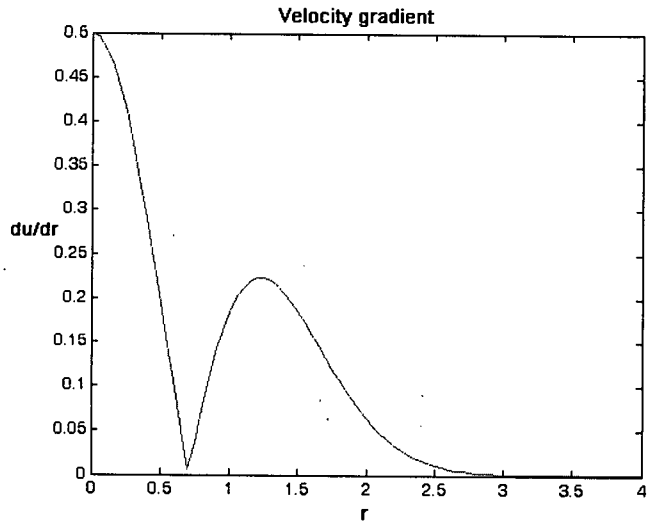


**Figure 7.2** Profile of the absolute value of the velocity gradient in the radial direction, in the horizontal plane of symmetry of a pancake vortex.

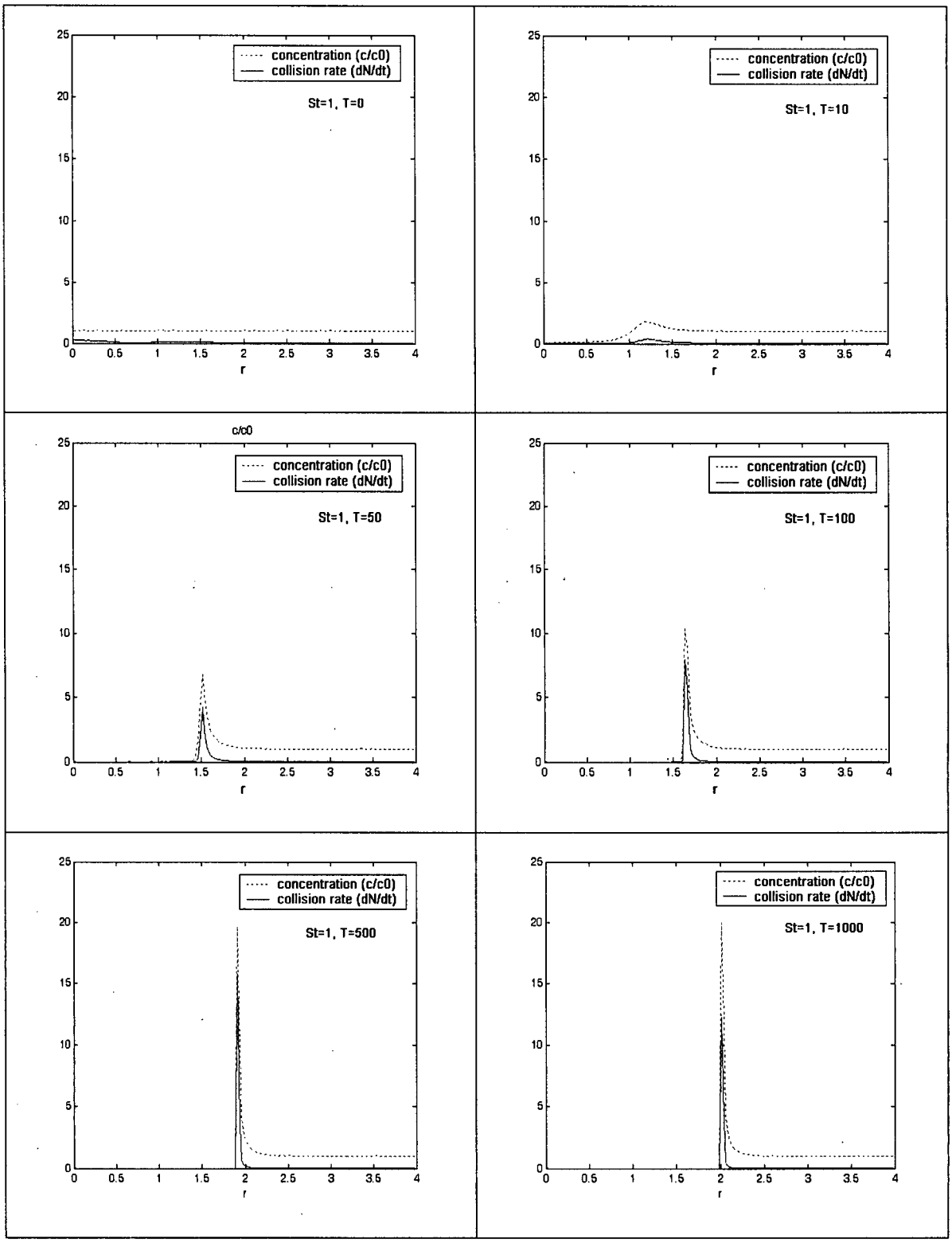


**Figure 7.3** Profiles of the particle concentration and of the collision rate in the radial direction for St=1 and T=0, 10, 50, 100, 500 and 1000.

Results of the simulations show that the collision rate's variation in the radial direction closely follows that of the concentration, hence a peak of the collision rate developing and following the peak of concentration (Figure 7.3). The value of the collision rate at the peak is represented on Figure 7.4, for St=0.1, St=1 and St=10. It increases with the Stokes number, and with time (in the overall). The radial profile of the velocity gradient modulates the value of the collision rate. In particular, for St=1 and St=10, the value of the collision rate at the peak starts to decrease at late times because the value of the velocity gradient tends to get quite small at the radial position reached by the peak.

Also, for St=10, the collision rate reaches a very large value at early times since a relatively high peak of concentration develops at a location where the velocity gradient is relatively large, thus creating optimal conditions for particle collision to occur. The peak of the collision rate goes as high as 236.5 (i.e. three orders of magnitude larger than for St=1) at $r = 1.4875$ and $T = 7$. It corresponds to the very moment where particles initially located in the central region of the vortex catch up particles initially located farther out, thus causing the local concentration to reach a relatively large value (see Chapter 5).

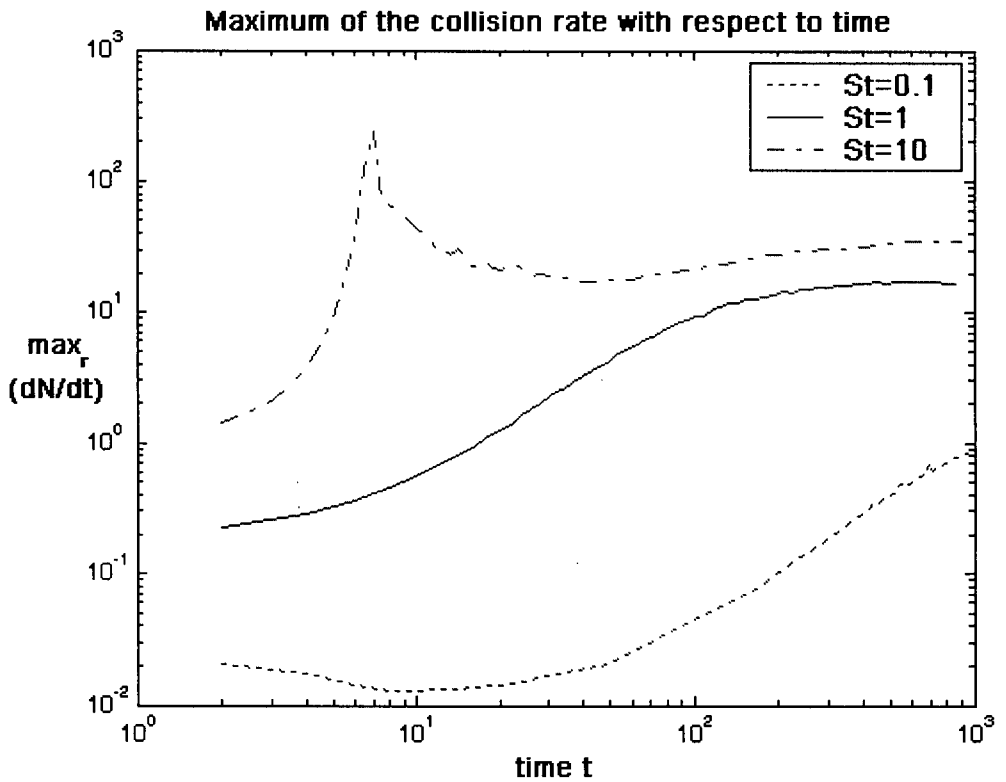


**Figure 7.4** Evolution of the maximum of the collision rate $\frac{dN}{dt}$, in the radial direction, with respect to time, for St=0.1, St=1 and St=10.

To measure the impact of the flocculation on the pool of particles, it is necessary to evaluate the number of particles that are expected to collide. Considering only the annular region where the collision rate involved is the highest (the region of the peak), and assuming that this region is roughly located at $r0 \sim 1.6$, is of width $dr = 0.05$, and that $\frac{dN}{dt}(r0) \approx 20$, the number of particles colliding per unit time is:

$$2(\frac{dN}{dt}(r0))(\pi((r0+dr)^2 - (r0)^2)) \approx 20$$

20 particles are expected to collide in that region per unit time. Therefore, for a time span T=100, 2000 would be expected to collide, which represents a fifth of the total number of particles ($P = 10000$).

**Conclusion**

As the particles go away from the vortex centre and accumulate, the rate of collision increases locally. However, the increase of the rate of collision is limited by the fact that the gradient of velocity –which is at the origin of particles collision- decreases significantly at large radial positions.

The scenario is more complex for particles having a large Stokes number (i.e. a large diameter). In that case, the rate of collision can reach very high value, especially at early times where some particles catch-up others. Therefore, flocculation is expected to have a significant impact in the dispersion process for large Stokes numbers ( $St \sim 10$ ).

# 8. CONCLUSIONS

The dispersion of small, spherical particles in a quasi-two-dimensional axisymmetric pancake-like vortex has been investigated numerically by substituting the velocity field for a pancake vortex into the Maxey-Riley (1983) equation of motion. The particles considered are heavy (i.e. denser than the surrounding fluid) with a fixed density.

In the first place, gravity was neglected. The analysis of the particle motion in the horizontal plane of symmetry of the vortex agreed with previous studies on the fact that:

1- contrary to light particles, heavy particles move away from the vortex centre

2- the Stokes number, which depends on both the particle size and density and measures the effect of the particle inertia relative to the drag, controls the dispersion process. Particles with a small Stokes number tend to follow the fluid elements. The larger the Stokes number, the further the particles are ejected. Also, when the flow is seeded with a large number of particles, inhomogeneities are created by the accumulation of particles in some regions of the vortex. Inhomogeneities are strongest for intermediate Stokes numbers (St~1) in general.

Also, by studying the dynamics of individual particles, it was found that particles of the same size and density cannot accumulate in the core region of the vortex, but they can do so in the outer region of the vortex. In addition, if the Stokes number is large enough, particles initially located in the central region of the vortex are able to overtake particles initially located farther from the vortex centre.

The flow was seeded with a homogeneous distribution of particles of the same size and density. The analysis of the concentration profiles in the horizontal plane of the vortex showed that accumulation of particles takes the form of a concentration wave that grows and travels away from the vortex centre, at a faster rate for larger Stokes numbers. The peak of concentration is the highest for intermediate values of the Stokes number ($St \sim 1$). For large Stokes numbers ($St \sim 10$), overtaking is observed visually. It occurs at very early times and substantially modifies the dispersion process, causing a second peak of concentration to appear. Just before the second peak of concentration appears, an exceptionally high peak of concentration is observed as a result of overtaking. Note that the characteristics of the concentration wave dependent on both the particles inertia (i.e. on the Stokes number) and on the vortex structure.

The analysis was then extended to the 3D case where particles settle through the vortex. The study showed that the second peak of concentration observed in the case of large Stokes numbers ($St \sim 10$) will not occur unless the vortex thickness is large enough. There is an intermediate value of the thickness ($\Lambda = 0.4$) for which particles with a large Stokes number are just brought to the point of overtaking, hence a high peak of concentration.

In reality, flocculation is expected to play an important role in regions of particle accumulation. The likelihood of orthokinetic flocculation was assessed, and was found to be exceptionally high for particles with a large Stokes number at the moment of overtaking.

# REFERENCES


ALCAN International, Ltd. Liquid metal launder. Eur. Patent Appl. No. 0289295 (1988).

Armi L., D. Herbert, N. Oakey, J. F. Prince, P. L. Richardson, H. T. Rossby, B. Ruddick, "Two years in the life of a Mediterranean salt lens", J. Phys. Oceanogr., 19, 354-370 (1989).

Auton T. R., Ph.D. thesis, University of Cambridge, Cambridge, United Kingdom (1981).

Beckers M., R. Verzicco, H. J. H. Clercx, G. J. F. Van Heijst, "Dynamics of pancake-like vortices in a stratified fluid: experiments, model and numerical simulations", J. Fluid Mech. 433, 1-27 (2001).

Bonnier M., O. Eiff, P. Bonneton, "On the density structure of far-wake vortices in a stratified fluid", Dyn. Atmos. Oceans, 31, 117-137 (2000).

Burns T. J., R. W. Davis, E. F. Moore, "A perturbation study of particle dynamics in a plane wake flow", J. Fluid Mech. 384, 1-26 (1999).

Carton X. J., G. R. Flierl, L. M. Polvani, "The generation of tripoles from unstable axisymmetric isolated vortex structures", Europhys. Lett. 9, 339-344 (1989).

Chahine G. L., "Bubble Interactions with Vortices," Chapter 18, *Fluid Vortices*, ed. S.Green, Kluwer Academic Publishing, (1994).

Chang E.J., M. Maxey, "Accelerated motion of rigid spheres in unsteady flow at low to moderate Reynolds number. Part I - Oscillatory motion ", J. Fluid Mech. 277, 347-379 (1994).

Chein R., J. N. Chung, "Effects of Vortex Pairing on Particle Dispersion in Turbulent Shear Flows," International Journal of Multiphase Flows, 13, No. 2, 785-802 (1987).

Chein R., J. N. Chung, "Simulation of particle dispersion in a two-dimensional mixing layer", AIChE J., 34, 946-954 (1988).

Chung J. N., T. R. Troutt, "Simulation of Particle Dispersion in an Axisymmetric Jet," J. Fluid Mech., 186, 199-222 (1988).

Corcos G. M., S. J. Lin, "The mixing layer: deterministic models of a turbulent flow. Part 2. The origin of the three-dimensional motion.", J. Fluid Mech., 139, 67-95 (1984).

Clift R., J. R. Grace, M. E. Weber, "Bubbles, drops and particles", Academic, New York, p. 285 (1978).

Crowe C.T., R. Gore, T. R. Troutt, "Particle Dispersion by Coherent Structures in Free Shear Flows," Particulate Science and Technology, 3, 149-158 (1985).

Crowe C. T., J. N. Chung, T. R. Troutt, "Particle Dispersion by Organized Turbulent Structures", Particulate Two-Phase Flow, Chapter 18, ed. M. Rocco Butterworth Pub. (1993).

Crowe C. T., T. R. Troutt, J. N. Chung, "Particle interactions with vortices", Chapter 19, *Fluid Vortices*, ed. S. Green, Kluwer Academic Publishing (1994).

Druzhinin O. A., "Concentration waves and flow modification in a particle-laden circular vortex", Phys. Fluids 6, 3276-3284 (1994).

Gañán-Calvo A. M., J. C. Lasheras, "The dynamics and mixing of small spherical particles in a plane, free shear layer", Phys. Fluids A 3, 1207 (1991).

Hardalupas Y., A. M. K. P. Taylor, J. H Whitelaw, "Velocity and Particle-Flux Characteristics of Turbulent Particle-laden Jets", Proc. R. Soc. Lond. A, 426, 31-78 (1989).

Hunt J. C. R., "Industrial and environmental fluid mechanics", Ann. Rev. Fluid Mech., 23, 1-42 (1991).

Ives K. J., "The scientific basis of flocculation", Nato Advanced Study Institute on the Scientific Basis of Flocculation, Christ's College, Cambridge university (1977).

Kamalu N., L. Tang, T. R. Troutt, J. N. Chung, C. T. Crowe, "Particle Dispersion in Developing Shear Layers," Proc. Intl. Conf. on Mechanics of Two Phase Flows, Taipei, Taiwan, 199-203 (1989).

Kiger K. T., J. C. Lasheras, "The effect of vortex pairing on particle dispersion and kinetic energy transfer in a two-phase shear layer", J. Fluid Mech., 302, 149-178 (1995).

Lazaro B. J., J. C. Lasheras, "Particle Dispersion in a Turbulent, Plane, Free Shear Layer," Physics of Fluids A, 1, 1035- 1050 (1989).

Lazaro B. J., J. C. Lasheras, "Particle dispersion in the developing free shear layer. Part 1. Unforced flow.", J. Fluid Mech., 235, 143-178 (1992).

Longmire E. K., J. K. Eaton, "Structure of a particle-laden round jet". J. Fluid Mech., Vol. 236, 217-257 (1992).

Lovalenti P. M., J. F. Brady, "The force on a sphere in a uniform flow with small-amplitude oscillations at finite Reynolds number", J. Fluid Mech. 256, 607 (1993a).

Lovalenti P. M., J. F. Brady, "The force on bubble, drop, or particle in arbitrary time-dependent motion at small Reynolds number", Phys. Fluids A 5, 2104 (1993b).

Lovalenti P. M., J. F. Brady, "The hydrodynamic force on a rigid particle undergoing arbitrary time-dependent motion at small Reynolds number", J. Fluid Mech. 256, 561 (1993c).

Lovalenti P. M., J. F. Brady, "The temporal behavior of the hydrodynamic force on a body in response to an abrupt change in velocity at small but finite Reynolds number", J. Fluid Mech. 293, 35 (1995).

McWilliams J. C., "Submesoscale coherent vortices in the ocean", Rev. Geophys. 23 (2), 165–182. (1985).

McWilliams J. C., "The emergence of isolated coherent vortices in turbulent flow", J. Fluid Mech., 146, 21–43. (1984).

Manton M. J., "On the motion of a small particle in the atmosphere", Boundary Layer Meteorol. , 6, 487, (1974).

Marcu B., E. Meiburg, P. K. Newton, "Dynamics of Heavy Particles in a Burgers Vortex", Phys. Fluids 7, 400-410 (1995).

Marcu B., E. Meiburg, "Three-Dimensional Features of Particle Dispersion in a Nominally Plane Mixing Layer, Phys. Fluids 8, 2266-2268 (1996).

Martin J. E., E. Meiburg, "The Accumulation and Dispersion of Heavy Particles in Forced Two-Dimensional Mixing Layers. Part I: The Fundamental and Subharmonic Cases", Phys. Fluids 6, 1116-1132 (1994).

Maxey M. R., J. J. Riley, "Equation of motion for a small rigid sphere in a nonuniform flow", Phys. Fluids 26, 883-889 (1983).

Mei R., C. J. Lawrence, R. J. Adrian, "Unsteady drag on a sphere with small fluctuations in the free-stream velocity", J. Fluid Mech. 233, 613 (1991a).

Mei R., R. J. Adrian, T. J. Hanratty, "Particle dispersion in isotropic turbulence under Stokes drag and Basset force with gravitational setting.", J. Fluid Mech. 225, 481 (1991b).

Mei R., R. J. Adrian, "Flow past a sphere with an oscillation in the free-stream velocity and unsteady drag at finite Reynolds number", J. Fluid Mech. 237, 323 (1992).

Mei R., "Flow due to an oscillating sphere and an expression for the unsteady drag on the sphere at finite Reynolds number", J. Fluid Mech. 270, 133-174 (1994).

Morrison F. A., M. B. Stewart, "Small bubble motion in an accelerating liquid", J. Appl. Mech. 43, 399-403 (1976).

Oseen C. W., Ark. Mat., Astron. Fys. 6, No 29 (1910).

Raju N., E. Meiburg, "The Accumulation and Dispersion of Heavy Particles in Forced Two-Dimensional Mixing Layers. II. The Effect of Gravity", Phys. Fluids 7, 1241 (1995).

Raju N., E. Meiburg, "Dynamics of Small, Spherical Particles in Vortical and Stagnation Point Flow Fields", Phys. Fluids 9, 299-314 (1997).

Stuart J. T., "On Finite Amplitude Oscillations in Laminar Mixing Layers," J. Fluid Mech. 29, 417-40 (1967).

Tang L., F. Wen, Y. Yang, C. T. Crowe, J. N. Chung, T. R. Troutt, "Self-organizing particle dispersion mechanism in a plane wake", Phys. Fluids A 4, 2244-2250 (1992).

Wen F., "A study on particle dispersion in a Two-Dimensional Mixing Layer", PhD dissertation, Dept. of Mech. And Matls Engr., Washington State University, (1990).

Wen F., N. Kamalu, R. Hanle, J. N. Chung, T. R. Troutt, "Particle Dispersion by Vortex Structures in Plane Mixing Layers," ASME J. Fluid Engineering, 114, 657-666 (1992).

Yang Y., J. N. Chung, T. R. Troutt, C. T. Crowe, "The Influence of Particles on the Spatial Stability of Two-Phase Mixing Layers," Phys. Fluids A 2, 1839-1845 (1990).

Yang Y., "Particle dispersion by coherent vortex structures in bluff body wake flows", PhD Dissertation, Washington State University (1993).

# APPENDIX A

## Equations of motion with a modified added mass term

In the Maxey-Riley (1983) equations, some authors have replaced the acceleration following the particle ($\frac{du}{dt}$) in the added mass term by that following a fluid element ($\frac{Du}{Dt}$).

By doing so, the equations of motion of the particles evolving in the pancake vortex are:

In polar coordinates:

$$(1+\frac{\delta}{2})\frac{\ddot{r}}{r} = -\frac{1}{St}\frac{\dot{r}}{r} - \frac{3}{2}(\frac{c}{2})^2 \delta \exp(-2r^2) + (1+\frac{\delta}{2})\dot{\theta}^2$$

$$(1+\frac{\delta}{2})\frac{d}{dt}(r^2\dot{\theta}) = \frac{1}{St}(\frac{c}{2}r^2\exp(-r^2) - r^2\dot{\theta})$$

$$(1+\frac{\delta}{2})\ddot{z} = -\frac{1}{St}\dot{z} - (1-\delta)g$$

In Cartesian coordinates:

$$(1+\frac{\delta}{2})\ddot{x} = \frac{1}{St}(-\frac{c}{2}y\exp(-r^2) - \dot{x}) - \frac{3}{2}(\frac{c}{2})^2 \delta x \exp(-2r^2)$$

$$(1+\frac{\delta}{2})\ddot{y} = \frac{1}{St}(\frac{c}{2}x\exp(-r^2) - \dot{y}) - \frac{3}{2}(\frac{c}{2})^2 \delta y \exp(-2r^2)$$

$$(1+\frac{\delta}{2})\ddot{z} = -\frac{1}{St}\dot{z} - (1-\delta)g .$$

# APPENDIX B

## Justification of the neglect of the Basset history term

The objective of this section is to check and make sure that the neglect of the Basset history term is justified. This can be done by taking the solution to the simplified equations of motion and using it to calculate the corresponding Basset history term. This term will then be compared to the drag term.

The Basset history term (B.H.T.) is equal to:

$$B.H.T. = -9\delta\left(\frac{\nu}{Ud}\right)\int_0^t \left\{\frac{d/d\tau[-\vec{w}(\vec{x},\tau)]}{[\pi\mu(t-\tau)\nu]^{\frac{1}{2}}}\right\}d\tau$$

$$= -9\delta\left(\frac{\nu}{Ud}\right)(\pi\mu\nu)^{(-1/2)}\int_0^t \left\{\frac{d/d\tau[-\vec{w}(\vec{x},\tau)]}{[t-\tau]^{\frac{1}{2}}}\right\}d\tau$$

The function under the integral is diverging when $\tau \to t$. To be able to calculate the integral numerically, for a given time t, one has to transform the integral.

By setting $x^2 = t - \tau$, the integral becomes:

$$\int_0^t \left\{\frac{d/d\tau[-\vec{w}(\vec{x},\tau)]}{[t-\tau]^{\frac{1}{2}}}\right\}d\tau = \int_{\sqrt{t}}^0 \left\{\frac{\frac{d}{d\tau}[-\vec{w}(\vec{x},\tau)]}{x}\right\} * -2 * x * dx$$

$$= 2\int_0^{\sqrt{t}} \frac{d}{d\tau}[-\vec{w}(\vec{x},\tau)] * dx$$

The value of $\frac{d}{d\tau}[\vec{w}(\vec{x},\tau)]$ is evaluated at regular, small time steps $\tau_i = t - x_i^2$, between 0 and t, such that $\Delta\tau = 0.01$. It is then multiplied by the corresponding $dx = x_{i+1} - x_i = (\sqrt{t-\tau_{i+1}}) - (\sqrt{t-\tau_i})$. Finally, all the $i-$terms are added together to get an approximation of the integral.

The case of a particle having a Stokes number of 1, released at $(x_0; y_0) = (0.01;0)$ in air, with the local fluid velocity, is now considered. The value of the different parameters is kept consistent with the rest of the thesis ($\delta = 4*10^{-4}$, $\nu = 10^{-5} m^2 s^{-1}$, $\mu = 10^{-5} N s m^{-2}$, U=3.3 $m\,s^{-1}$, L=0.03 m). First, we make sure that the time step $\Delta\tau = 0.01$ is sufficiently small for the integral to converge, by comparing the value of the Basset history term found for that time step with the one found for $\Delta\tau' = 0.001$, at t=100 (Table B.1).

| | $\Delta\tau = 0.01$ | $\Delta\tau' = 0.001$ |
|---|---|---|
| B.H.T. in the radial direction (t=100) | $-6.5392*10^{-10}$ | $-6.5387*10^{-10}$ |
| B.H.T. in the azymuthal direction (t=100) | $-1.3956*10^{-9}$ | $-1.3955*10^{-9}$ |

**Table B.1** Comparison of the value of the Basset history term obtained, at t=100, with a time step $\Delta\tau = 0.01$, with that obtained with a time step $\Delta\tau' = 0.001$.

The values found for the Basset history term are very close to each other in both cases, so we will keep the time step equal to $\Delta\tau = 0.01$.

Figure B.1 presents the absolute value of the Basset history term compared to that of the drag term. The figure illustrates that the magnitude of the Basset history term is negligible compared to the drag force term. It is seven orders of magnitude smaller approximately (Figure 1).

Therefore, the neglect of the Basset history term (mentioned in section 2.4.2) is justified *a posteriori*.

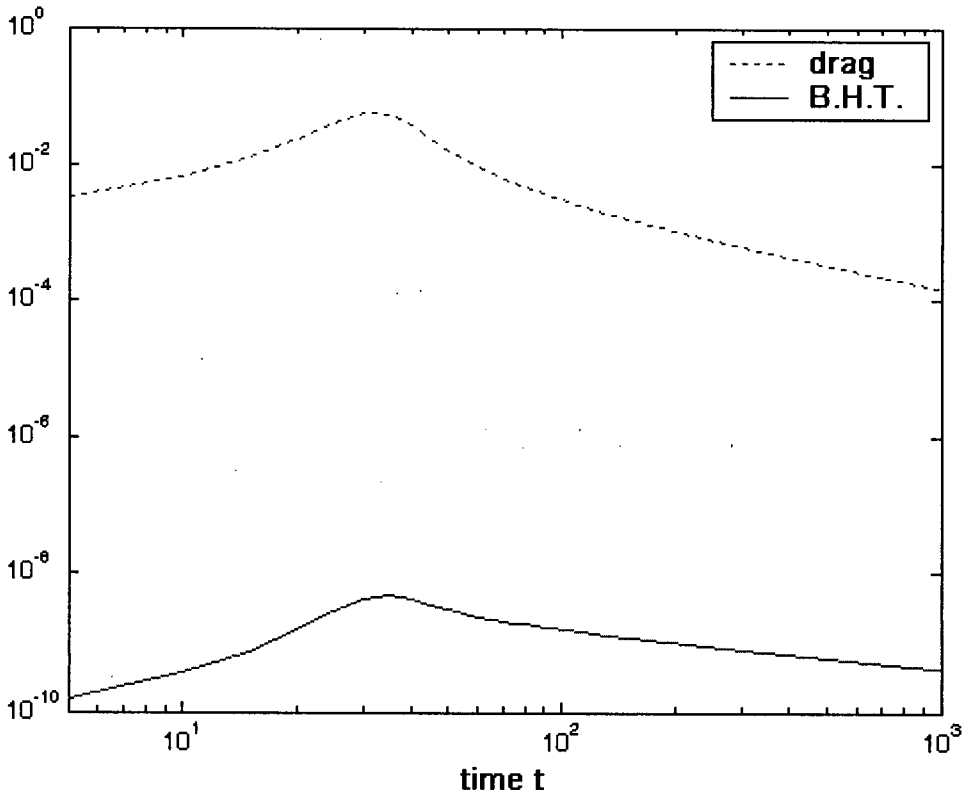


**Figure B.1** Absolute value of the drag term and of the Basset History term, with respect to time, in the case of a particle of Stokes number St=1, released at (x0;y0)=(0.01;0) with the local fluid velocity.

# APPENDIX C

## Origin of the Maxey-Riley equation's assumptions

In deriving the equation (Maxey-Riley - 1983), the force on the sphere was evaluated by separating the flow field into two components: the undisturbed and the disturbed flows. In order to obtain a simple form of the force acting on the sphere from the undisturbed flow, the particle diameter has to be small compared to the characteristic length scale of the fluid motion (referred to as Assumption 3 in section 2.4.3: $\frac{d}{L} << 1$). In order to obtain a simplified equation for the force due to the disturbance flow, the convective terms were neglected, implying Stokes flow, which requires the particle Reynolds number based on the slip velocity to be small:

$$\mathrm{Re}_p = \frac{d.|\vec{v}_p - \vec{u}|}{\nu} << 1$$

or

$$\mathrm{Re}_p = \frac{Ud}{\nu}|\vec{v}_p - \vec{u}|_{\mathrm{dim}ensionless} << 1 \qquad \text{Assumption 1 (section 2.4.3)}$$

Also, the ratio of the particle diameter squared times the characteristic velocity scale to the product of the kinematic viscosity of the fluid and of its characteristic length scale –which is representative of the gradients of the velocity U- has to be small compared to one:

$$(\frac{d}{L})^2 \mathrm{Re}_f = \frac{d^2 U}{L\nu} << 1. \qquad \text{Assumption 2 (section 2.4.3)}$$

As long as $\frac{d}{L} << 1$, $\mathrm{Re}_f = \frac{UL}{\nu}$ can be large up to $O(\frac{L}{d})$ while $\mathrm{Re}_p << 1$ is still satisfied (as long as $|\vec{v}_p - \vec{u}|$ is small compared to $U$).

The assumption of a zero Reynolds number for the relative motion actually enables many effects to be neglected. For finite values of the Reynolds number, corrections such as the Oseen correction to the Stokes drag, of order $O(\mathrm{Re}_p) = O(\frac{d|\vec{v}_p - \vec{u}|}{\nu})$ for rectilinear motion, will have to be considered. Some other corrections would also intervene if the particle were to spin, but we won't look at spinning particles in this project.